A MODEL FOR THE DOPPLER SPREAD OF BACKSCATTERED SOUND FROM A COMPOSITE ROUGHNESS SEA SURFACE

SACLANT ASW Research Centre

PREPARED FOR
North Atlantic Treaty Organization

1 May 1976

SACLANTCEN Memorandum
SM - 86

SACLANT ASW
RESEARCH CENTRE
MEMORANDUM

A MODEL FOR THE DOPPLER SPREAD OF BACKSCATTERED SOUND FROM A COMPOSITE ROUGHNESS SEA SURFACE

by

HERWARD SCHWARZE

1 MAY 1976

NORTH
ATLANTIC
TREATY
ORGANIZATION

VIALE SAN BARTOLOMEO 400
I - 19026 - LA SPEZIA, ITALY

SACLANTCEN MEMORANDUM SM-86

NORTH ATLANTIC TREATY ORGANIZATION
SACLANT ASW Research Centre
Viale San Bartolomeo 400
I 19026 — La Spezia, Italy

A MODEL FOR THE DOPPLER SPREAD OF BACKSCATTERED SOUND FROM A COMPOSITE ROUGHNESS SEA SURFACE

by

Herward Schwarze

1 May 1976

This memorandum has been prepared within the SACLANTCEN Deep Water Research Group.

i

W. Bachmann
Group Leader

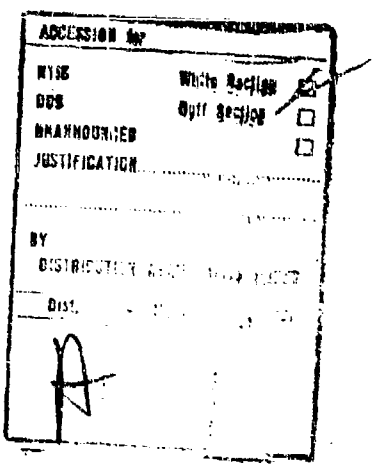

i (a)

Published by

TABLE OF CONTENTS

		Pages
ABSTRACT		1
INTRODUCTION		2
1.	RESONANT BACKSCATTERING THEORY FOR SMALL SEA-SURFACE ROUGHNESS	2
2.	DOPPLER SPECTRUM FOR A COMPOSITE-ROUGHNESS SEA SURFACE	5
	2.1 Introductory	5
	2.2 Facet statistics	6
	2.3 Choice of the facet length	10
	2.4 The Doppler spectrum	12
3.	APPLICATIONS	14
	3.1 Examples of sea-surface spectra	14
	3.2 Variances of facet slope and velocities	14
	3.3 Calculation of the facet length	18
	3.4 Resulting doppler spectra	20
CONCLUSION		21
APPENDIX A -	SEA-SURFACE DESCRIPTION	45
APPENDIX B -	SMALL SCALE ROUGHNESS BACKSCATTERING AND EXTENSION OF THE THEORY	57
APPENDIX C -	STATISTICAL DESCRIPTION OF THE FACETS	64
APPENDIX D -	CALCULATION OF THE DOPPLER SPECTRUM FOR AN ARBITRARY SEA-SURFACE ROUGHNESS	87
REFERENCES		92

List of Figures

1.		Geometry for scattering from the sea surface	3
2.		Geometry for the facet description	7
3.	n = 2	Facet slope	24
4.	n = 2	Vertical facet velocity	25
5.	n = 2	Horizontal facet velocity	26
6.	n = 2	Correlation between slope and vertical velocity	27
7.	n = 2	Correlation coefficient	28

TABLE OF CONTENTS (Cont'd)

List of Figures (Cont'd)

			Pages
8.	n = 4	Facet slope	29
9.	n = 4	Vertical facet velocity	30
10.	n = 4	Horizontal facet velocity	31
11.	n = 4	Correlation between slope and vertical velocity	32
12.	n = 4	Correlation coefficient	33
13.	n = 2	Roughness on the facet	34
14.	n = 4	Roughness on the facet	35
15.	n = 2	Relative facet length	36
16.	n = 4	Relative facet length	36
17 to 26		Doppler spectral density vs doppler shift	37 - 41
27 to 31		Doppler spectral density vs normalized doppler shift	42 - 44

A MODEL FOR THE DOPPLER SPREAD OF BACKSCATTERED SOUND FROM A COMPOSITE ROUGHNESS SEA SURFACE

by

Herward Schwarze

ABSTRACT

A theoretical model for the doppler spread of backscattered acoustic waves from the rough sea surface is described on the basis of a two component structure (facet model) of the sea surface. The facet statistics are derived for a general gaussian sea surface. The results are evaluated for a Pierson-Moskowitz spectrum. A procedure for choosing the facet length is developed. Approximate, simple formulae for the Pierson-Moskowitz case are given. The general result for the doppler spread of the backscattered acoustic wave is evaluated for a sea surface spectrum due to Scott and examples for doppler spectra are given for different windspeeds, wind directions, grazing angles and acoustic frequencies.

INTRODUCTION

The important problem of scattering of acoustic waves from the rough moving sea surface has often been investigated, but a general, exact and tractable solution has not yet been obtained.
For special cases, solutions are known, e.g. for the cases where the amplitudes of the sea surface waves are much smaller [Ref. 1] or much larger [Ref. 2] than the length of the incident wave.
For arbitrary roughnesses of the sea surface, approximate solutions are obtained by applying the small-scale backscattering results to a composite-roughness sea-surface model [Refs. 3, 4, 5, 6]. This means that the small waves with lengths up to some 10 cm, causing the resonant or "Bragg" scattering, are carried by long waves. The long waves are approximated by plane facets whose movements depend on the large-scale roughness of the sea surface.

In this paper, the interest is focussed on the frequency spreading of a backscattered monochromatic acoustic plane wave. This case is of special interest in active sonar applications because the moving sea surface limits the detectability of slowly-moving targets.
Special effort has been devoted to obtain a set of formulae that are simple to use in already existing sonar models, especially in the RAIBAC program system developed at SACLANTCEN [Ref. 7].

The main text of this paper contains the results obtained, together with some physical explanations. All mathematical derivations and proofs are given in appendices.
In the main text, the existing resonant scattering theory is first reviewed and the facets are then introduced. The statistical properties of the facets are given in terms of the sea-surface covariance function or the three-dimensional sea-surface spectrum. The concept is applied to the small-scale roughness results. Several special cases are considered.
The general formalism is worked out in several examples of idealized sea-surface spectra and the computer results are shown.

1. RESONANT BACKSCATTERING THEORY FOR SMALL SEA-SURFACE ROUGHNESS

The geometry shown in Fig. 1 is used. A source $S(x_0, 0, z_0)$ illuminates a surface area $A = ab$ with a plane wave of frequency f_0 and pressure amplitude p_0. The distance r_0 is considered much larger than $\sqrt{A}$. Without loss of generality the y-coordinate of S is set to zero. Besides the specular reflection, the rough sea surface causes a scattered field in all directions. For backscattering, source S and receiver R coincide.

The doppler spectrum $\Phi(f)$ of the backscattered wave $p(t)$ is the Fourier transform of its correlation function, viz:

$$\Phi(f) = \int_{-\infty}^{\infty} E\{p^*(t)p(t+T)\} \exp\{-2\pi jfT\}\, dt \qquad [Eq.1]$$

where $E\{...\}$ denotes expectation and $*$ the conjugate complex.

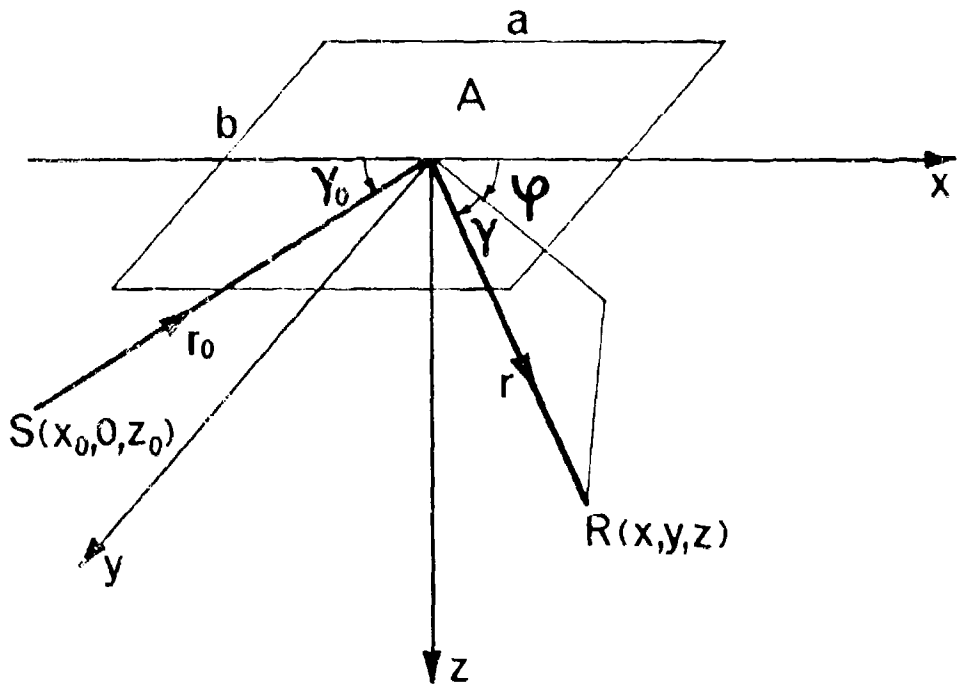

FIG. 1 GEOMETRY FOR SCATTERING FROM THE SEA SURFACE

A normalization is introduced, yielding a backscattering doppler density

$$\varphi(f) = \frac{\Phi(f) r_0^2}{p_0^2 A} \quad . \qquad \text{[Eq. 2]}$$

Starting from Ref. 8, for example, the basic equation for the backscattering doppler density for the slightly rough sea surface is

$$\varphi(f) = (4\pi)^2 \sin^4 \gamma_0 k_0^4 X_3(-2k_0 \cos \gamma_0, 0, f-f_0) \quad . \qquad \text{[Eq. 3]}$$

In Eq. 3, $k_0 = \frac{1}{\lambda_0} = \frac{f_0}{c}$ is the wave parameter of the acoustic plane wave and $X_3(k_x, k_y, f)$ is the three-dimensional wave parameter frequency spectrum of the sea surface. The wave parameter $k = \frac{1}{\lambda}$ was introduced here instead of the wave number $\frac{2\pi}{\lambda}$, because it offers some notational advantage. Equation 3 is derived in detail in App. B. When integrated over f, Eq. 3 becomes the backscattering strength, known from the literature [Refs. 9, 4].

The general small-scale roughness result is simplified by the assumption that the dispersion relation

$$2\pi f^2 = g k \qquad \text{[Eq. 4]}$$

is valid, where g is the gravity constant.
Using the relations in App. A, Eq. 3 is written in terms of the frequency angle spectrum $F_2(f, \varphi)$

$$\varphi(f) = \frac{2g^2 k_0^4 \sin^4 \gamma_0}{f_0^{*3}} F_2(f_0^*, 0) \qquad \text{[Eq. 5]}$$

$$[W(f_0^*, \pi)\ \delta(f-f_0-f_0^*) + W(f_0^*, 0)\ \delta(f-f_0+f_0^*)],$$

where

$$f_0^* = \sqrt{\frac{g k_0 \cos \gamma_0}{\pi}} \qquad \text{[Eq. 6]}$$

is the dispersion relation. In Eq. 5, $F_2(f, \varphi)$ and $W(f, \varphi)$ are the frequency angle spectrum and the wave-mixing function, respectively.

The mixing function describes the ratio of incoming and outgoing surface waves for a given wave parameter vector or a given frequency and direction. The introduction of this function leads to the same results as the theory of Neumann and Pierson [Ref. 10, p. 330] but it is felt that the formulation used here is simpler. For details of the definition of W and its relation to the wave parameter frequency spectrum X_3 the reader is referred to App. A.

A simple practical case is the omnidirectional sea-surface spectrum with $W = 0.5$, which seems reasonable for short surface waves. In this case one obtains

$$\varphi(f) = \frac{g^2 \sin^4 \gamma_0 k_0^4}{2\pi f_0^{*3}} F_1(f_0^*)[\delta(f-f_0-f_0^*) + \delta(f-f_0+f_0^*)]. \qquad \text{[Eq. 7]}$$

Equations 5 and 7 are considered to be valid under the following conditions:

1)	$\lambda_0 >> \sigma_h \cdot 2\pi \sin\gamma_0$ σ_h: standard deviation of the sea surface height	"Bragg" scattering, Rayleigh theory [Ref. 11]	[Eq. 8]
2)	$\lambda_0 << \sqrt{A}$	Implicit assumption for Eqs. 5 and 7, explanation see App. B	[Eq. 9]
3)	$r_0 >> \sqrt{A}$	Assumption of incident plane wave	[Eq. 10]
4)	$\frac{1}{k} > 0.05$ m	Approximation rule for the validity of the dispersion relation, Eq. 4	[Eq. 11]

As most acoustic wavelengths in sonar applications are between 0.1 and 1 m, the condition of Eq. 8 is often not fulfilled. Therefore it is necessary to introduce the composite roughness sea surface model, which circumvents this condition. This model is developed in the next chapter.

2. DOPPLER SPECTRUM FOR A COMPOSITE-ROUGHNESS SEA SURFACE

2.1 Introductory

The derivations of this chapter are based on the facet model as used by Bachmann [Refs. 5, 14] for the calculation of the backscattering strength.

The facet model assumes basically a two-component structure of the rough-moving sea surface: the small-scale high-frequency roughness (ripples), responsible for the resonant scattering are carried by the low-frequency large-scale sea-surface waves (swell). These carrier waves are locally approximated by plane facets of finite extend. The movements of these facets have influences on the back-scattering strength and the doppler shifts of the backscattered sound.

In the first part of this chapter the facet model is developed and the statistics of the facets are calculated. In the second part, the effects of the facet movements on the small-scale roughness results are considered.

2.2 Facet statistics

The facets are statistically described by a five-dimensional random process: the inclinations ϵ_x and ϵ_y and the velocities u_x, u_y, and u_z. If the incident acoustic-wave vector lies in the x-z plane, the influences of ϵ_y and u_y can be considered small and are neglected [Ref. 14]. Consequently one deals with a three-dimensional process only and the facet can be represented by a straight line, thus reducing the mathematical effort.

As it is assumed that the sea surface is described as a gaussian process, the facet movement is also considered to be normal distributed. As the mean values of the stochastic variables $\epsilon = \epsilon_x(t)$, $u_x(t)$ and $u_z(t)$ are zero by definition, their covariance matrix is sufficient for their complete description.

The geometry shown in Fig. 2 is used in the calculation. To obtain an expression for $\epsilon(t)$ and $b(t)$, the sea surface function $h(x, y, t)\big|_{y=0}$ is approximated by a least-square-error straight line

$$f(x, t) = \epsilon(t)\, x + b \qquad \text{[Eq. 12]}$$

in the interval $|x| \leq \frac{L}{2}$. This yields

$$\epsilon(t) = \frac{12}{L^3} \int_{-\frac{L}{2}}^{\frac{L}{2}} x\, h(x, y, t)\, dx \qquad \text{[Eq. 13]}$$

and

$$b(t) = \frac{1}{L} \int_{-\frac{L}{2}}^{\frac{L}{2}} h(x, y, t)\, dx \; . \qquad \text{[Eq. 14]}$$

The vertical velocity u_z follows from Eq. 14

$$u_z(t) = \frac{\partial b(t)}{\partial t} = \frac{1}{L} \int_{-\frac{L}{2}}^{\frac{L}{2}} \frac{\partial h(x, y, t)}{\partial t}\, dx \; . \qquad \text{[Eq. 15]}$$

For the horizontal velocity u_x the following argument applies. From the linear theory of surface waves it follows that the horizontal particle velocity u in the x-direction is

$$\frac{\partial u}{\partial t} = -g \quad \frac{\partial h(x, y, t)}{\partial x} \; . \qquad \text{[Eq. 16]}$$

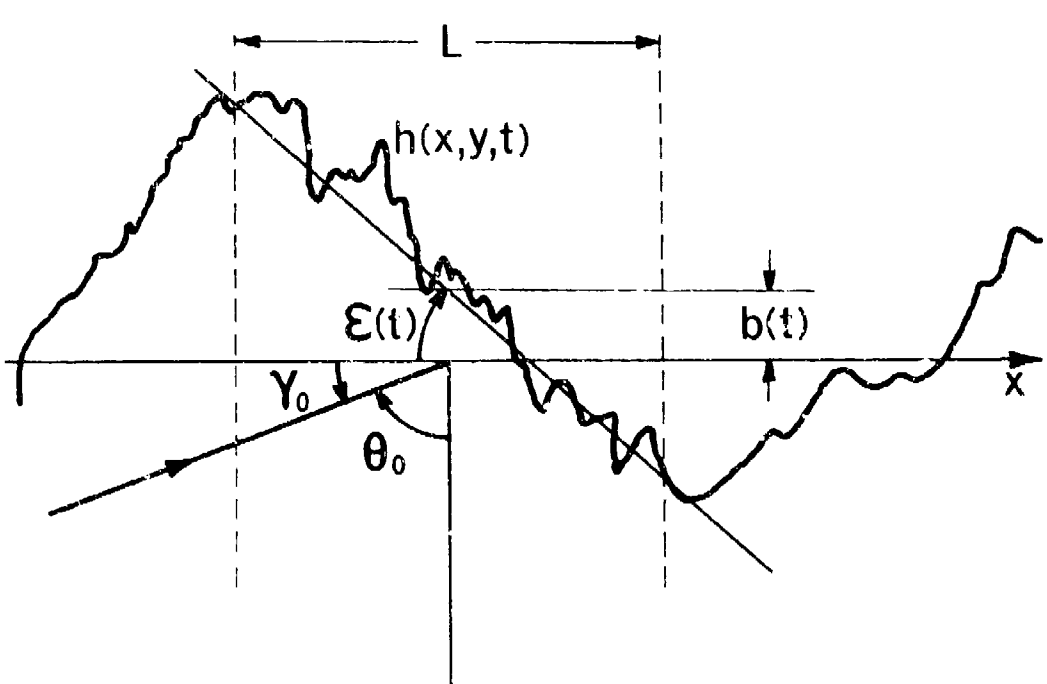

FIG. 2 GEOMETRY FOR THE FACET DESCRIPTION

The horizontal velocity of the facet u_x is defined as the mean horizontal particle velocity on the facet

$$u_x(t) = \frac{1}{L} \int_{-\frac{L}{2}}^{\frac{L}{2}} u\,dx \quad . \qquad \text{[Eq. 17]}$$

Inserting Eq. 16 into Eq. 17 gives

$$u_x(t) = -\frac{g}{L} \int_{t_o}^{t} \left[h\left(\frac{L}{2}, y, t_1\right) - h\left(-\frac{L}{2}, y, t_1\right) \right] dt_1 + u_x(t_o). \qquad \text{[Eq. 18]}$$

From Eqs. 13, 15 and 17 the variances and cross-variances of the facet movement are calculated. The results are given below, the derivation of the formulae is found in App. C

$$E_t\{\epsilon^2\} = \frac{24}{L^3} \int_o^L C(x, y, \tau)\Big|_{\substack{y=0 \\ \tau=0}} \left(1 - \frac{3x}{L} + \frac{2x^3}{L^3}\right) dx, \qquad \text{[Eq. 19]}$$

$$E_t\{u_z^2\} = -\frac{2}{L} \int_o^L \frac{\partial^2 C(x, y, \tau)}{\partial \tau^2}\Big|_{\substack{y=0 \\ \tau=0}} \left(1 - \frac{x}{L}\right) dx, \qquad \text{[Eq. 20]}$$

and

$$E_t\{u_x^2\} = -\frac{g^2}{L^2} \int_{-\infty}^{\tau} \int_{t_1}^{\tau} \left[2C(0, y, t) - C(L, y, t) - C(-L, y, t) \right] dt\, dt_1 \Big|_{\substack{\tau=0 \\ y=0}} .$$

[Eq. 21]

The cross variances are

$$E_t\{\epsilon\, u_z\} = -\frac{12}{L^3} \int_o^L \frac{\partial C(x, y, \tau)}{\partial \tau}\Big|_{\substack{y=0 \\ \tau=0}} \left(x - \frac{x^2}{L}\right) dx \qquad \text{[Eq. 22]}$$

and

$$E_t\{\epsilon\, u_x\} = E_t\{u_x u_z\} = 0. \qquad \text{[Eq. 23]}$$

Using the results of App. A, the above equations can be written in terms of the wave parameter frequency spectrum or the frequency angle spectrum. As the latter is of importance in the applications, the formulation of the facet statistics in terms of $F_2(f, \varphi)$ is given here.

It is

$$E_t\{\epsilon^2\} = \frac{144}{L^6}\int_{-\pi}^{+\pi}\int_{0}^{\infty}\frac{F_2(f,\varphi)}{a^4}\left(La\cos\frac{aL}{2} - 2\sin\frac{aL}{2}\right)^2 df d\varphi\,, \qquad \text{[Eq. 24]}$$

$$E_t\{u_z^2\} = \frac{2g^2}{L^2}\int_{-\pi}^{+\pi}\int_{0}^{\infty}\frac{F_2(f,\varphi)(1-\cos aL)}{(2\pi f\cos\varphi)^2} df d\varphi\,, \qquad \text{[Eq. 25]}$$

$$E_t\{u_x^2\} = \frac{2g^2}{L^2}\int_{-\pi}^{+\pi}\int_{0}^{\infty}\frac{F_2(f,\varphi)(1-\cos aL)}{(2\pi f)^2} df d\varphi\,, \qquad \text{[Eq. 26]}$$

and

$$E_t\{\epsilon u_z\} = \frac{-12}{L^3}\int_{-\pi}^{+\pi}\int_{0}^{\infty}F_2(f,\varphi)(2W(f,\varphi)-1)\,2\pi f$$

$$\left[-\frac{\sin aL}{a^3} + \frac{2}{La^3}(1-\cos aL)\right] df d\varphi\,, \qquad \text{[Eq. 27]}$$

where

$$a = \frac{(2\pi f)^2\cos\varphi}{g}\,. \qquad \text{[Eq. 28]}$$

The derivation of the above formulae is also found in App. C.

The horizontal velocity u_x is uncorrelated to ϵ and u_z, as is seen from Eq. 23. As ϵ, u_z and u_x are assumed to be normally distributed, u_x is therefore independent of ϵ and u_z. Then the three-dimensional probability density $w_3(\epsilon, u_z, u_x)$ has the form

$$w_3(\epsilon, u_z, u_x) = w_2(\epsilon, u_z)\, w_1(u_x)\,, \qquad \text{[Eq. 29]}$$

where

$$w_1(u_x) = \frac{1}{\sqrt{2\pi}\,\sigma_x}\exp\left\{-\frac{u_x^2}{2\sigma_x^2}\right\} \qquad \text{[Eq. 30]}$$

$$= N(u_x, 0, \sigma_x)$$

and

$$w_2(\epsilon, u_z) = \frac{1}{2\pi\sigma_\epsilon\sigma_z\sqrt{1-\rho_{\epsilon z}^2}} \exp\left\{\frac{1}{2(1-\rho_{\epsilon z}^2)}\left(\frac{u_z^2}{\sigma_z^2} - \frac{2\rho_{\epsilon z}u_z\epsilon}{\sigma_z\sigma_\epsilon} + \frac{\epsilon^2}{\sigma_z^2}\right)\right\} .$$

[Eq. 31]

The abbreviations in Eqs. 30 and 31 are

$$\sigma_\epsilon = \sqrt{E_t\{\epsilon^2\}},\ \sigma_z = \sqrt{E_t\{u_z^2\}},\ \sigma_x = \sqrt{E_t\{u_x^2\}} \qquad \text{[Eq. 32]}$$

and

$$\rho_{\epsilon z} = \frac{E\{\epsilon\, u_z\}}{\sigma_\epsilon\, \sigma_z} \quad . \qquad \text{[Eq. 33]}$$

Equation 29 describes the facet statistics and is used in the following for the calculation of the doppler density.

2.3 Choice of the facet length

The facet statistics as derived in the preceding section depend entirely on the facet length L. In practical cases, this L has to be chosen. The choice is directed by two influences. Firstly, the facet length should be greater than the wave length of the incident acoustic wave to reduce the finite aperture error as much as possible. That leads to the condition

$$L >> \lambda_o \quad . \qquad \text{[Eq. 34]}$$

Secondly, the sea-surface roughness $\sigma_h(L)$ on the facet should be much smaller than the acoustic wave length λ_o to fulfil the Rayleigh condition [Eq. 8]

$$\lambda_o >> \sigma_h(L) \quad . \qquad \text{[Eq. 35]}$$

It seems to be extremely complicated to calculate the finite aperture error and the finite roughness error and to choose that facet length, L_{opt}, where the sum of both is a minimum. Therefore the following procedure for choosing the facet length is performed: A number N is chosen that transforms the two above inequalities [Eqs. 34 and 35] to the equations

$$L = \lambda_o \cdot N \qquad \text{[Eq. 36]}$$

and

$$\frac{\lambda_o}{N} = \sigma_h(L) \quad . \qquad \text{[Eq. 37]}$$

Combining them gives

$$L \cdot \sigma_h(L) = \lambda_o^2 \quad . \qquad \text{[Eq. 38]}$$

This implicit equation has to be solved to find the facet length L. The number N is a quality number that shows how far L is away from the limit where the conditions for the validity of the composite sea surface model are no longer valid. If N is less than about 2, this indicates that the facet model will yield no correct results.

To solve Eq. 38, an expression for $\sigma_h(L)$ has to be found. The roughness $r(t)$ on the facet is

$$r(x, t) = h(x, y, t)|_{y=0} - f(x, t) \quad , \qquad \text{[Eq. 39]}$$

where $f(x, t)$ is the facet equation in Eq. 12.

The mean square error $\rho^2(t)$ is a random variable in time

$$\rho^2(t) = \frac{1}{L} \int_{-\frac{L}{2}}^{+\frac{L}{2}} r^2(x, t)\, dx \quad . \qquad \text{[Eq. 40]}$$

The sea-surface roughness $\sigma_h^2(t)$ is the expectation of $\rho^2(t)$

$$\sigma_h^2(L) = E_t\{\rho^2\} \quad . \qquad \text{[Eq. 41]}$$

Using App. A, is it shown in App. C that this takes the form

$$E_t\{\rho^2\} = C(o, o, o) - \frac{4}{L} \int_o^L C(x, y, \tau)|_{y=\tau=o} \left(1 - \frac{2x}{L} + \frac{x^3}{L^3}\right) dx \qquad \text{[Eq. 42]}$$

or, written in terms of the frequency angle spectrum $F_2(f, \varphi)$,

$$E\{\rho^2(t)\} = \int_{-\pi}^{+\pi} \int_o^\infty F_2(f, \varphi) \left\{1 - \frac{4}{a^2 L^2}\left[\left(1 - \frac{6}{a^2 L^2}\right)\cos aL - \frac{6}{aL}\sin aL + 2 + \frac{6}{L^2 a^2}\right]\right\} df\, d\varphi \,, \qquad \text{[Eq. 43]}$$

where the factor a is seen from Eq. 28.

With Eq. 42 or Eq. 43 it is possible to solve Eq. 38 by an interactive procedure for a practical case, where $C(x, y, x)$ or $F_2(f, \varphi)$ is known explicitly. This will be investigated in Chapter 3.

2.4 The Doppler spectrum

The doppler spectrum for an arbitrarily rough surface takes into account the facet movements whose statistics were described in the preceding chapter.

The grazing angle γ_o and the incident frequency f_o are modulated by the facet inclination $\varepsilon(t)$ and the facet velocities $u_x(t)$ and $u_z(t)$ respectively and accordingly the small scale result in Eq. 5 is changed.
The modulation changes γ_o and f_o to statistic variables of the following form

1) Influence of the facet slope

$$\gamma_f(t) = \gamma_o + \varepsilon(t) \ . \qquad \text{[Eq. 44]}$$

2) Influence of the facet velocities

$$f_f(t) = f_o + \frac{2f_o}{c} \left[u_z(t)\sin\gamma_f(t) - u_x(t)\cos\gamma_f(t)\right]. \qquad \text{[Eq. 45]}$$

To obtain the backscattered doppler density $\varphi(f)$, the weighted sum for all ε, u_x, and u_z has to be taken. Using Eq. 6 one finds

$$\varphi(f) = 2g^2 \int_{-\infty}^{\infty}\int\int\int \frac{k_{of}^4 \sin^4\gamma_f}{f_f^{*8}} F_2(f_f^*, o)$$

$$\left[W(f_f^*, \pi)\ \delta(f - f_f - f_f^*) + W(f_f^*, o)\ \delta(f - f_f + f_f^*)\right]. \qquad \text{[Eq. 46]}$$

$$w_3(\varepsilon, u_z, u_x)\ d\varepsilon du_z du_x \ .$$

This integral can be solved in closed form for a small facet slope ε and other minor neglections that are found, together with a derivation of the general result, in App. D. The general formula for the doppler density $\varphi(f)$ is

$$\varphi(f) = \sqrt{\frac{\pi g \cos^5\gamma_o}{c^3}} \ \frac{1}{4f_o \sin\gamma_o}$$

$$\left[\sqrt{(f - f_o^*)^5}\ F_2(f_-^*, o)\, W(f_-^*, \pi)\, I_- \right. \qquad \text{[Eq. 47]}$$

$$\left. + \sqrt{(f + f_o^*)^5}\ F_2(f_+^*, o)\, W(f_+^*, o)\, I_+\right] \ ,$$

where

$$f^{*}_{-,+} = \sqrt{\frac{g \cos\gamma_o (f \mp f_o)^3}{\pi c}} \qquad \text{[Eq. 48]}$$

and

$$I_{-,+} = N(u_{-,+}, o, \sigma_1) \left[3\sigma_\epsilon^4 (1 - \rho_{\epsilon z}^2)^2 + 6\sigma_\epsilon^2 (1 - \rho_{\epsilon z}^2) (\sigma_2^2 + m_{-,+}^2) + 3\sigma_2^4 + 6\sigma_2^2 m_{-,+}^2 + m_{-,+}^4 \right] . \qquad \text{[Eq. 49]}$$

In Eq. 49 the abbreviations are

$$u_{-,+} = \frac{(f - f_o \mp f_o^{*}) c}{2 f_o \sin\gamma_o} , \qquad \text{[Eq. 50]}$$

$$\sigma_1 = \frac{\sqrt{\sigma_x^2 + \sigma_z^2 \tan^2\gamma_o}}{\tan\gamma_o} , \qquad \text{[Eq. 51]}$$

$$\sigma_2 = \frac{\sigma_\epsilon \sigma_x \rho_{\epsilon x}}{\sqrt{\sigma_x^2 + \sigma_z^2 \tan^2\gamma_o}} = \frac{\sigma_x \sigma_\epsilon}{\sigma_1 \tan\gamma_o} , \qquad \text{[Eq. 52]}$$

and

$$m_{-,+} = \frac{\sigma_\epsilon \sigma_z \rho_{\epsilon z} u_{-,+} \tan^2\gamma_o}{\sigma_x^2 + \sigma_z^2 \tan^2\gamma_o} + \tan\gamma_o . \qquad \text{[Eq. 53]}$$

From this general result every required simplification can be easily deduced. For example, if the facet slope is considered of little influence in a certain case, the expression $I_{-,+}$ in Eq. 49 reduces to

$$I_{-,+} = N(u_{-,+}, o, \sigma_1) \tan^4\gamma_o . \qquad \text{[Eq. 54]}$$

Another special case is the assumption of an omnidirectional sea surface spectrum $F_1(f)$ and a mixing function $W = 0.5$ (see App. A). Using Eq. A.26, the doppler density for this case can easily be found.

The general result of Eq. 47 has been programmed on a computer for sea-surface spectra of practical importance. These applications are discussed in the next chapter.

3. APPLICATIONS

3.1 Examples of sea-surface spectra

For demonstrating the use of the model described in the preceding chapters a sea-surface spectrum needs to be chosen as an example. This spectrum should have a well defined frequency and directionality variation with the wind speed and wind direction. On the other hand it should be mathematically simple enough to allow the calculation of the facet statistics with not too much effort. Therefore the well known Pierson-Moskowitz spectrum was chosen for the facet statistics in slightly modified form. It can be found in App. A, Eqs. A.50 and A.51, and is given here for convenience

$$F_2(f, \varphi) = F_1(f) \frac{\cos^n(\varphi - \varphi_0)}{x_n} \quad , \qquad \text{[Eq. 55]}$$

where

$$F_1(f) = \begin{cases} \dfrac{\alpha g^2}{(2\pi)^4 f^5} \; , & f > f_s = \dfrac{g}{2\pi v} \sqrt[4]{\beta} \\ 0 \; , & \text{else} \end{cases} \qquad \text{[Eq. 56]}$$

and

$$x_n = \int_{-\pi}^{\pi} \cos^n \varphi \, d\varphi \, , \qquad \alpha = 0.0081 \quad \text{and} \quad \beta = 0.74.$$

The mixing function W used for these calculations is given by Eq. A.40.

For the calculation of the doppler density a more flexible spectrum was employed, which takes into consideration the frequency dependence of the surface-wave directivity. This spectrum, due to Scott [Ref. 15] is found in Eqs. 60 and A.64 of Appendix A.

3.2 Variances of facet slope and velocities

In this section the general formulae for the facet statistics [Eqs. 24 to 28] are evaluated for the Pierson-Moskowitz sea-surface spectrum. Again the derivations are found in App. C, the results are given in the following.

The starting point is the Pierson-Moskowitz spectrum of the form of Eq. 56. This spectrum is inserted into Eqs. 24 to 27. Then the integration over the frequency f is performed, yielding

$$\sigma_\epsilon^2 = \frac{\alpha\, v^4}{\beta\, x_n\, L^2\, g^3} \int_0^\pi \cos^n(\varphi - \varphi_0) \left\{ \frac{18}{u_0^2} + \frac{48}{u_0^4} + \cos u_0 \left(-1 + \frac{6}{u_0^2} - \frac{48}{u_0^4}\right) + \sin u_0 \left(u_0 - \frac{2}{u_0} - \frac{48}{u_0^3}\right) - u_0^2\, \mathrm{Ci}(|u_0|) \right\} d\varphi \quad , \qquad \text{[Eq. 57]}$$

$$\sigma_z^2 = \frac{2\alpha v^2}{3\sqrt{\beta}\, x_n} \int_0^\pi \cos^n(\varphi - \varphi_0) \left\{ 1 + \cos u_0 \left(\frac{1}{2} - \frac{1}{u_0^2}\right) + \frac{\sin u_0}{2u_0} + \frac{|u_0|}{2}\, \mathrm{Si}(|u_0|) \right\} d\varphi \quad , \qquad \text{[Eq. 58]}$$

$$\sigma_x^2 = \frac{2\alpha\, v^6}{3\beta^{1.5}\, x_n L^2 g^2} \int_0^\pi \cos^n(\varphi - \varphi_0) \left\{ 1 + \cos u_0 \left(-1 + \frac{u_0^2}{2}\right) \frac{u_0 \sin u_0}{2} + \frac{|u_0|^3}{2}\, \mathrm{Si}(|u_0|) \right\} d\varphi \quad , \qquad \text{[Eq. 59]}$$

and

$$E_t\{\epsilon\, u_z\} = \sigma_{\epsilon z} = \frac{12(1 - 2W_0)\alpha v^4}{\beta^{0.75}\, x_n\, L\, g} \int_{\varphi_w - \frac{\pi}{2}}^{\varphi_w + \frac{\pi}{2}} \cos^n(\varphi - \varphi_0) \cdot \left\{ \sin u_0 \left(\frac{k_1}{u_0^2} + k_2\right) + \cos u_0 \left(\frac{k_3}{u_0^3} + \frac{k_4}{u_0} + k_5 \cdot u_0\right) - \frac{k_3}{u_0^3} - 2 k_5\, u_0 \sqrt{\frac{\pi}{2}\,|u_0|} \left(\frac{1}{2} - S\left(\sqrt{\frac{2|u_0|}{\pi}}\right)\right) \right\} d\varphi \quad , \qquad \text{[Eq. 60]}$$

where

$$u_0 = a_0 \cos\varphi \qquad \text{[Eq. 61]}$$

and

$$a_0 = \frac{(2\pi f_s)^2\, L}{g} = \frac{\sqrt{\beta}\, Lg}{v^2} \qquad \text{[Eq. 62]}$$

The constants k_1 to k_5 are $k_1 = -10/63$, $k_2 = 8/189$, $k_3 = -4/9$, $k_4 = -4/63$, and $k_5 = 16/189$. The functions Si, Ci and S are the sine integral, the cosine integral and the Fresnel integral [Ref. 13], respectively.

The variances in Eqs. 57 to 60 have been programmed on a digital computer, using numerical integration techniques. Inspection of the equations shows that the variances are functions of the following form

$$\sigma_\epsilon = f_1\left(\frac{L}{v^2}\right)$$

$$\frac{\sigma_z}{v} = f_2\left(\frac{L}{v^2}\right) \quad ,$$

$$\frac{\sigma_x}{v} = f_3\left(\frac{L}{v^2}\right) \quad , \qquad \text{[Eq. 63]}$$

$$\frac{\sigma_{\epsilon z}}{v} = f_4\left(\frac{L}{v^2}\right)$$

and

$$\rho_{\epsilon z} = \frac{\sigma_{\epsilon z}}{\sigma_\epsilon \sigma_z} = f_5\left(\frac{L}{v^2}\right) \quad .$$

Therefore, the results are shown as a function of L/v^2 rather than the facet length L, thus eliminating the variation of the results as a function of the windspeed v.

The remaining parameters are the direction angle φ_0, the direction angle φ_w of the mixing function, and the exponent n of the cosine directivity function. In Figs. 3 to 12 the facet statistics are shown for $\varphi_0 = \varphi_w = 0°$, 45° and 90° and $n = 2$ and $n = 4$. From the figures, the facet statistics can be found for practical cases.

The important region for L/v^2 between 0.1 and 1 s^2/m is shown in a linear scale in addition to the general double logarithmic plots. The facet slope σ_ϵ diverges for $L \to 0$; therefore the curves in figures 3b and 7b start at the maximum value on the σ_ϵ-scale. For $\frac{L}{v^2} < 0.1$, Figs. 3a and 7a should be used.

For certain applications it is desirable to have analytical expressions for the variances. This can be achieved by approximate solutions of Eqs. 57 to 60 for $a_0 \ll 1$ and $a_0 \gg 1$ and combining the results. Again, the derivations are found in App. C; for the important practical case $n = 2$ it is

for $a_0 \ll 1$

$$\sigma_\epsilon = \sqrt{\frac{\alpha}{8}\left[(3.85 - 3\ln a_0)\cos^2\varphi_0 + (1.31 - \ln a_0)\sin^2\varphi_0\right]}$$

$$\frac{\sigma_z}{v} = \sqrt{\frac{\alpha}{2\sqrt{\beta}}} = 6.86 \cdot 10^{-2}$$

$$\frac{\sigma_x}{v} = \sqrt{\frac{\alpha}{8\sqrt{\beta}} \left(3 \cos^2 \varphi_0 + \sin^2 \varphi_0\right)} \qquad \text{[Eq. 64a]}$$

$$\frac{\sigma_{\epsilon z}}{v} = \frac{8(1 - 2W_0)\, \alpha \cos\varphi_0}{3\pi \sqrt[4]{\beta}} \left(1 - 0.596 \sqrt{a_0}\right)$$

$$= 7.413 \cdot 10^{-3} \cos \varphi_0 \,(1 - 2W_0)\left(1 - 1.732 \sqrt{\frac{L}{v^2}}\right),$$

for $a_c >> 1$

$$\sigma_\epsilon = \frac{\sqrt{18\,\alpha}}{\beta g^2 \left(\frac{L}{v^2}\right)^2} \sqrt{\cos^2 \varphi_0 + \frac{(2a_0 - \pi)}{\pi} \sin^2 \varphi_0}$$

$$\frac{\sigma_z}{v} = \sqrt{\frac{2\alpha}{3\beta^{1.5}}} \quad \frac{1}{g\frac{L}{v^2}} \sqrt{\cos^2 \varphi_0 + \frac{(2a_0 - \pi)}{\pi} \sin^2 \varphi_0}$$

[Eq. 64b]

$$\frac{\sigma_x}{v} = \sqrt{\frac{\alpha}{3\beta^{1.5}}} \quad \frac{1}{g\frac{L}{v^2}}$$

$$\frac{\sigma_{\epsilon z}}{v} = \frac{16(1 - 2W_0)\,\alpha}{3a_0^{\,4}\pi \sqrt[4]{\beta}} \begin{cases} \left[\left(\cos^2 \varphi_0 - \frac{1}{2} \sin^2 \varphi_0\right) \ln \frac{1 + \cos \varphi_0}{1 - \cos \varphi_0} \right. \\ \left. \quad + 4 \cos \varphi_0 \,(-1 + a_0 |\sin \varphi_0|)\right] & , \text{if } \varphi_0 \neq 0 \\ \left[2 \ln(2a_0)\right] , \quad \text{if } \varphi_0 = 0. \end{cases}$$

The dimension of σ_ϵ and $\sigma_{\epsilon z}/v$ is in radians, the other quantities are dimensionless.

With a simple interpolation formula it is possible to combine the limiting cases in Eq. 64 to general valid formulae that can more easily be used than the numerical integration procedure described earlier in this chapter. The interpolation formula appropriate for Eq. 64 is

$$f(x) = \frac{1}{\left(\frac{1}{f_1^m(x)} + \frac{1}{f_2^m(x)} \right)^{1/m}} \quad . \qquad \text{[Eq. 65]}$$

The functions $f_1(x)$ and $f_2(x)$ are the approximations for $a_0 << 1$ and $a_0 >> 1$ in Eq. 64, respectively, with one modification: the approximation for σ_ϵ should read

$$\sigma_\epsilon = \sqrt{\frac{\alpha}{8} \left[(3.85 + |\ln a_0|) \cos^2 \varphi_0 + (1.31 + |\ln a_0|) \sin^2 \varphi_0 \right]} \qquad \text{[Eq. 66]}$$

to provide a defined function for all values $\frac{L}{v^2}$. The exponent m in Eq. 65 can be chosen arbitrarily; $m = 2$ has shown to approximate the equations with sufficient accuracy.

The relations in Eq. 64 contain the facet length L as the independent variable. For practical applications this length L has to be chosen. The calculation of L is discussed in the next chapter.

3.3 Calculation of the facet length

The facet length L is calculated following the general procedure of Sect. 2.3. The starting equation is Eq. 38, which is evaluated for the Pierson-Moskowitz spectrum [Eq. 55]. First, the variance $\sigma_h^2 = E_t\{\rho^2\}$ is calculated, employing Eq. 42

$$\sigma_h^2 = \frac{2\alpha v^4}{\beta x_n g^2} \int_0^\pi \cos^n(\varphi - \varphi_0) \qquad \text{[Eq. 67]}$$

$$\left(\frac{1}{4} - \frac{1}{u_0^2} - \frac{2}{u_0^4} + \frac{2\cos u_0}{u_0^4} + \frac{2 \sin u_0}{u_0^3} \right) d\varphi \quad ,$$

where u_0 is defined in Eq. 61. The derivation of Eq. 67 can be found in App. C. From Eq. 67 it is seen that

$$\frac{\sigma_h}{v^2} = f_8\left(\frac{L}{v^2}\right) \quad ; \qquad \text{[Eq. 68]}$$

therefore the results in Figs. 13 and 14 are given in this form.

As for the facet statistics, the limiting forms for $a_0 \ll 1$ and $a_0 \gg 1$ are calculated in App. C. It is, for $n = 2$:

for $a_0 \ll 1$

$$\frac{\sigma_h}{v^2} = \sqrt{\frac{\alpha}{288}(3\cos^2\varphi_0 + \sin^2\varphi_0)}\ \frac{L}{v^2} \qquad \text{[Eq. 69]}$$

for $a_0 \gg 1$

$$\frac{\sigma_h}{v^2} = \sqrt{\frac{\alpha}{\beta}}\ \frac{1}{2g} \quad .$$

For these limiting forms, Eq. 38 is solved in closed form, giving

for $a_0 \ll 1$

$$\frac{L}{\lambda_0} = \frac{1}{\sqrt[4]{\frac{\alpha}{288}(3\cos^2\varphi_0 + \sin^2\varphi_0)}} \qquad \text{[Eq. 70]}$$

and for $a_0 \gg 1$

$$\frac{L}{\lambda_0} = \frac{2g\sqrt{\beta}}{\sqrt{\alpha}\left(\frac{v}{\sqrt{\lambda_0}}\right)^2} .$$

The two parts of Eq. 70 are interpolated to a general formula with the result

$$\frac{L}{\lambda_0} = \sqrt{\frac{1}{\sqrt{\frac{\alpha}{288}}(3\cos^2\varphi_0 + \sin^2\varphi_0)} + \frac{4g^2\beta}{\alpha\left(\frac{v}{\sqrt{\lambda_0}}\right)^4}} . \qquad \text{[Eq. 71]}$$

This is an important result, as it relates the surface parameters of wind speed v and wind direction φ_0 and the acoustic wave length λ_0 to the facet length L. Equation 71 is plotted in Fig. 15, together with the exact result obtained by the solution of Eq. 38 with an iterative procedure on the digital computer. The figure shows that the maximum error does not exceed 20%; thus

the approximation should be sufficient in most cases. It is further seen that the quality number $N = \frac{L}{\lambda_0}$ [Eq. 30] is always greater than 10, therefore the errors induced by the facets are negligible and the problem of choosing the facet length does not need further investigation.

The same procedure was performed for the exponent $n = 4$ of the directivity law, the result is shown in Fig. 16. Figures 15 and 16 are similar, the only difference is a larger variation of L with the direction angle φ_0 .

3.4 Resulting doppler spectra

The computer results for doppler spectra will now be discussed, the facet statistics being calculated as described in the preceding section. The doppler-density spectra use Eqs. 47 and 48; the sea surface spectrum $F_z(f, \varphi)$ employed here is the spectrum due to Scott [Eq. A.60] and the mixing function $W(f, \varphi)$ is found in Eq. A.64. This choice of the sea-surface spectra seems to be the best possibility at present. It should be understood, however, that the general result for the doppler density of backscattered sound can be evaluated for any sea-surface spectrum written in a form used here.

In Fig. 17 the influence of the grazing angle γ_0 on the doppler density is demonstrated. The x-axis shows the doppler shift $f - f_0$ in hertz, the y-axis shows the doppler density $\varphi(f)$ in 1/Hz. The angle γ_0 is changed from 2° to 20°, the wind speed is $v = 8$ m/s, the incident acoustic frequency is 3.5 kHz, and the main direction of the surface waves points away from the sound source. This causes an asymmetry in the spectrum, which is explained as follows: The correlation between the facet slope and the facet vertical velocity is negative in this case; this means that a large angle belongs to a negative velocity. This velocity causes negative doppler shift; as the slope is greater for the negative velocity than for the positive velocity the backscattered energy is greater. In this figure the sea-surface spectrum is omnidirectional in the frequency range where resonant scattering occurs: about 2.7 Hz or 20 cm wavelength. The lack of symmetry is due only to the facet movement.

If the orientation of the sea surface specturm is 90° off the incident wave vector, this effect does not occur, as is seen from Fig. 18.

At this point it is instructive to compare these results with those of another, very simple approximation. In this approximation the variances of u_x and u_z are calculated as second-order moments of the sea-surface spectrum. This is the special case of the facet model with facet length $L = 0$. The slope of the sea surface is not considered.

Figure 19 shows the result of the approximation for a limiting frequency $f_g = 1$ Hz. Compared to the previous figure it can be said that for small grazing angles, $\gamma_0 = 2°$ to 6°, the differences are up to 20 dB. Moreover, the asymmetry of the curves, which must be expected from physical reasons, is not incorporated in the model. The small asymmetries in the frequency region from 0 to 2 Hz are due

because the Bragg frequency is shifted to the omnidirectional part of the sea-surface spectrum. The limiting frequency is $f_g = 5$ Hz in this case; this means that for $f_0 = 33$ kHz the Bragg frequency is $f_0^* = 8.25$ Hz and accordingly the spectral density $\varphi(f)$ is almost symmetrical. In this figure the modified Scott sea-surface spectrum is used. If, instead, the unmodified spectrum is used up to $f_g = 5$ Hz and above a omnidirectional spectrum, the result of Fig. 28 is obtained. The asymmetry of the lower acoustic frequencies is considerably higher than in the previous figure. For $f_0 = 33$ kHz the curves are almost identical. This shows that the choice of the limiting frequency and the modification of the Scott spectrum is important. A comparison with measurements will be necessary to find out the optimum values for this parameter.

The last three figures show the results for the doppler density at higher wind speeds. The limiting frequency was chosen as $f_g = 2.5$ Hz. In Fig. 29 all parameters are the same as in Fig. 28, except that the wind speed is doubled. In Fig. 30 the direction angle is changed to $\varphi_0 = 90^\circ$, thus giving symmetric curves in this crosswind case. Figure 31 shows an example for an extreme wind speed $v = 32$ m/s, where even the low acoustic frequency $f_0 = 100$ Hz produces a doppler spectrum with a double gaussian shape instead of δ-function peaks.

CONCLUSION

A theoretical model for the doppler spread of the backscattered acoustic waves from the rough sea surface is developed that makes use of a two-component structure (facet model) of the sea surface.

The model requires a description of the statistical properties of the sea-surface roughness including the directivity and the mixing of incoming and outgoing waves in one direction as a function of frequency. The concept of the mixing function is necessary to obtain asymmetrical doppler spectra as a function of the wind direction. The parameters of this function need experimental verification; in particular, the optimal value for the limiting frequency is not yet known.

The general result of this paper is a set of formulae for both the facet statistics and the doppler spectrum in terms of the sea-surface covariance function or the sea-surface spectrum. The results can be used in two ways:

1. Measured sea-surface data are used to fit the parameters of analytical spectra such as the Pierson-Moskowitz spectrum or the Scott spectrum.

2. Measured spectra are inserted into the general formulae.

The procedure, developed for the choice of the facet length L shows that the quality number $N = L/\lambda_0$, where λ_0 is the acoustic wavelength, is never smaller than 10, thus the aperture error due to finite facet length can be neglected.

only to the different results of the small-scale roughness backscattering. They depend linearily on the sea-surface spectrum and have nothing to do with the facet movements and the correlation between slope and vertical velocity. This effect can be quite important if the sea-surface spectrum is assumed to be directional up to high frequencies.

Figure 20 shows the same case as before but for $f_g = 5$ Hz, where the asymmetrical effect is clearly seen. If the facet slope is considered for the simple approximation, a considerable change occurs in the results. The standard deviation σ_ε of the facet slope tends to infinity when L approaches zero. To avoid numerical instability a facet length of $L = 0.0001$ m was taken. In Fig. 21 the result is shown. As is to be expected, the influence of the grazing angle γ_0 is smaller and the total backscattered power is much higher.

These considerable differences show the need for the facet model in the doppler-spread calculation.

The result of the facet theory lies between the extremes of the two previous figures and is shown in Fig. 22. Here the asymmetry of the curves depends on both the correlation of the facet slope and velocity and the asymmetric results of the resonant backscattering.

The curves depend quite strongly on the limiting frequency f_g, which is specially apparent if f_g tends to infinity, leading to a spectrum that has a directivity up to the highest frequencies. This case is shown in Fig. 23 for the same parameters as in the previous figures. In fact, the figure contains only one branch of the usual two, as only one δ-function occurs in the Bragg-scattering case. This is of course a somewhat academic example.

Figure 24 shows the variation of the doppler density with the orientation angle φ_0 for a grazing angle $\gamma_0 = 6°$, a wind speed $v = 8$ m/s, and an incident frequency $f_0 = 3.5$ kHz. The angle φ_0 is varied from 0° to 180° in steps of 20°. Of course, for $\varphi_0 = 0°$ and $\varphi_0 = 180°$ the antisymmetric result occurs. The influence of φ_0 reaches from about 5 dB variation at low doppler frequencies to 10 dB at about 10 Hz doppler shift. Again, the sea-surface spectrum is considered omnidirectional at the Bragg frequency of about 2.7 Hz.

Figures 25 and 26 show the influence of the wind speed for a fully developed sea. The grazing angle γ_0 is 6°, the orientation angle φ_0 is 0°, and the acoustic frequency f_0 is 3.5 kHz. In Fig. 25 the wind speed varies from 2 m/s to 32 m/s in geometrical progression, in Fig. 26 from 2 to 20 m/s linearily. Fow low wind speeds the facet model is seen to be superfluous, as the doppler density consists virtually of two δ-functions due to the Bragg resonant scattering. For high wind speeds the backscattered energy is considerable higher, but it is spread over a higher frequency range; the backscattered energy at the Bragg frequency does not change considerably.

The next figures show the dependence of the results on the incident acoustic frequency f_0. Figure 27 shows the doppler density versus the normalized frequency $\frac{\Delta f}{f_0} = \frac{f - f_0}{f_0}$ for $f_0 = 0.33$, ., 3.3, 10 and 33 kHz. For the low frequency $f_0 = 330$ Hz the Rayleigh condition is fullfilled; thus the doppler spectral density consists of two sharp peaks. With increasing frequency the facets become more important and at the same time the asymmetry of the curves disappears,

The general results for the statistics of the facets are evaluated for a Pierson-Moskowitz spectrum. An approximate closed-form solution is obtained.

For the numerical evaluation of the general result for the doppler spectral density, a more general sea-surface spectrum due to Scott is employed, which contains the Pierson-Moskowitz spectrum as a special case.

Examples for different wind speeds, wind directions, grazing angles, and acoustic frequencies are calculated via a computer program.

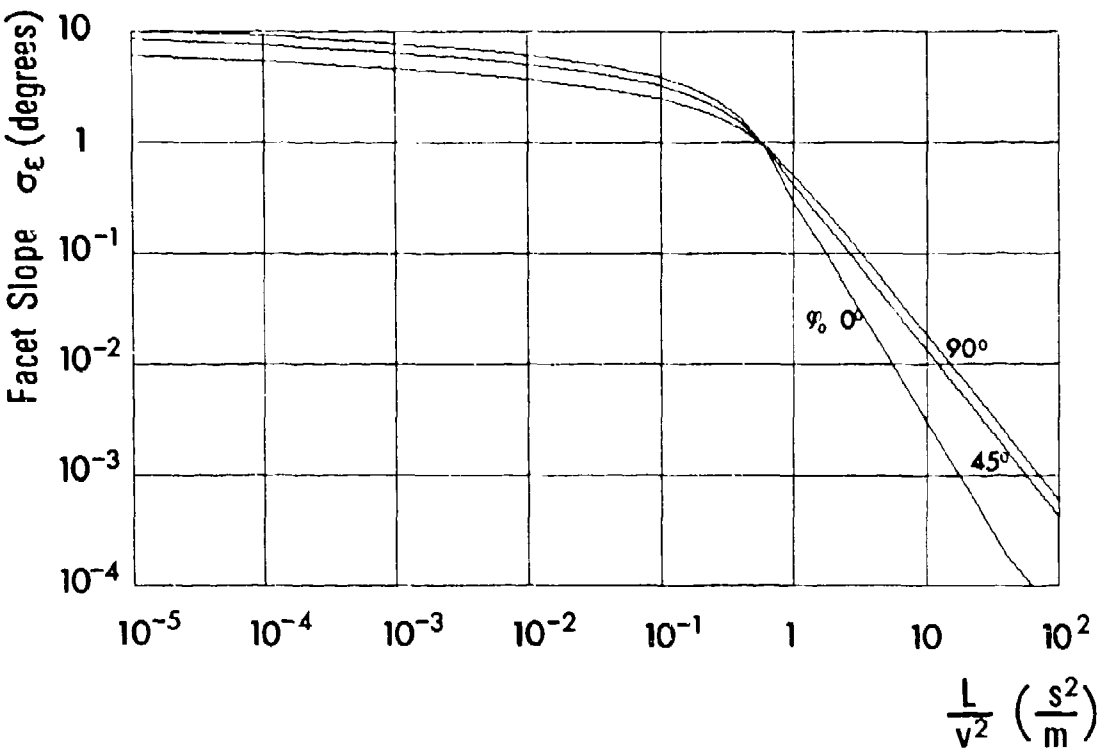

FIG. 3a FACET SLOPE σ_ε vs $\frac{L}{v^2}$
Parameter: Wind direction φ_0 [°]
Facet length: L [m]
Wind speed: v [m/s]
Directivity exponent: n = 2

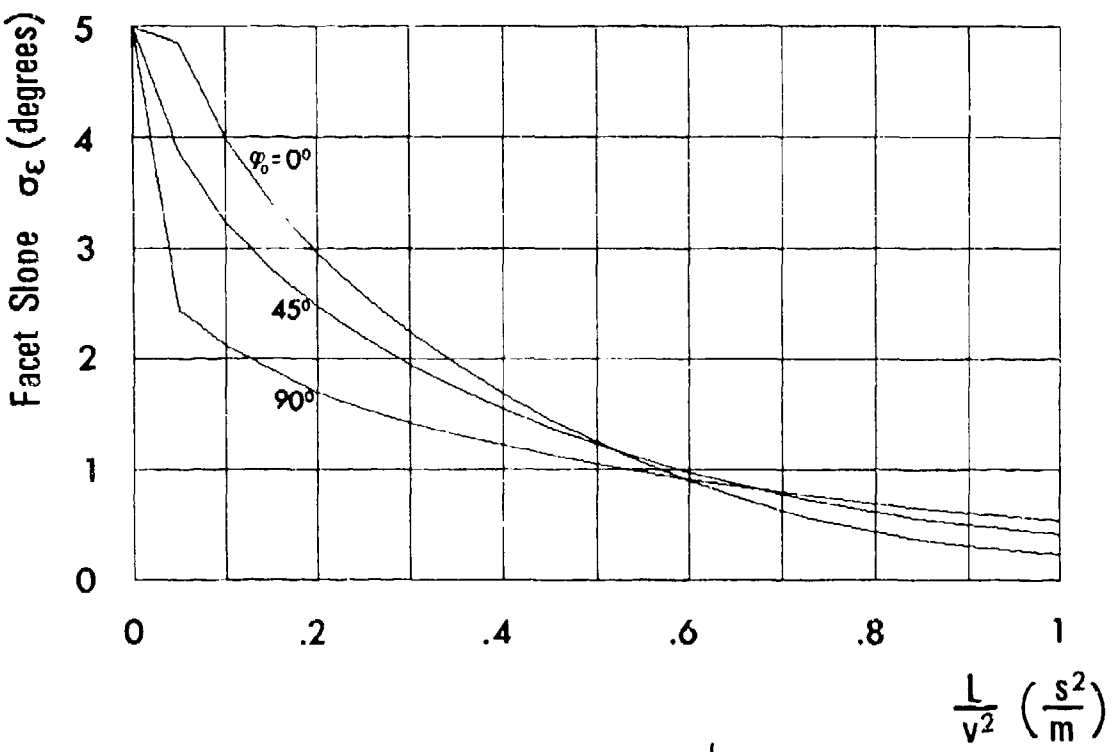

FIG. 3b FACET SLOPE σ_ε vs $\frac{L}{v^2}$
Parameters: see Fig. 3a

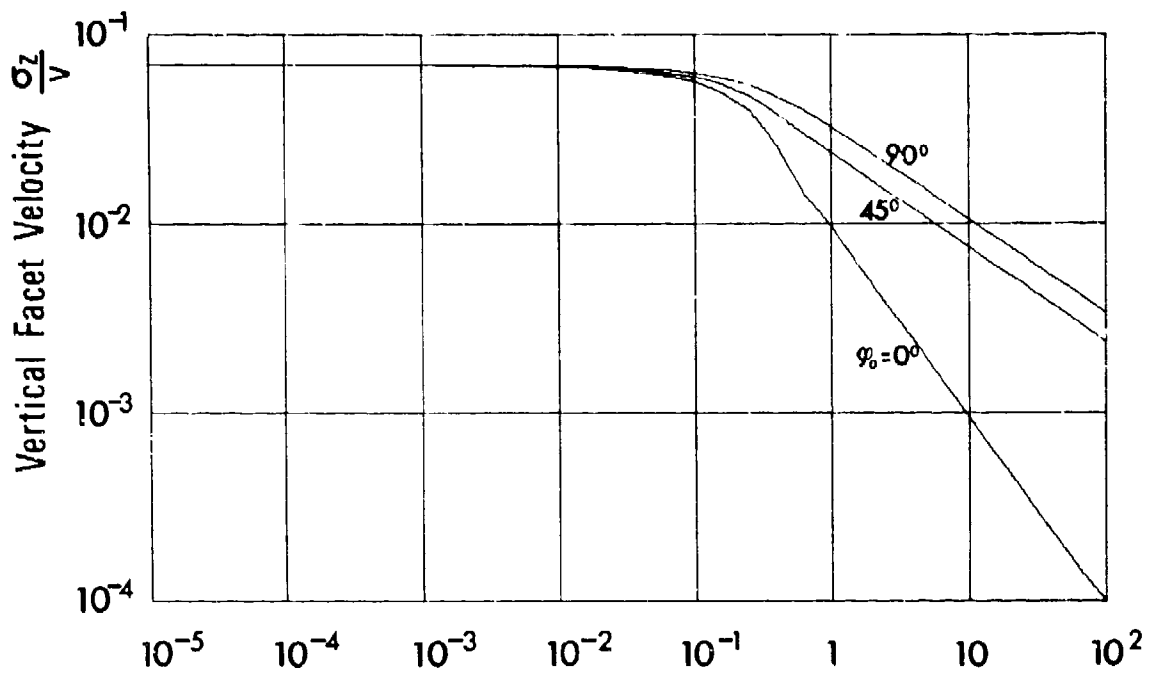

FIG. 4a VERTICAL FACET VELOCITY $\frac{\sigma_z}{v}$ vs $\frac{L}{v^2}$
Parameters: see Fig. 3a

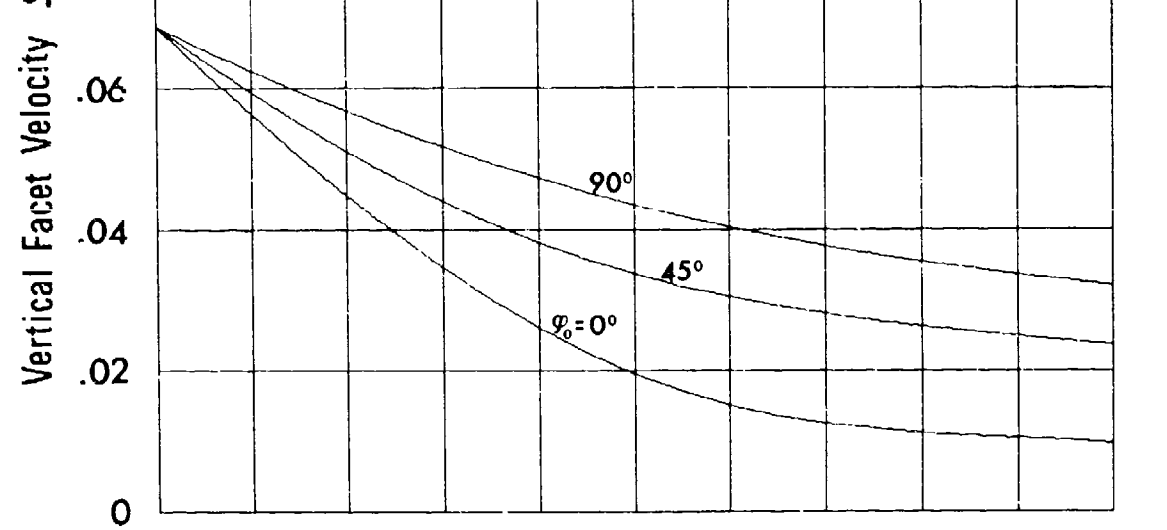

FIG. 4b VERTICAL FACET VELOCITY $\frac{\sigma_z}{v}$ vs $\frac{L}{v^2}$
Parameters: see Fig. 3a

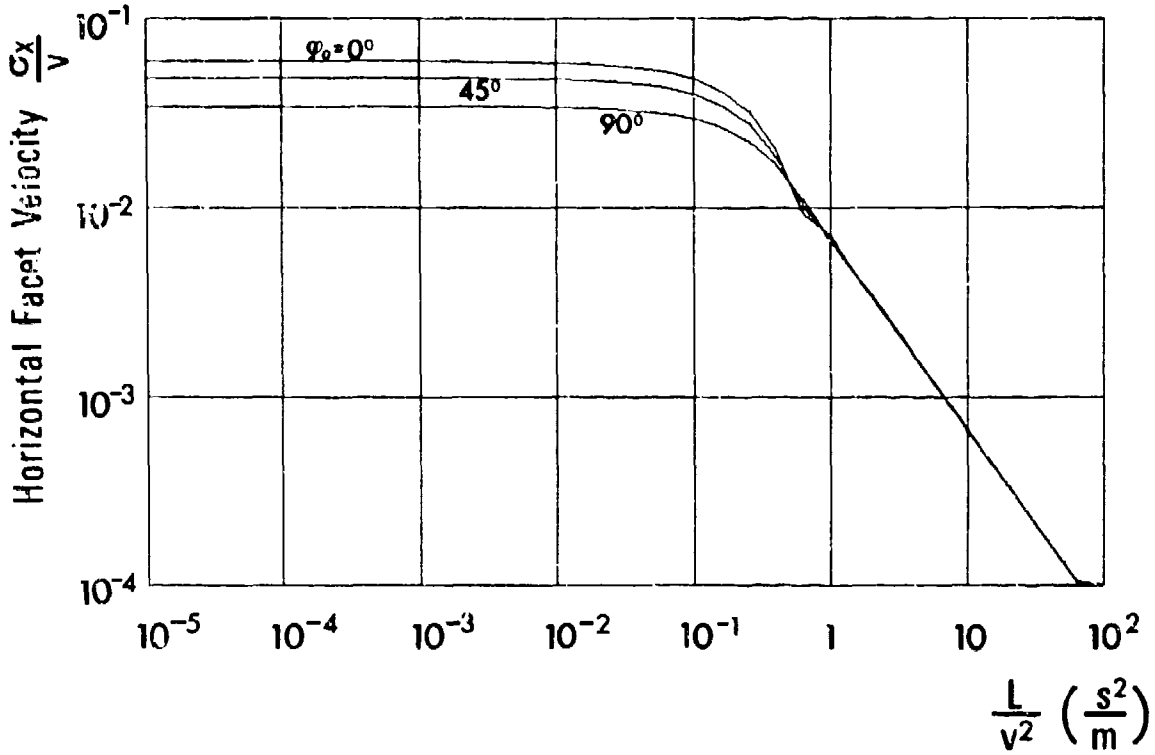

FIG. 5a HORIZONTAL FACET VELOCITY $\frac{\sigma_x}{v}$ vs $\frac{L}{v^2}$
Parameters: see Fig. 3a

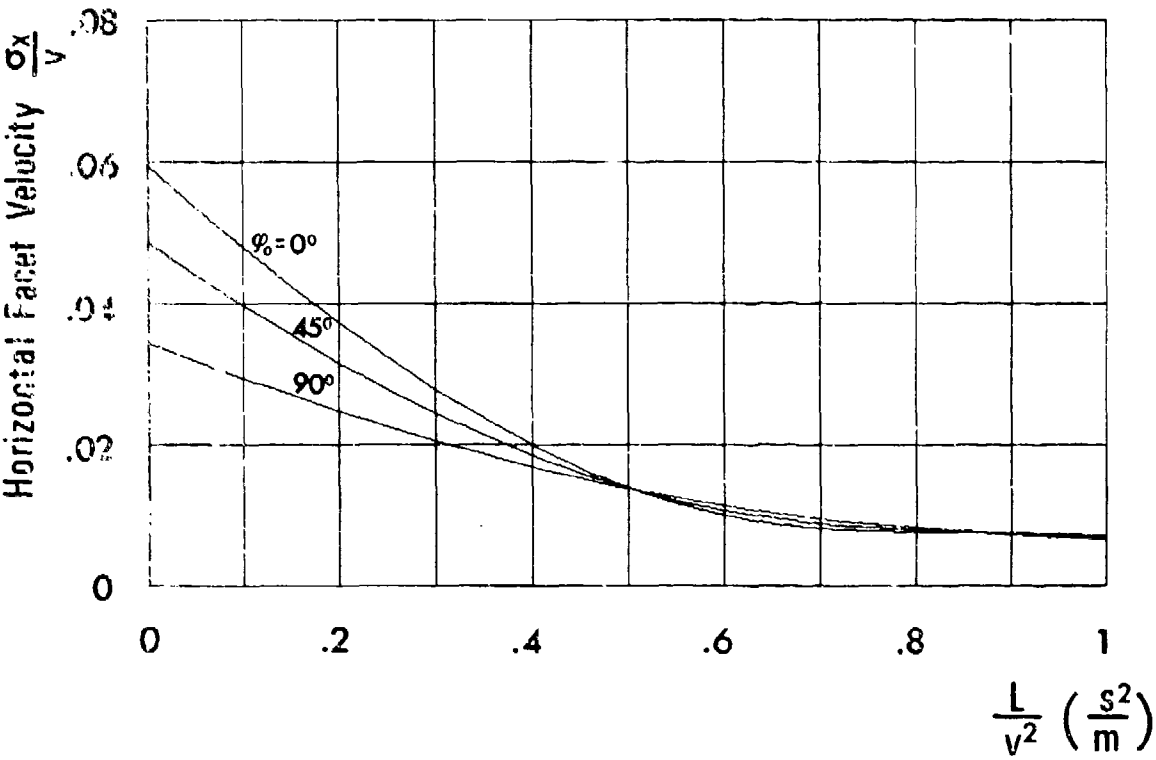

FIG. 5b HORIZONTAL FACET VELOCITY $\frac{\sigma_x}{v}$ vs $\frac{L}{v^2}$
Parameters: see Fig. 3a

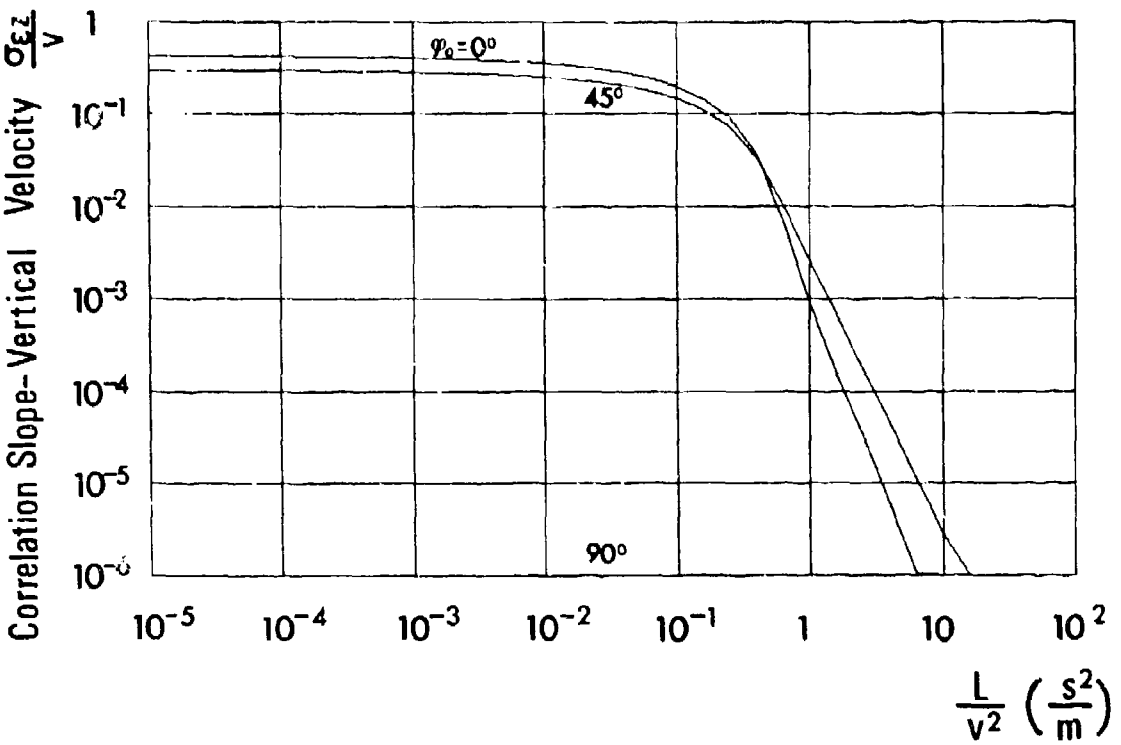

FIG. 6a CORRELATION BETWEEN SLOPE AND VERTICAL VELOCITY $\frac{\sigma_{\epsilon z}}{v}$ vs $\frac{L}{v^2}$
Parameters: see Fig. 3a

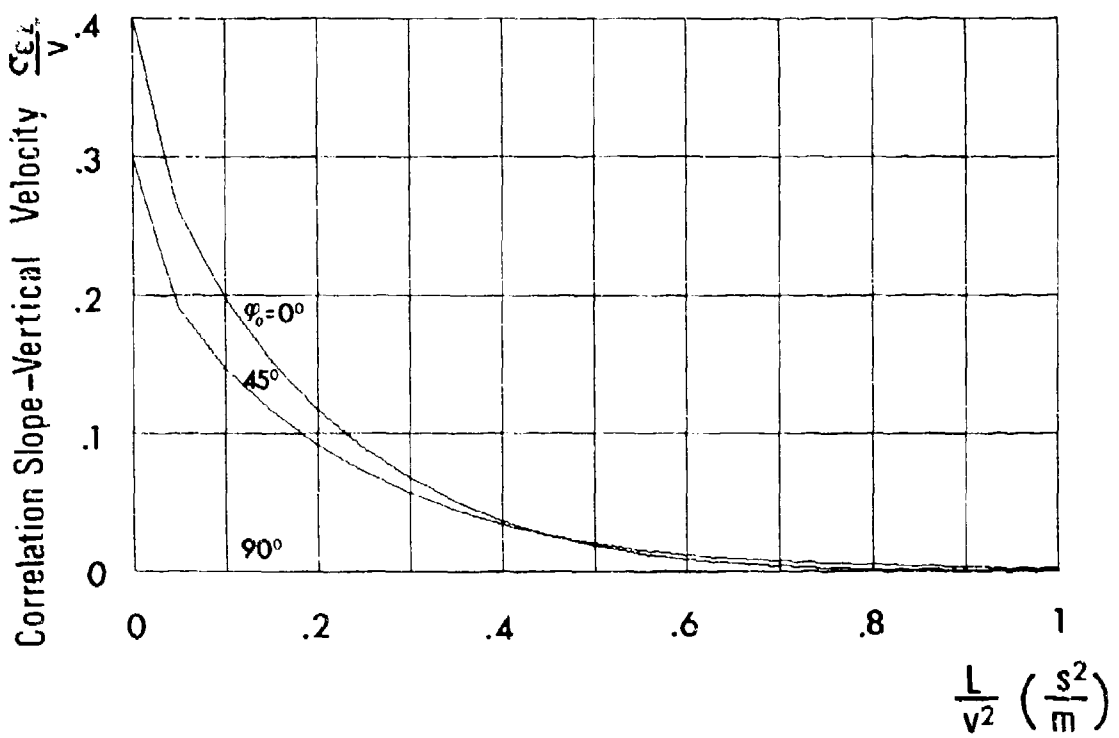

FIG. 6b CORRELATION BETWEEN SLOPE AND VERTICAL VELOCITY $\frac{\sigma_{\epsilon z}}{v}$ vs $\frac{L}{v^2}$
Parameters: see Fig. 3a

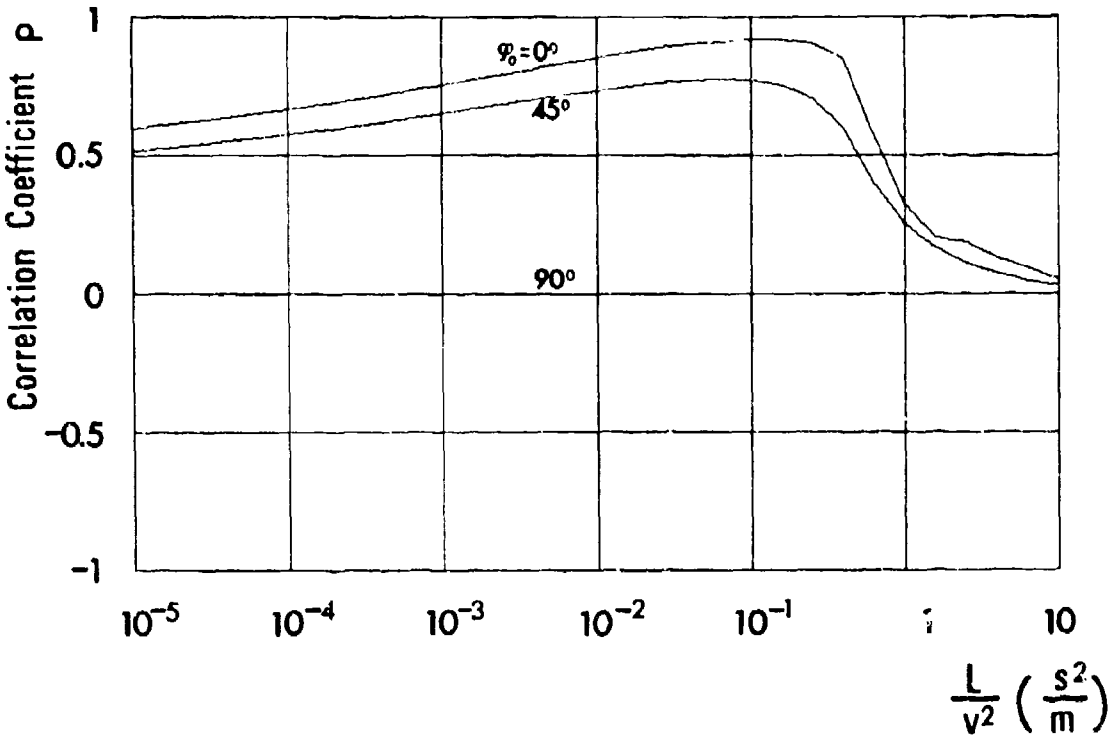

FIG. 7 CORRELATION COEFFICIENT ρ vs $\frac{L}{v^2}$
Parameters: see Fig. 3a

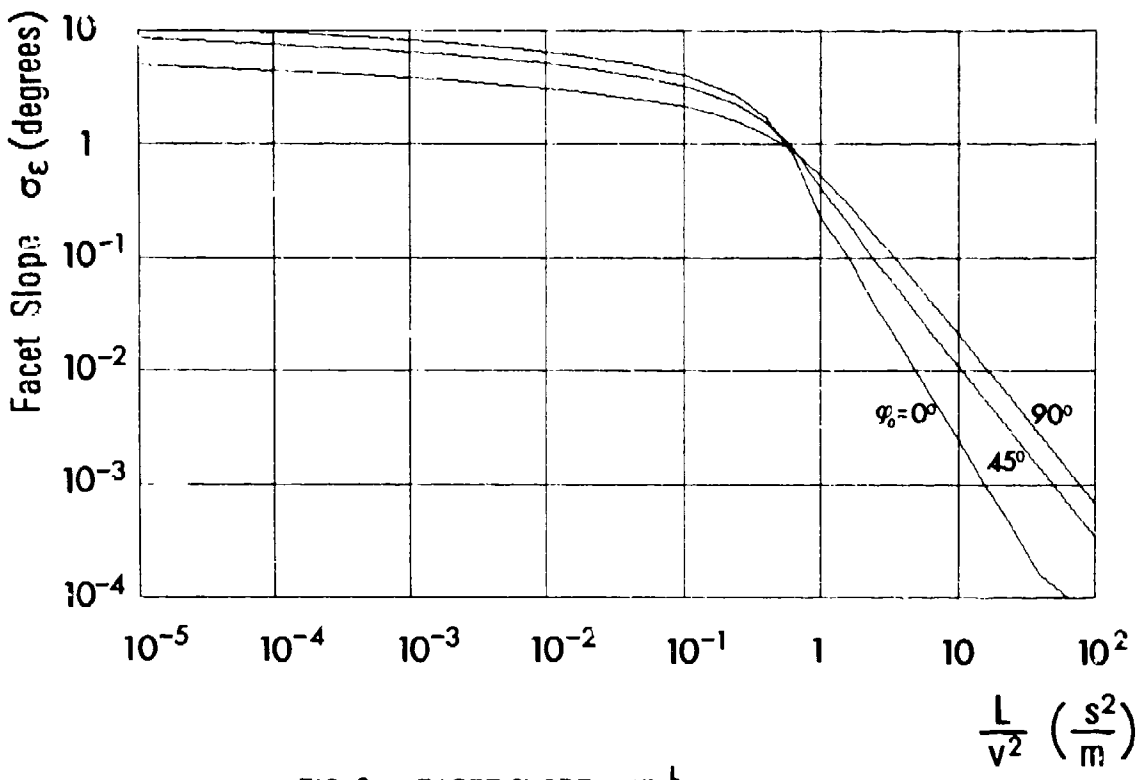

FIG. 8a FACET SLOPE σ_ε vs $\frac{L}{v^2}$
Parameter: Wind direction φ_0 [°]
Facet length: L [m]
Wind speed: v [m/s]
Directivity exponent: n = 4

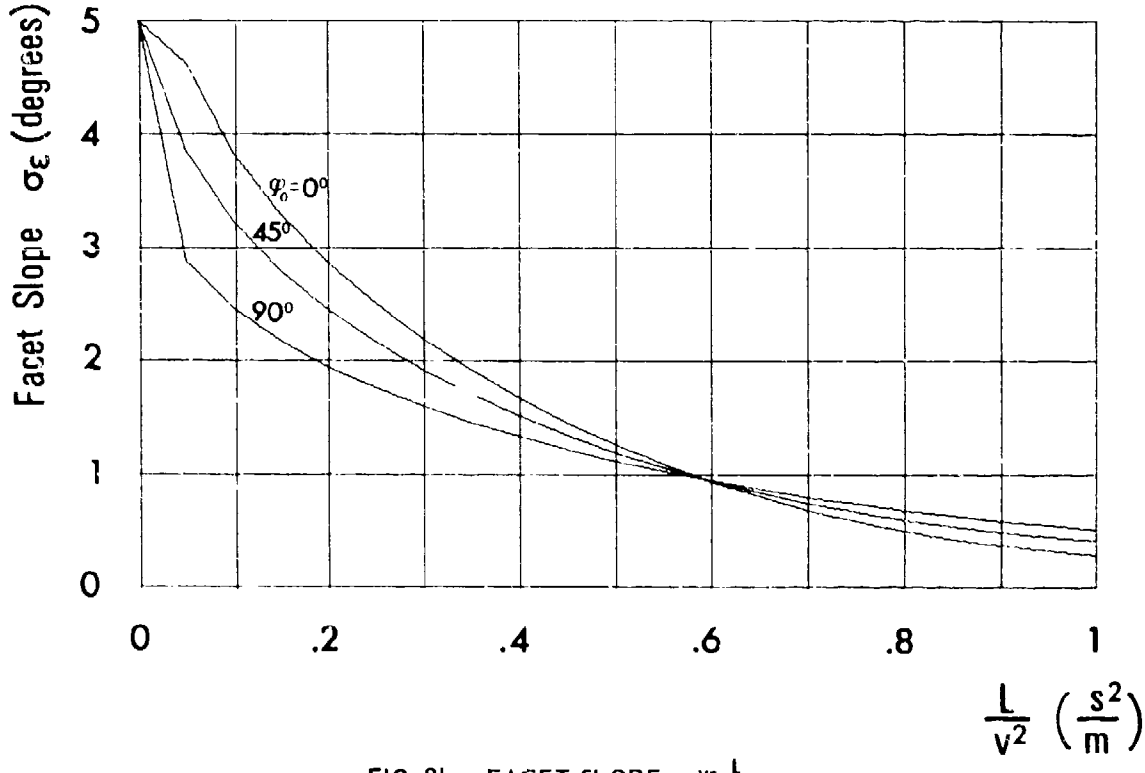

FIG. 8b FACET SLOPE σ_ε vs $\frac{L}{v^2}$
Parameters: see Fig. 8a

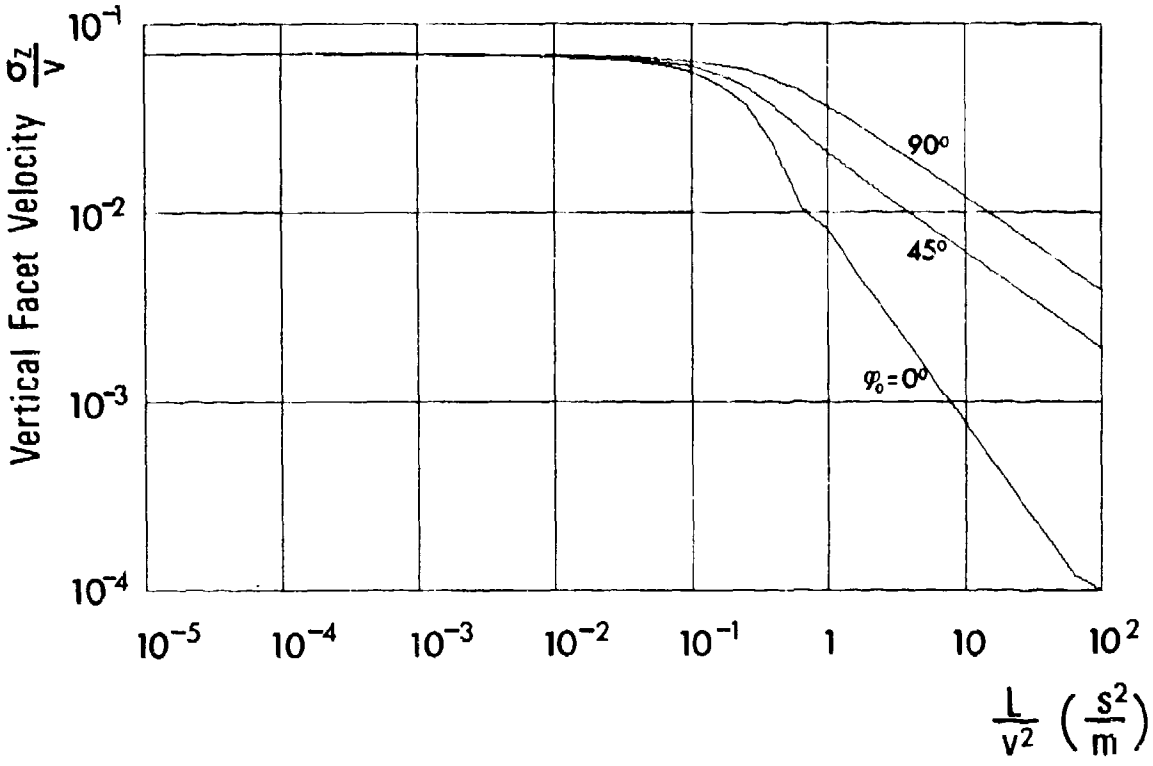

FIG. 9a VERTICAL FACET VELOCITY $\frac{\sigma_z}{v}$ vs $\frac{L}{v^2}$
Parameters: see Fig. 8a

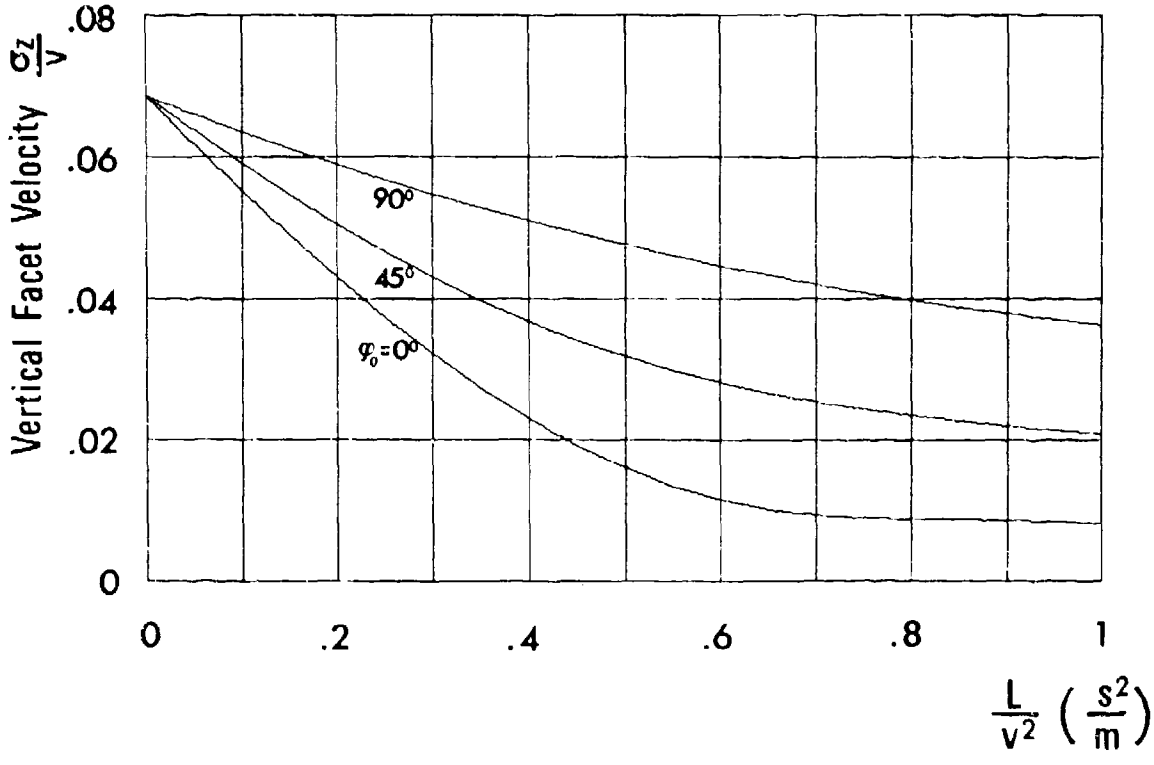

FIG. 9b VERTICAL FACET VELOCITY $\frac{\sigma_z}{v}$ vs $\frac{L}{v^2}$
Parameters: see Fig. 8a

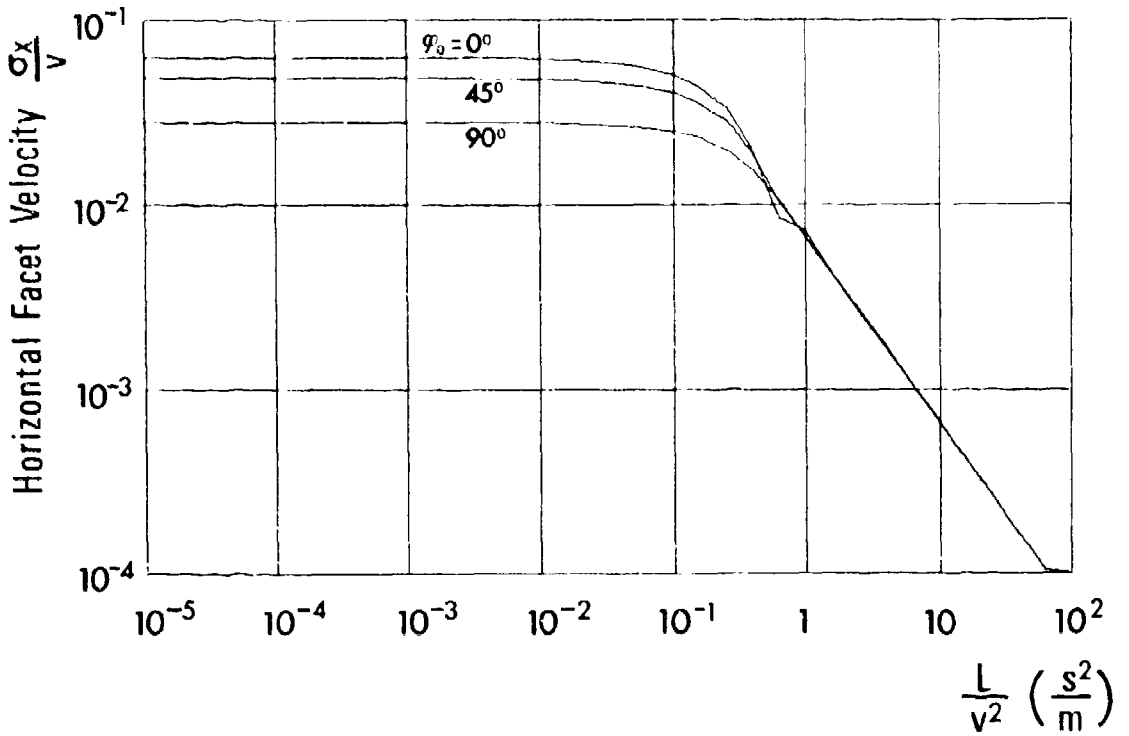

FIG. 10a HORIZONTAL FACET VELOCITY $\frac{\sigma_x}{v}$ vs $\frac{L}{v^2}$
Parameters: see Fig. 8a

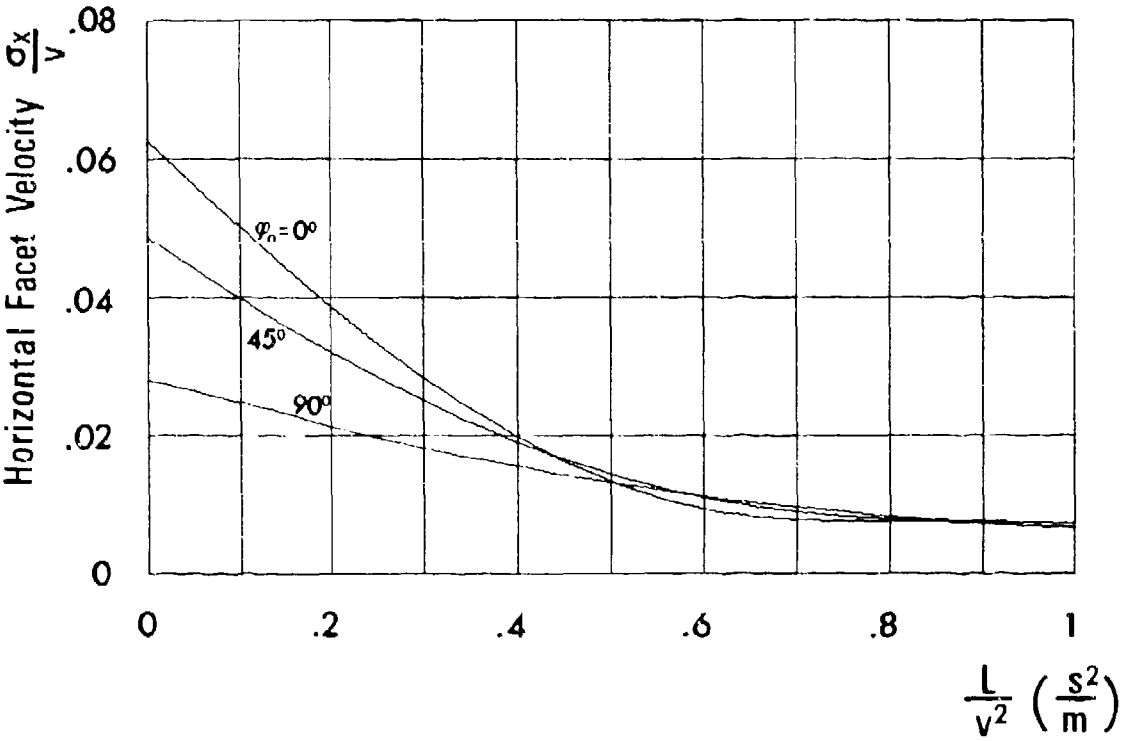

FIG. 10b HORIZONTAL FACET VELOCITY $\frac{\sigma_x}{v}$ vs $\frac{L}{v^2}$
Parameters: see Fig. 8a

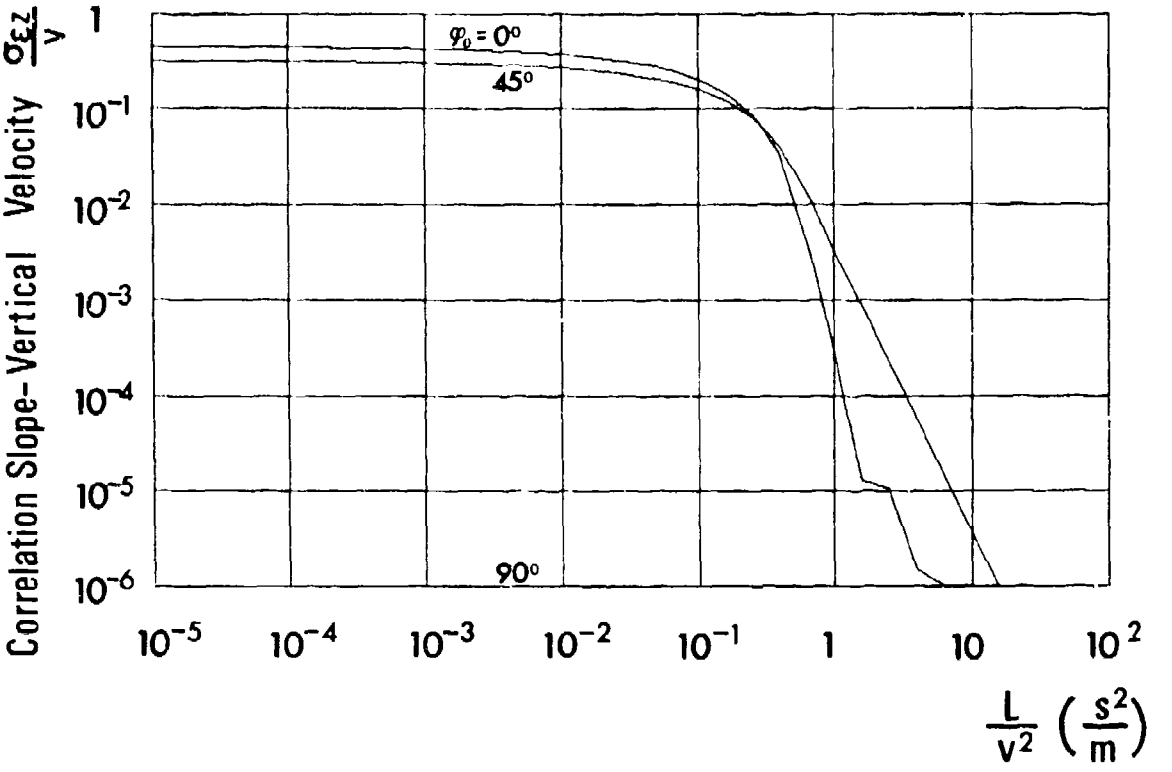

FIG. 11a CORRELATION BETWEEN SLOPE AND VERTICAL VELOCITY $\frac{\sigma_{\epsilon z}}{v}$ vs $\frac{L}{v^2}$
Parameters; see Fig. 8a

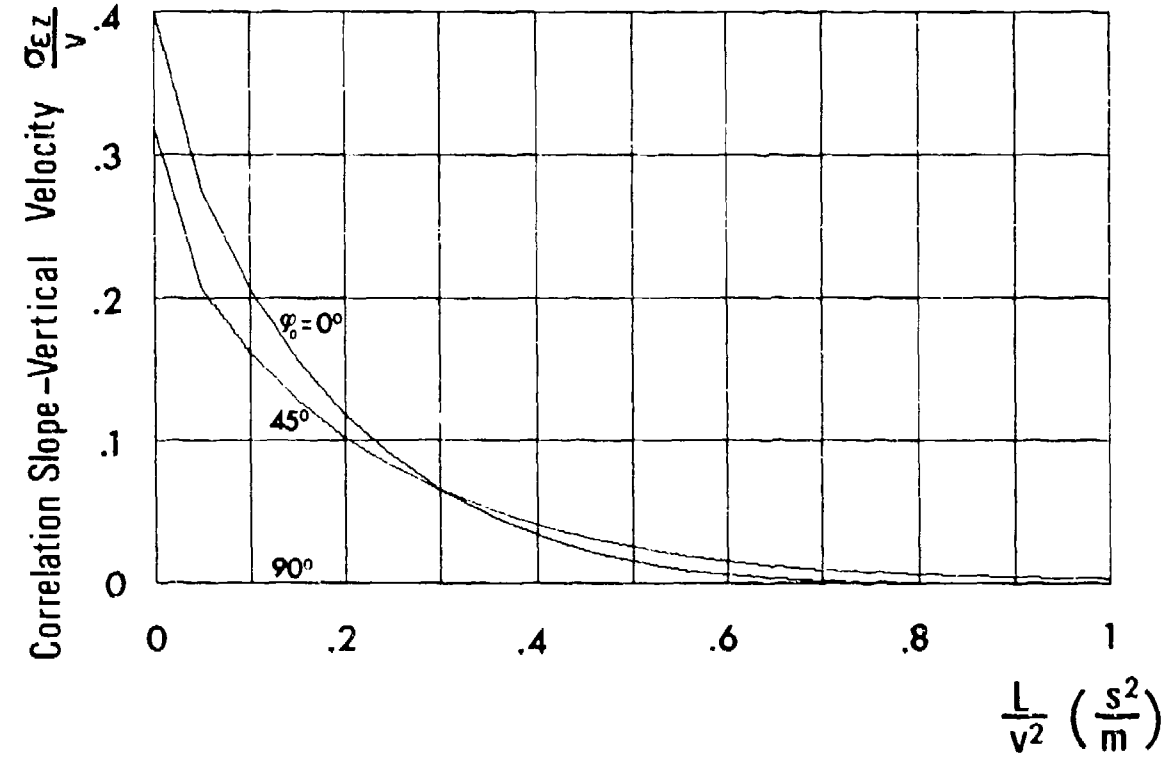

FIG. 11b CORRELATION BETWEEN SLOPE AND VERTICAL VELOCITY $\frac{\sigma_{\epsilon z}}{v}$ vs $\frac{L}{v^2}$
Parameters: see Fig. 8a

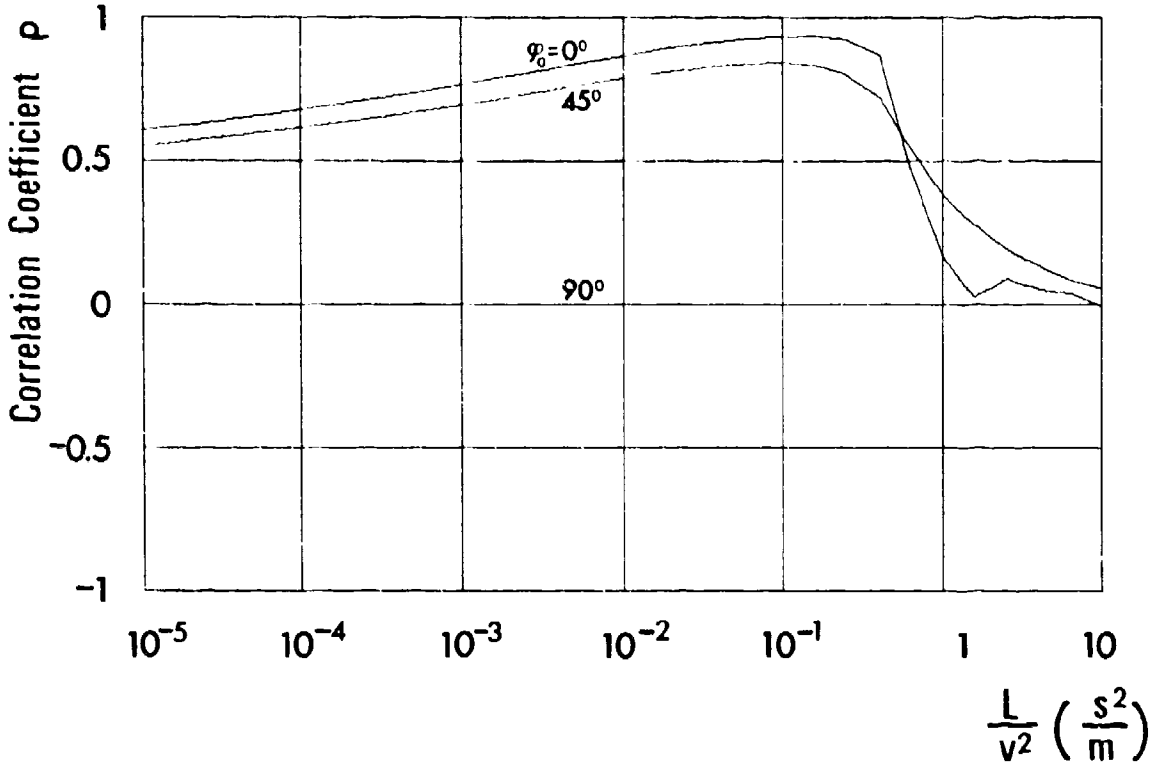

FIG. 12 CORRELATION COEFFICIENT ρ vs $\frac{L}{v^2}$
Parameters: see Fig. 8a

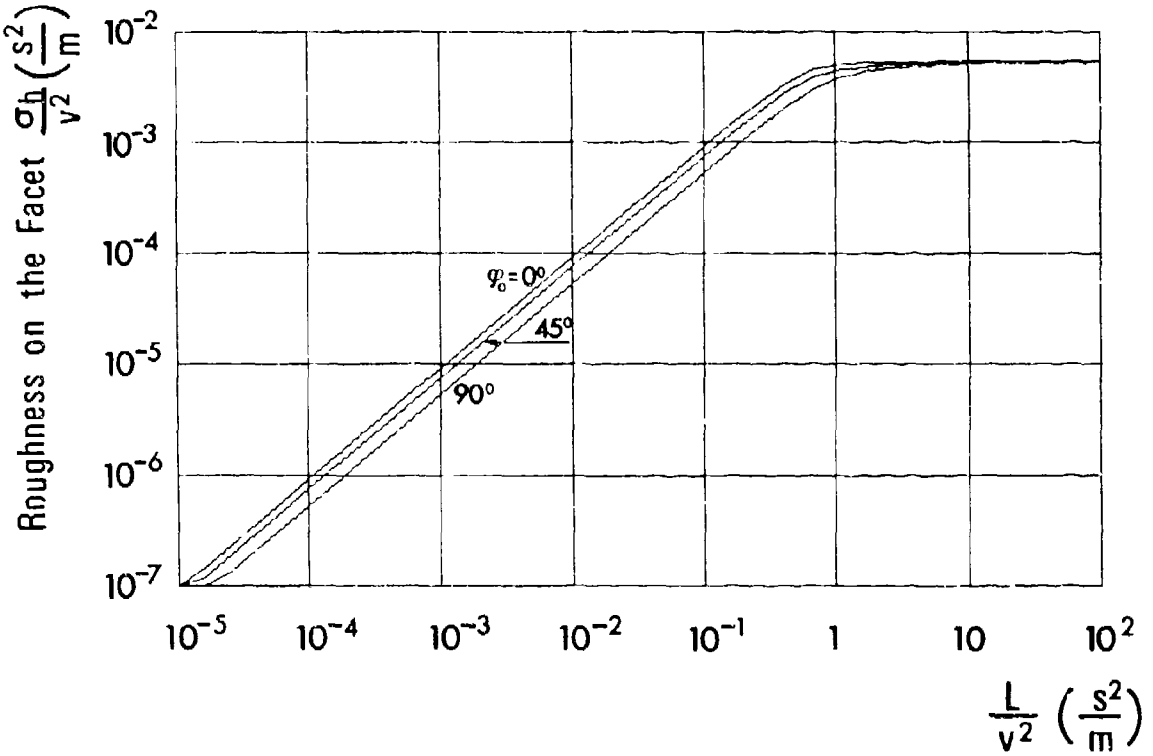

FIG. 13a ROUGHNESS ON THE FACET $\frac{\sigma_h}{v^2}$ vs $\frac{L}{v^2}$
Parameters: see Fig. 3a

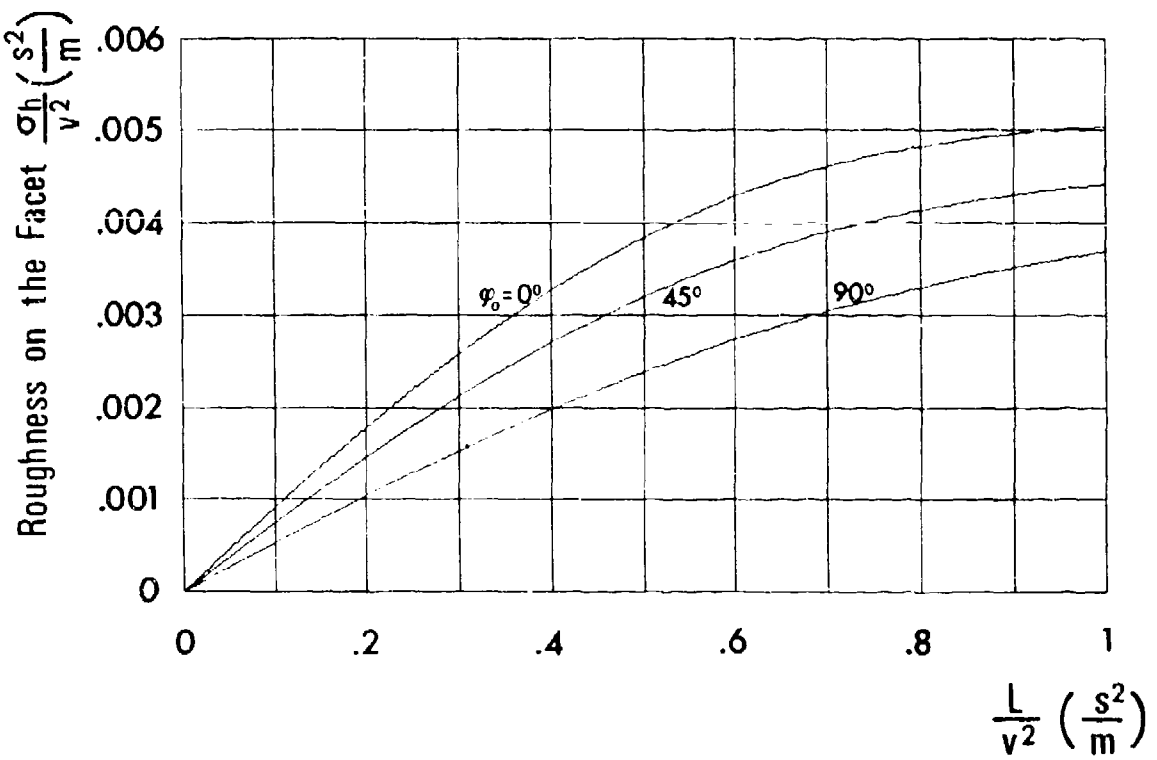

FIG. 13b ROUGHNESS ON THE FACET $\frac{\sigma_h}{v^2}$ vs $\frac{L}{v^2}$
Parameters: see Fig. 3a

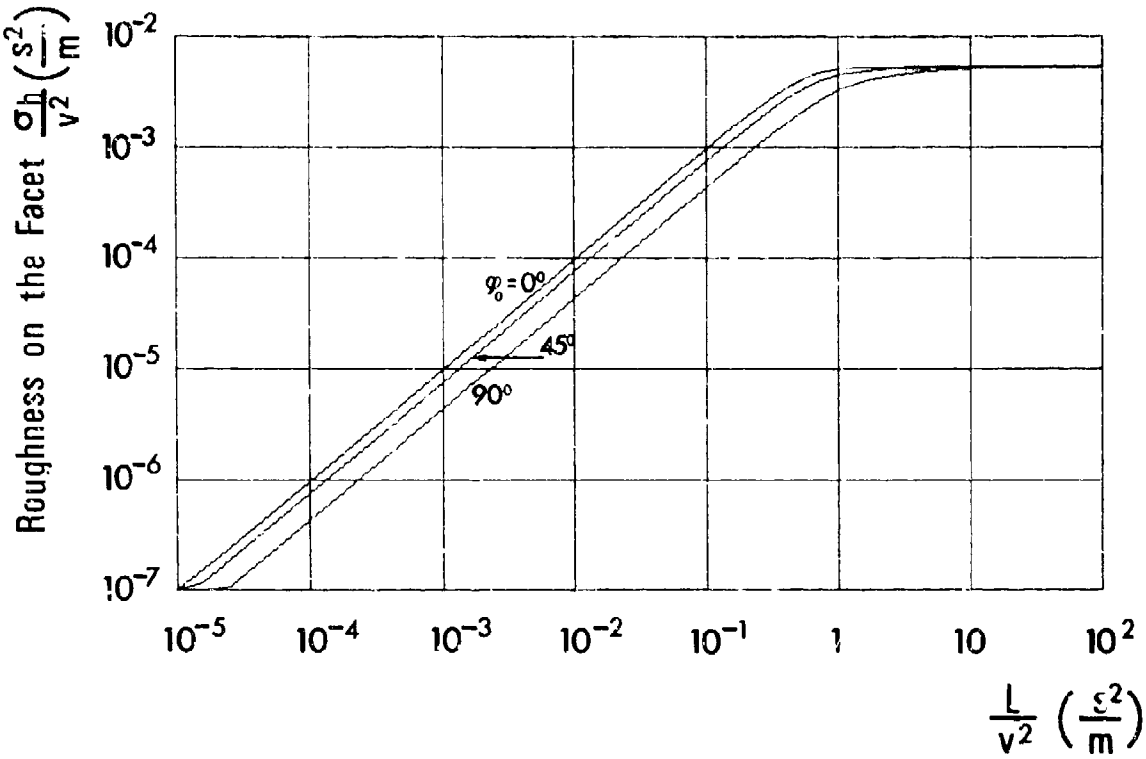

FIG. 14a ROUGHNESS ON THE FACET $\frac{\sigma_h}{v^2}$ vs $\frac{L}{v^2}$
Parameters: see Fig. 8a

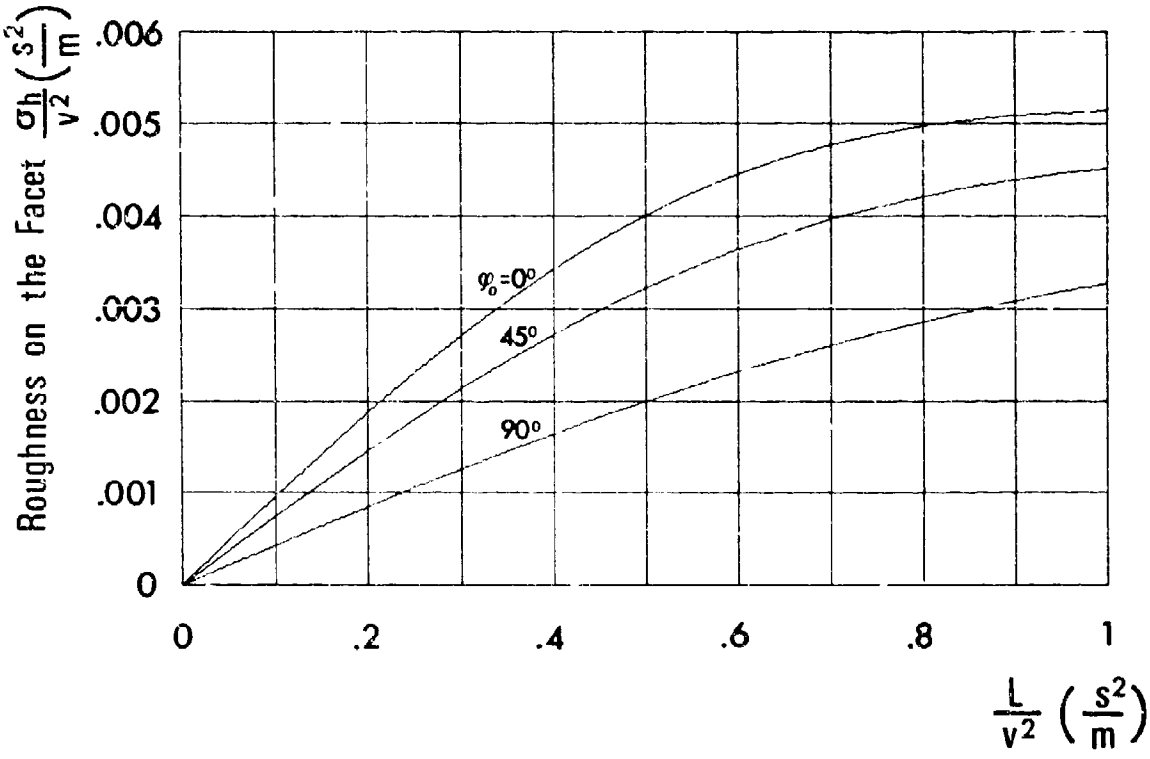

FIG. 14b ROUGHNESS ON THE FACET $\frac{\sigma_h}{v^2}$ vs $\frac{L}{v^2}$
Parameters: see Fig. 8a

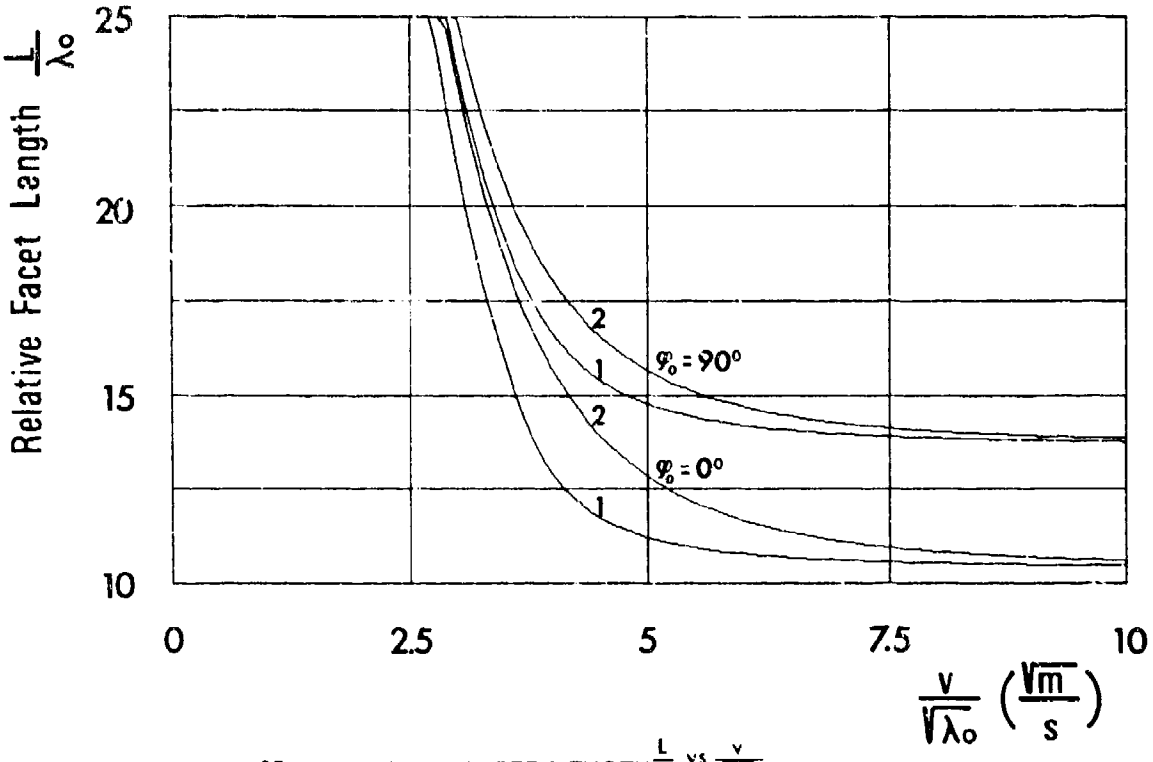

FIG. 15 RELATIVE FACET LENGTH $\frac{L}{\lambda_o}$ vs $\frac{v}{\sqrt{\lambda_o}}$
Parameter: Wind direction φ_o [°]
Facet length: L [m]
Wind speed: v [m/s]
Acoustic wavelength: λ_o [m]
Directivity exponent: n = 2

1: Exact result
2: Approximation

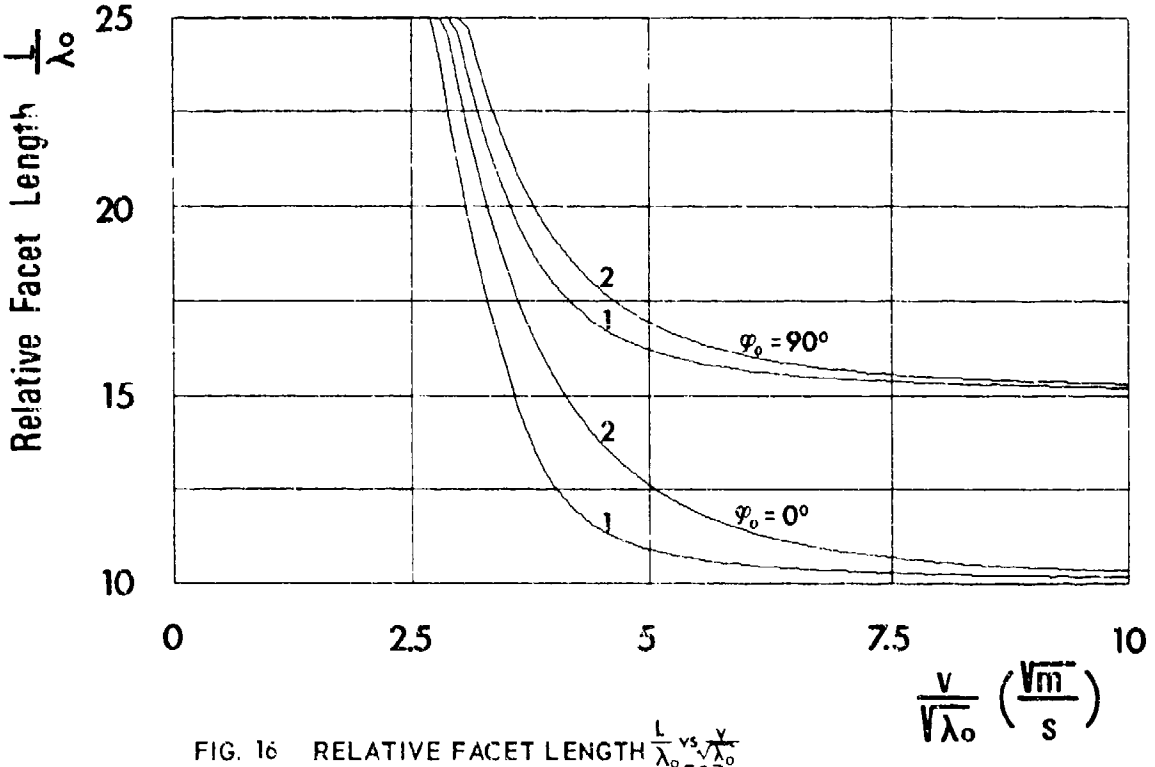

FIG. 16 RELATIVE FACET LENGTH $\frac{L}{\lambda_o}$ vs $\frac{v}{\sqrt{\lambda_o}}$
Parameter: Wind direction φ_o [°]
Facet length: L [m]
Wind speed: v [m/s]
Acoustic wavelength: λ_o [m]
Directivity exponent: n = 4

1: Exact result
2: Approximation

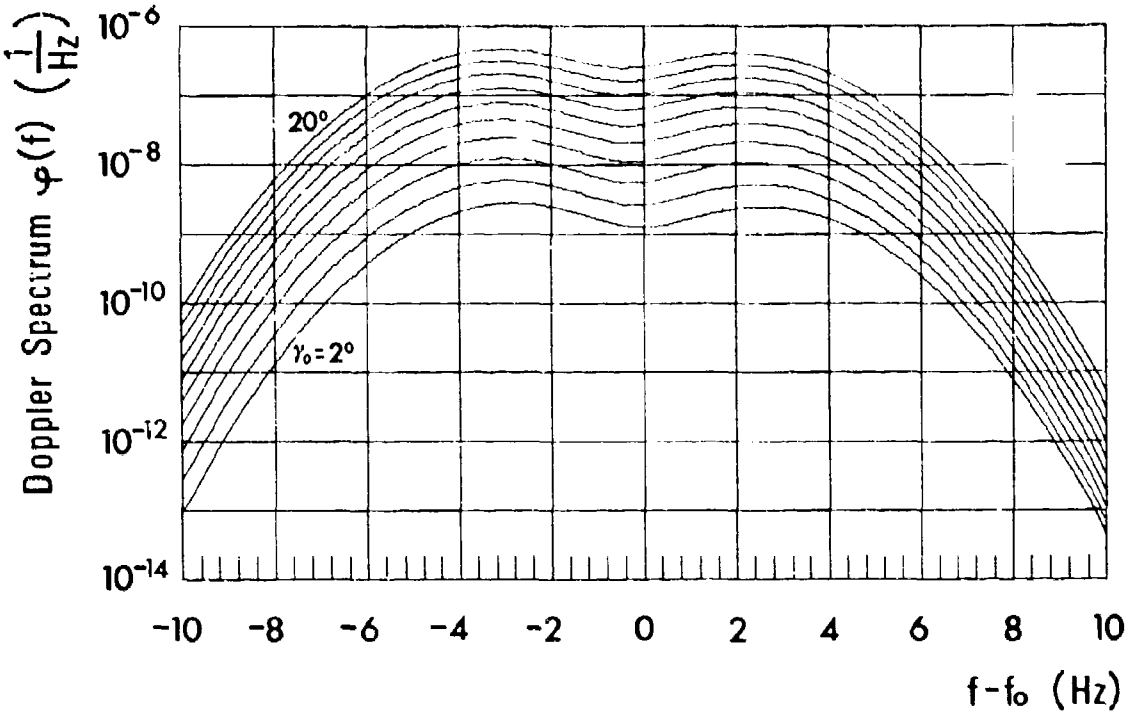

FIG. 17 DOPPLER SPECTRAL DENSITY $\varphi(f)$ vs DOPPLER SHIFT $f - f_o$
Parameter: Grazing angle: $\gamma_c = 2°$ to 20°
Centre frequency: $f_o = 3.5$ kHz
Wind speed: $v = 8$ m/s
Wind direction: $\varphi_o = 0°$ (downwind)
Limiting frequency: $f_g = 1$ Hz

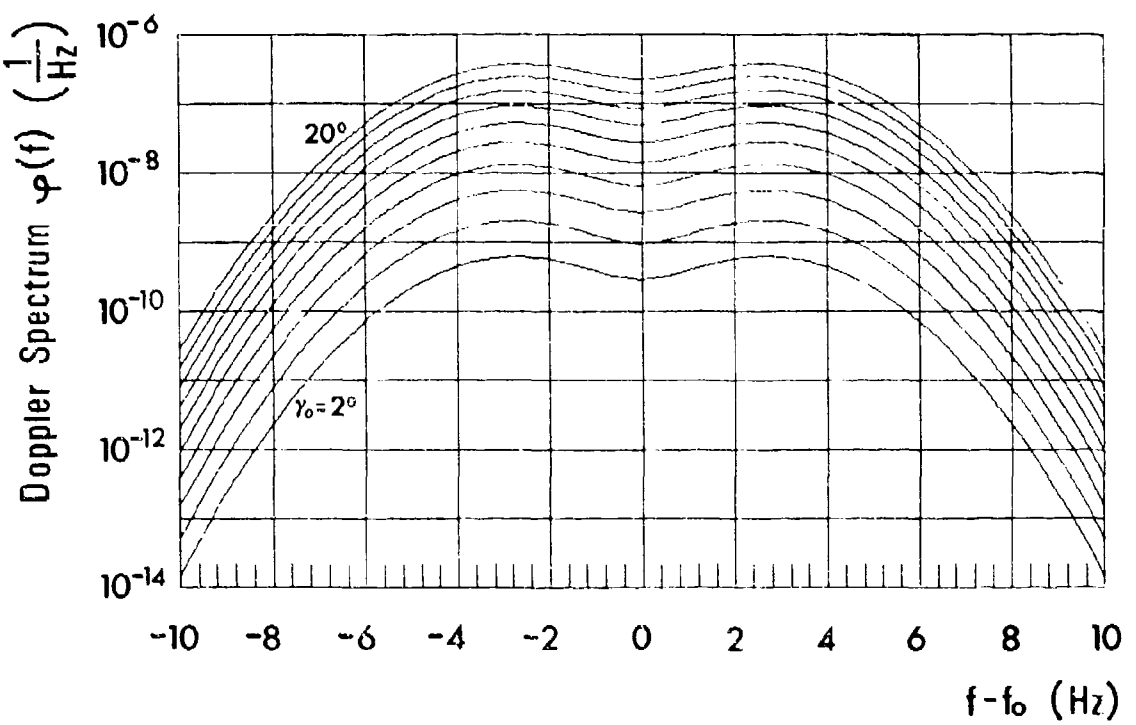

FIG. 18 DOPPLER SPECTRAL DENSITY $\varphi(f)$ vs DOPPLER SHIFT $f - f_o$
Parameters: see Fig. 17
except: Wind direction: $\varphi_o = 90°$ (crosswind)

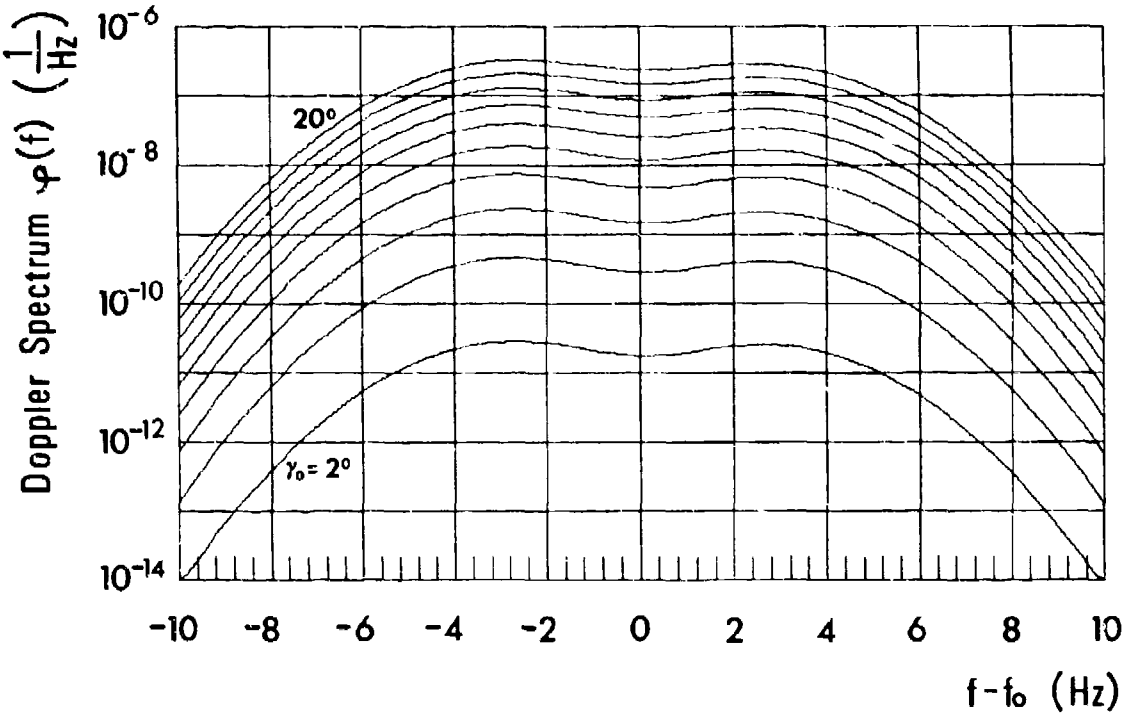

FIG. 19 DOPPLER SPECTRAL DENSITY $\varphi(f)$ vs DOPPLER SHIFT $f - f_o$
Parameters: see Fig. 17
addition: Simplified model: $\sigma_\varepsilon = 0$

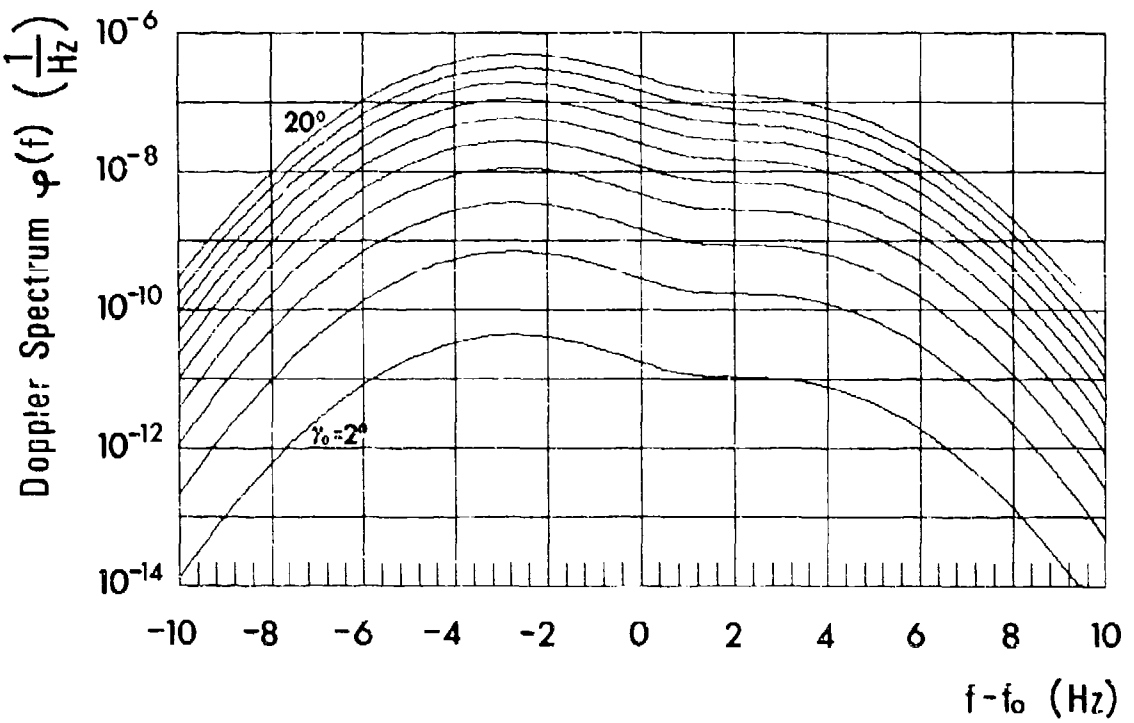

FIG. 20 DOPPLER SPECTRAL DENSITY $\varphi(f)$ vs DOPPLER SHIFT $f - f_c$
Parameters: see Fig. 17
except: Limiting frequency: $f_g = 5$ Hz
addition: Simplified model: $\sigma_\varepsilon = 0$

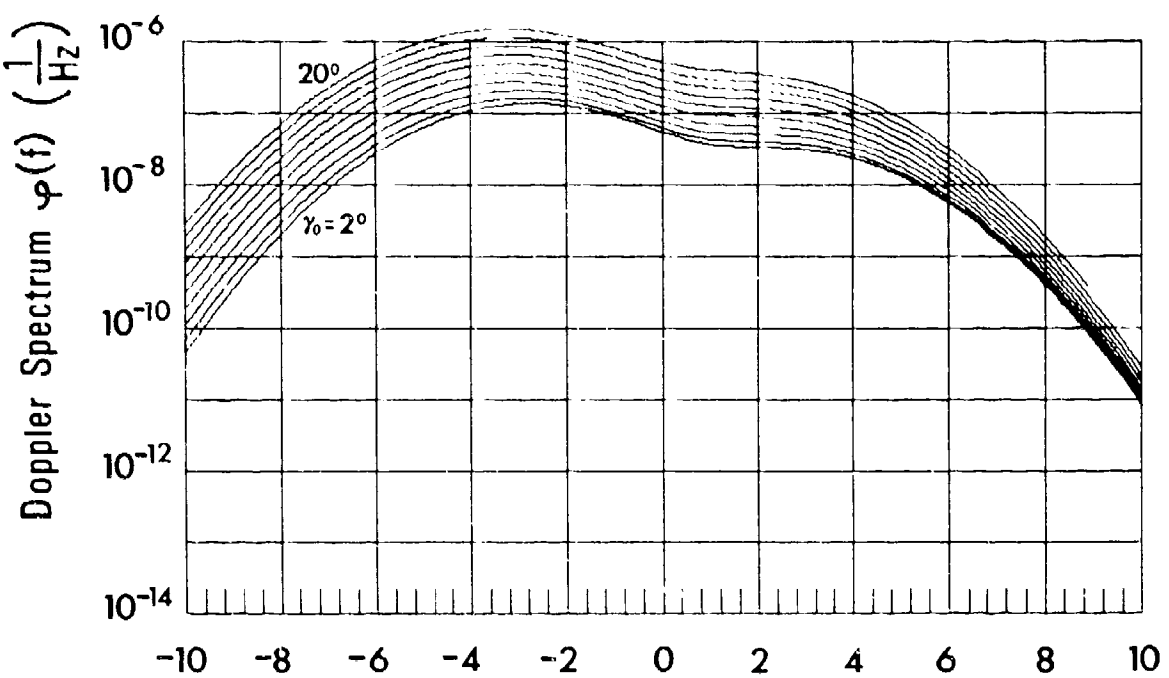

FIG. 21 DOPPLER SPECTRAL DENSITY $\Phi(f)$ vs DOPPLER SHIFT $f - f_o$
Parameters: see Fig. 17
except: Limiting frequency: $f_g = 5$ Hz
addition: Simplified model: Face: length $L \to 0$

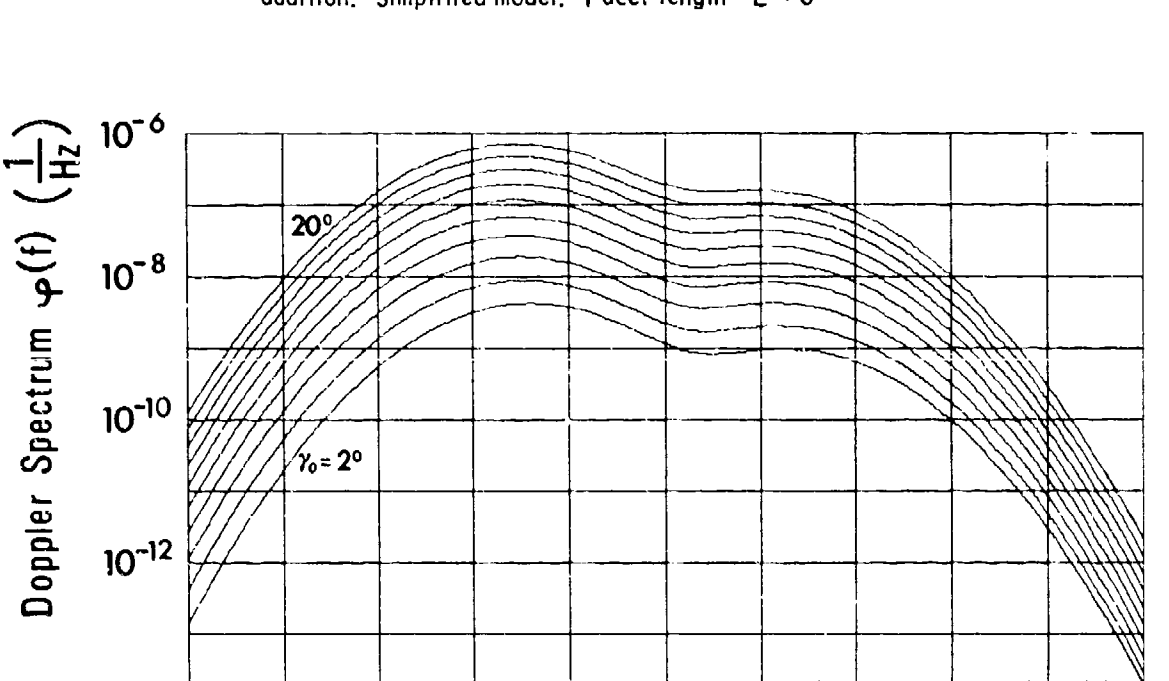

FIG. 22 DOPPLER SPECTRAL DENSITY $\Phi(f)$ vs DOPPLER SHIFT $f - f_o$
Parameters: see Fig. 17
except: Limiting frequency: $f_g = 5$ Hz

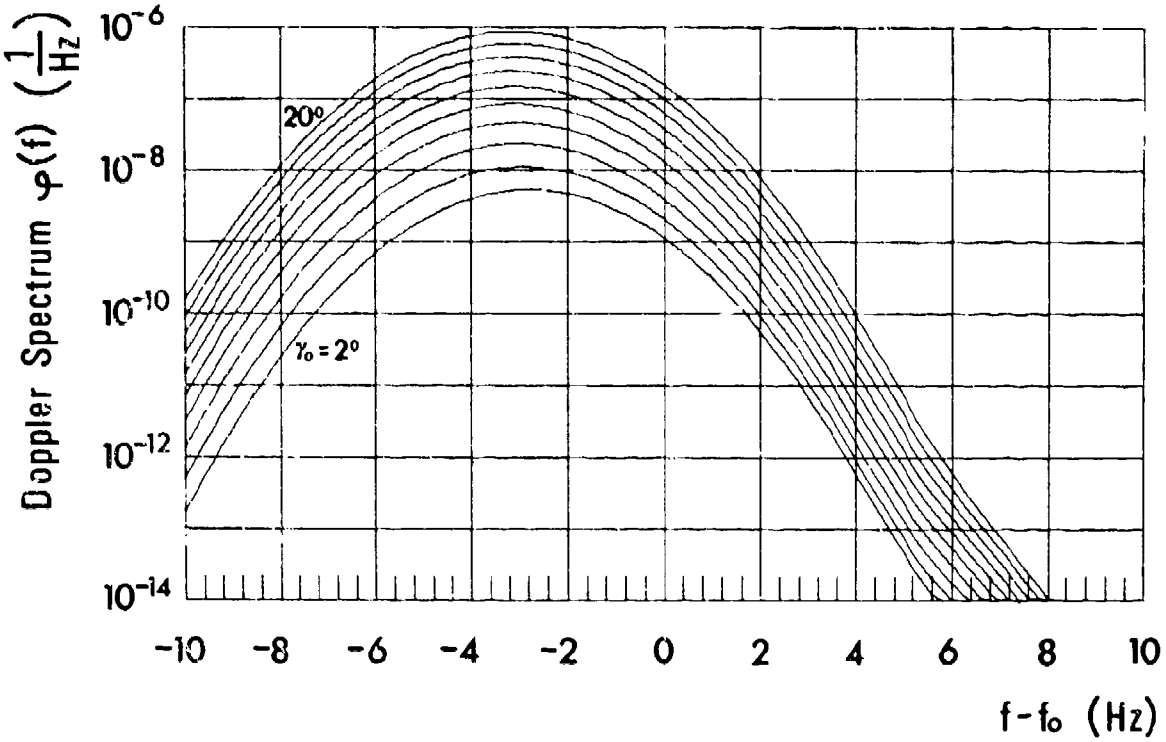

FIG. 23 DOPPLER SPECTRAL DENSITY $\Phi(f)$ vs DOPPLER SHIFT $f - f_o$
Parameters: see Fig. 17
except: Limiting frequency: $f_g \rightarrow \infty$

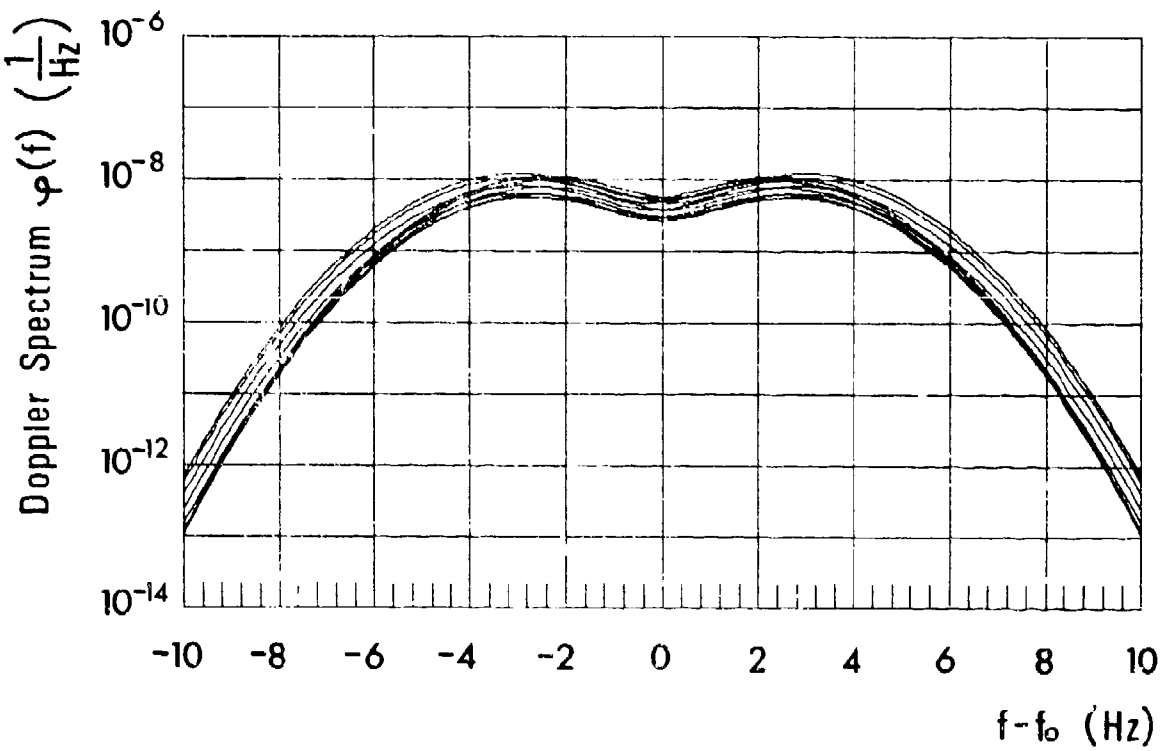

FIG. 24 DOPPLER SPECTRAL DENSITY $\Phi(f)$ vs DOPPLER SHIFT $f - f_o$
Parameter: Wind direction $\Phi_o = 0°$ to 180°
Centre frequency: $f_o = 3.5$ kHz
Grazing angle: $\gamma_o = 2°$
Wind speed: $v = 8$ m/s
Limiting frequency: $f_g = 1$ Hz

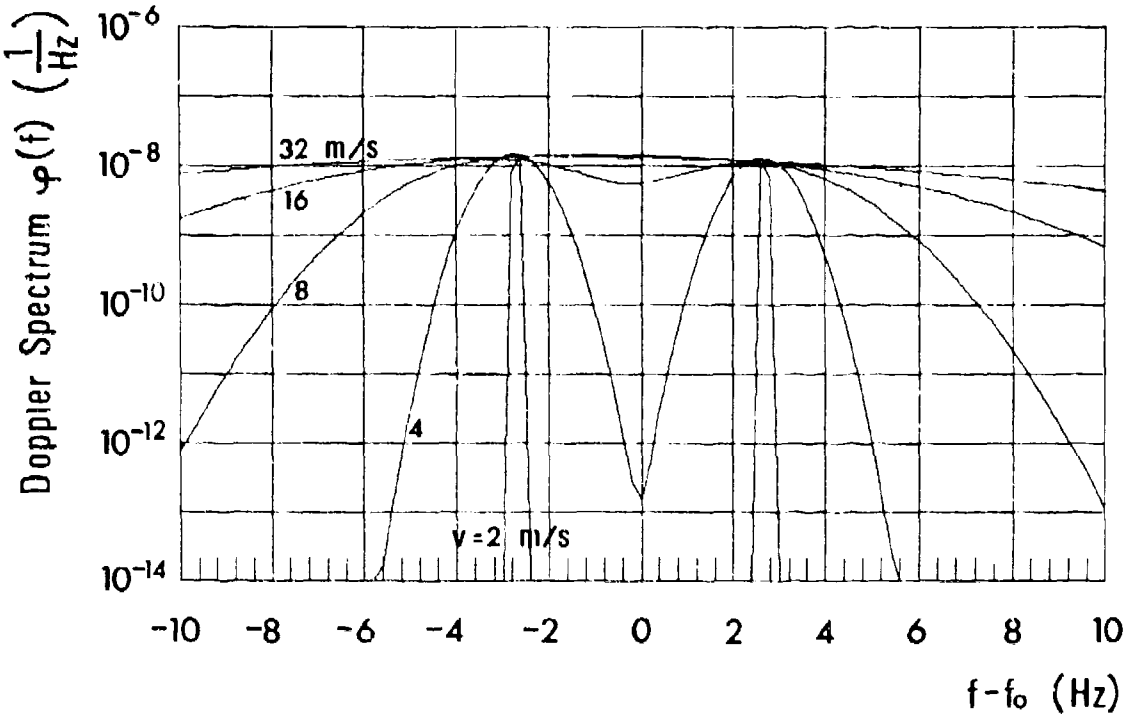

FIG. 25 DOPPLER SPECTRAL DENSITY $\Phi(f)$ vs DOPPLER SHIFT $f - f_o$
Parameter: Wind speed: $v = 2$ m/s to 32 m/s
Centre frequency: $f_o = 3.5$ kHz
Grazing angle: $\gamma_o = 6°$
Wind direction: $\bar{\Psi}_o = 0°$ (downwind)
Limiting frequency: $f_g = 1$ Hz

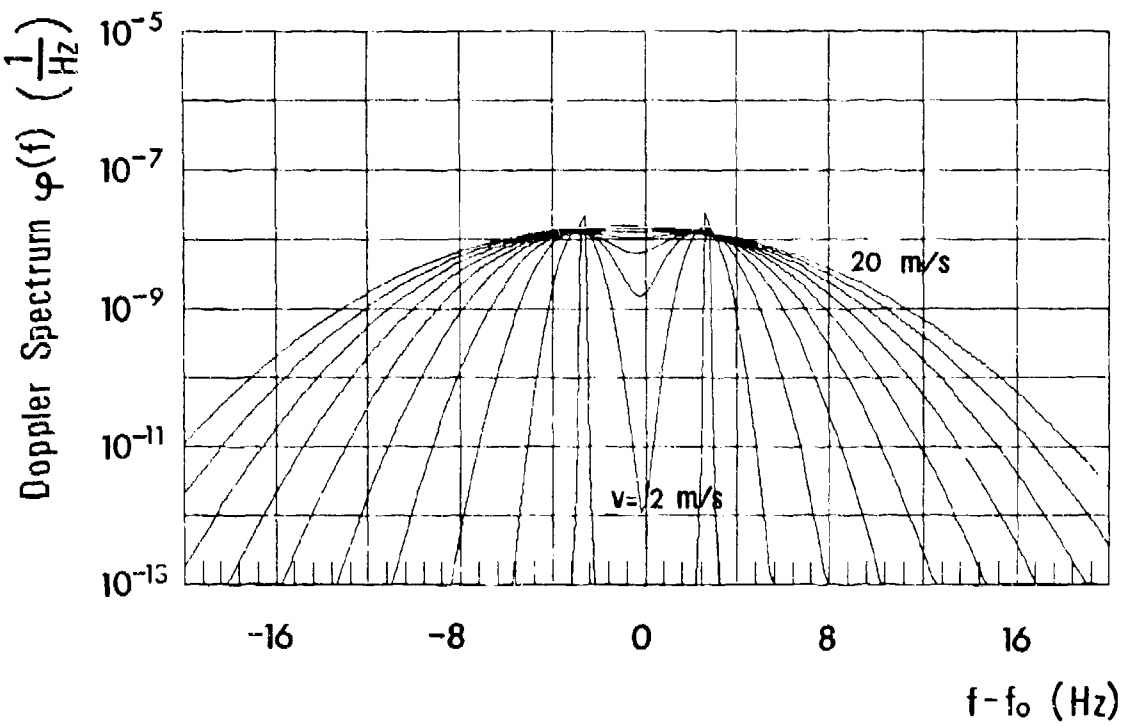

FIG. 26 DOPPLER SPECTRAL DENSITY $\Phi(f)$ vs DOPPLER SHIFT $f - f_o$
Parameters: see Fig. 25
except: Wind speed: $v = 2$ m/s to 20 m/s

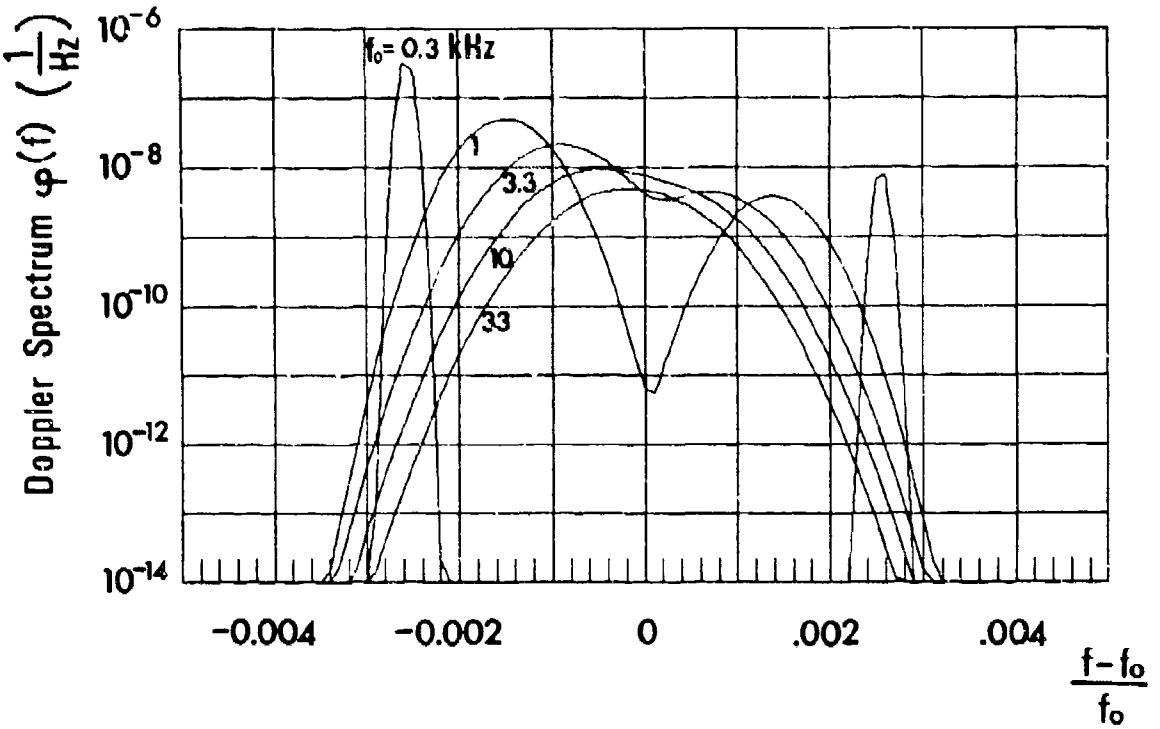

FIG. 27 DOPPLER SPECTRAL DENSITY $\varphi(f)$ vs NORMALIZED DOPPLER SHIFT $\frac{f-f_o}{f_o}$
Parameter: Centre frequency: f_o= 0.3 kHz to 33 kHz
Grazing angle: $\gamma_n = 6°$
Wind speed: $v = 8$ m/s
Wind direction: $\varphi_o = 0°$ (downwind)
Limiting frequency: $f_g = 5$ Hz

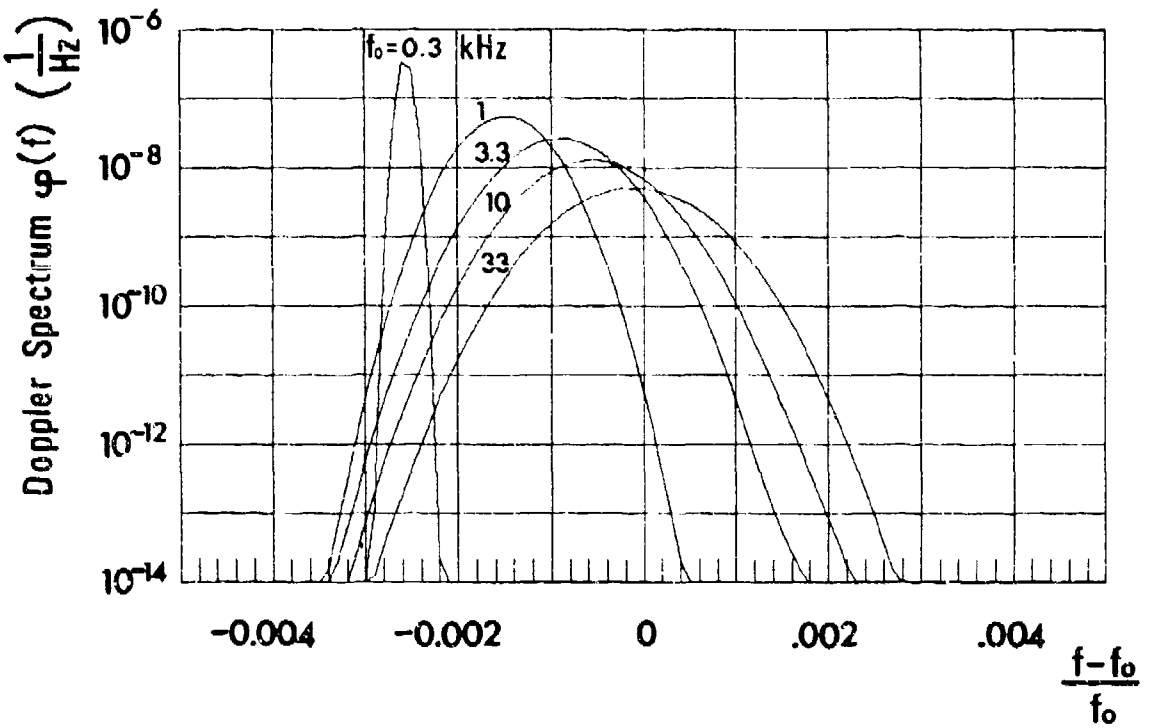

FIG. 28 DOPPLER SPECTRAL DENSITY $\Phi(f)$ vs NORMALIZED DOPPLER SHIFT $\frac{f-f_o}{f_o}$
Parameters: see Fig. 27
except: Limiting frequency: $f_g = 5$ Hz, unmodified Scott spectrum

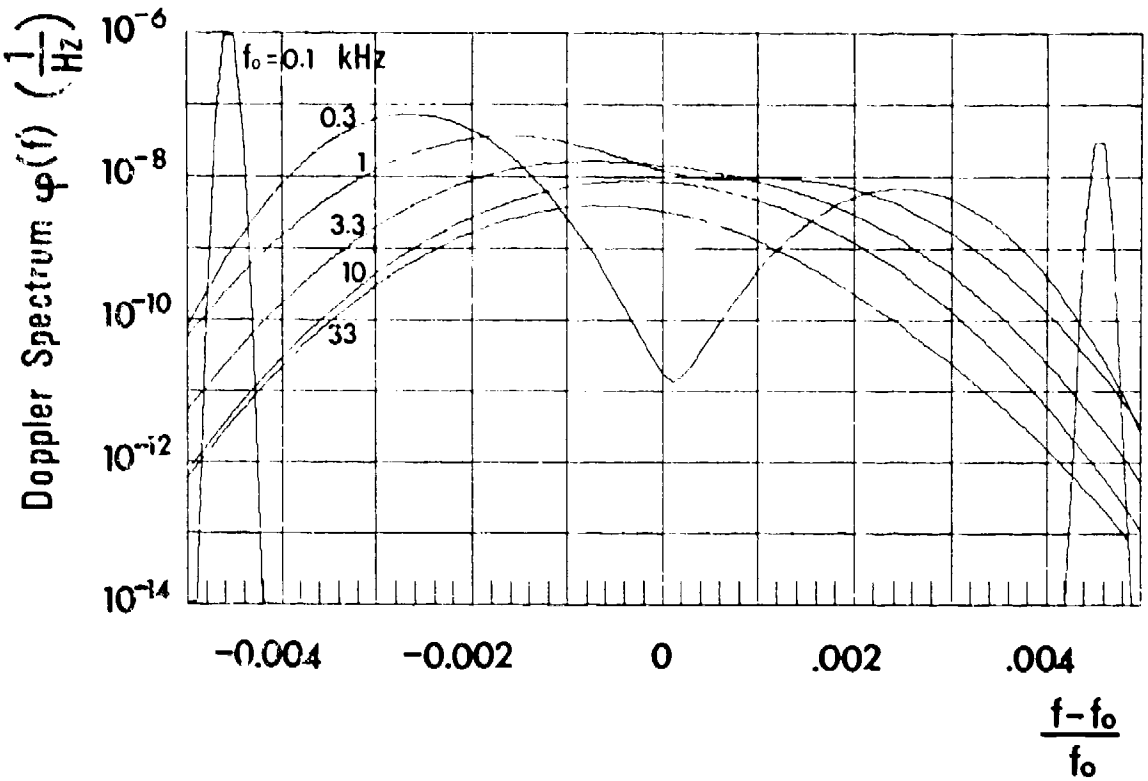

FIG. 29 DOPPLER SPECTRAL DENSITY $\Phi(f)$ vs NORMALIZED DOPPLER SHIFT $\frac{f-f_0}{f_0}$
Parameters: see Fig. 27
except: Wind speed: $v = 10$ m/s
Limiting frequency: $f_g = 2.5$ Hz

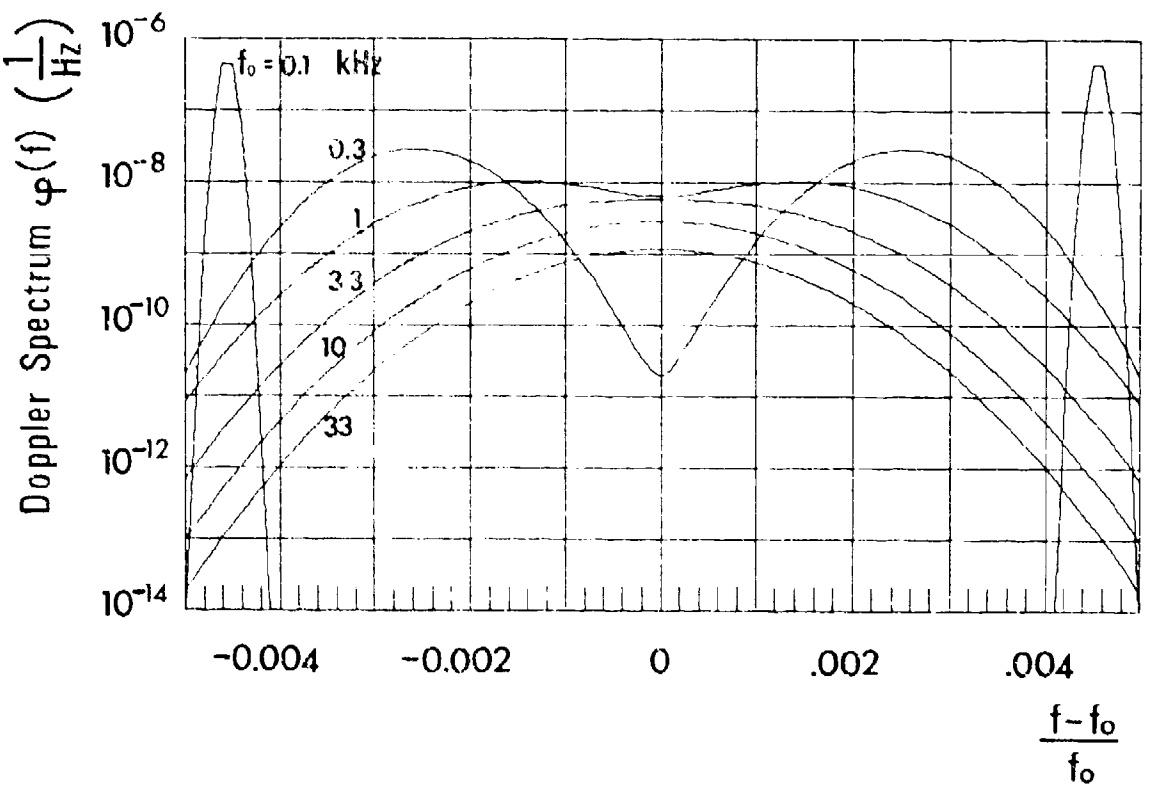

FIG. 30 DOPPLER SPECTRAL DENSITY $\Phi(f)$ vs NORMALIZED DOPPLER SHIFT $\frac{f-f_0}{f_0}$
Parameters: see Fig. 29
except: Wind direction: $\Phi_0 = 90°$

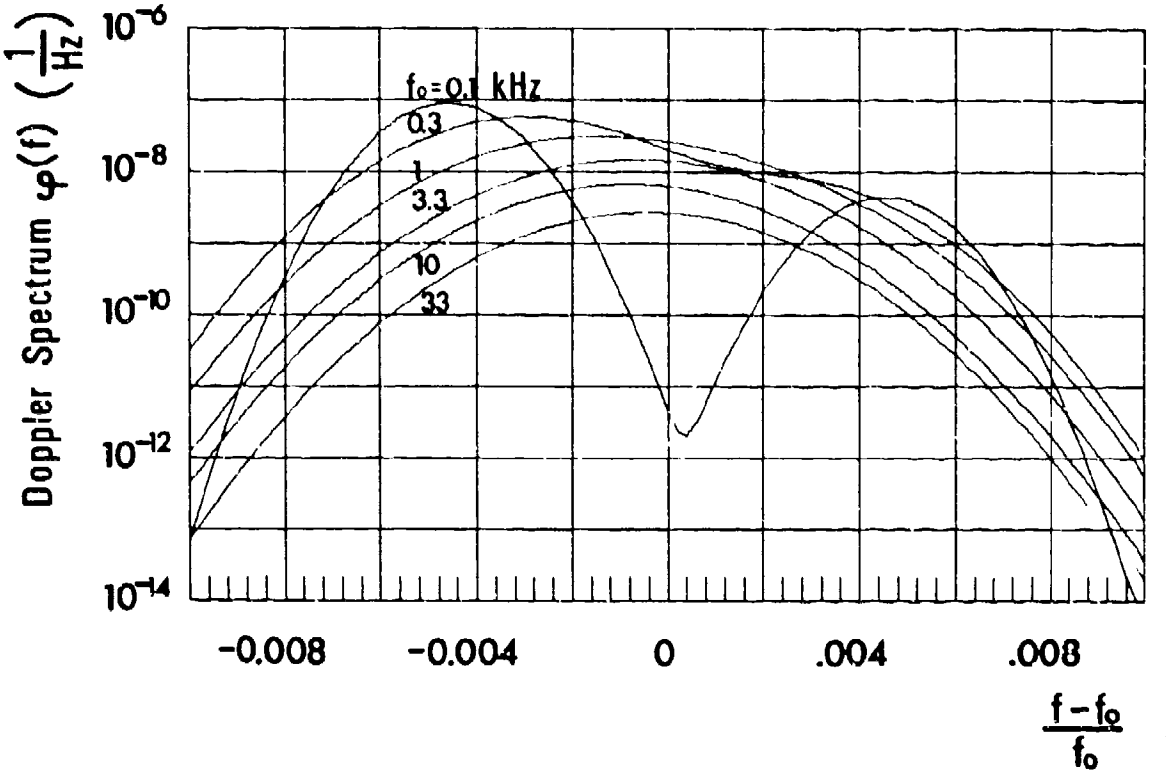

FIG. 31 DOPPLER SPECTRAL DENSITY $\varphi(f)$ vs NORMALIZED DOPPLER SHIFT $\frac{f - f_o}{f_o}$
Parameters: see Fig. 27
except: Wind speed: $v = 32$ m/s
Limiting frequency: $f_g = 2.5$ Hz

APPENDICES

APPENDIX A

SEA-SURFACE DESCRIPTION

A.1 Introductory

The sea surface $h(x, y, t)$ is considered as a stationary three-dimensional process that is assumed to be gaussian distributed. Then the statistical properties of this process are completely described by its covariance function C, which is defined as

$$C(x_1, y_1, t_1, x_2, y_2, t_2) = E\{h(x_1, y_1, t_1)\, h(x_2, y_2, t_2)\}. \qquad \text{[Eq. A.1]}$$

The symbol $E\{...\}$ denotes expectation.

Because of the assumption of stationarity in space and time, the covariance function is dependent only on the difference of the variables. The following notation is used

$$x_1 - x_2 = x,\ y_1 - y_2 = y,\ t_1 - t_2 = \tau\ , \qquad \text{[Eq. A.2]}$$

where x and y are spatial displacements, τ is the time displacement.

The covariance function is related to the three-dimensional wave parameter frequency spectrum $X_3(k_x, k_y, f)$ via the three-dimensional Fourier transform

$$\left.\begin{aligned} X_3(k_x,k_y,f) &= \int_{-\infty}^{+\infty}\!\!\iiint C(x,y,\tau)\, \exp\{-j2\pi(-k_x x - k_y y + f\tau)\}\, dx dy d\tau \\ \text{and} \\ C(x,y,\tau) &= \int_{-\infty}^{+\infty}\!\!\iiint X_3(k_x,k_y,f)\, \exp\{j2\pi(-k_x x - k_y y + f\tau)\}\, dk_x dk_y df, \end{aligned}\right\} \qquad \text{[Eq. A.3]}$$

where both, X_3 and C are real-valued functions and f is the frequency. The components k_x and k_y of the wave parameter k are

$$k_x^2 + k_y^2 = k^2 \quad \text{and} \quad k = \frac{1}{\lambda}\ , \qquad \text{[Eq. A.4]}$$

where λ is the wavelength of the corresponding surface wave.

Equation A.3 states that the sea surface, with the assumptions made, is described by the covariance function C or the wave parameter frequency function X_3.

In the following, both forms are considered in more detail.

A.2 The wave parameter frequency spectrum

Assuming that the dispersion relation, (Eq. 4 of the main text) is valid, the three-dimensional spectrum $X_3(k_x,k_y,f)$ can be written as

$$X_3(k_x,k_y,f) = X_2(k_x,k_y)\, W[k_x \operatorname{sgn}(f),\ k_y \operatorname{sgn}(f)]\,[\delta(f-f^*) + \delta(f+f^*)]\,, \qquad \text{[Eq. A.5]}$$

where

$$f^* = \sqrt{\frac{g}{2\pi}\sqrt{k_x^2 + k_y^2}}\ . \qquad \text{[Eq. A.6]}$$

In Eq. A.5, the function $X_2(k_x,k_y)$ is the wave parameter spectrum. $X_2(k_x,k_y)$ contains the orientational information of the frozen sea surface. The "mixing function" W describes the ratio of incoming and outgoing waves for a given wave parameter vector. The function W(x,y) has the properties

$$\left.\begin{aligned} &0 \le W(x,y) \le 1 \\ &\text{and} \\ &W(x,y) = 1 - W(-x,-y)\ . \end{aligned}\right\} \qquad \text{[Eq. A.7]}$$

It is used in Eq. A.5 with the complicated argument $W[k_x\operatorname{sgn}(f),k_y\operatorname{sgn}(f)]$ to fulfill the symmetry relations imposed on the wave parameter spectra $X_3(k_x,k_y,f)$ and $X_2(k_x,k_y)$, namely

$$\left.\begin{aligned} X_3(k_x,k_y,f) &= X_3(-k_x,-k_y,-f) \\ &\text{and} \\ X_2(k_x,k_y) &= X_2(-k_x,-k_y)\ , \end{aligned}\right\} \qquad \text{[Eq. A.8]}$$

which are necessary to obtain a real covariance function. Apparently, the normalization for X_3 and X_2 has to be

$$\left.\begin{aligned} C(0,0,0) &= \int_{-\infty}^{+\infty}\!\!\int\!\!\int X_3(k_x,k_y,f)\ dk_x dk_y df \\ &\text{and} \\ C(0,0,0) &= \iint X_2(k_x,k_y)\ dk_x dk_y\ . \end{aligned}\right\} \qquad \text{[Eq. A.9]}$$

The basic equation [Eq. A.5] will now be formulated in terms of other functions describing the statistics of the sea surface as well.

First, a description in polar coordinates is given. Equation A.9 is rewritten as

$$\sigma_h^2 = \int_{-\infty}^{\infty}\int_{-\infty}^{\infty} X_2(k_x, k_y)\, dk_x\, dk_y \qquad \text{[Eq. A.10]}$$

$$= \int_{0}^{\infty}\int_{-\pi}^{+\pi} X_2(k\cos\varphi, k\sin\varphi)\, k\, dk\, d\varphi \quad , \qquad \text{[Eq. A.11]}$$

where σ_h is the standard deviation of the sea-surface height and

$$k_x = k\cos\varphi, \quad k_y = k\sin\varphi \; . \qquad \text{[Eq. A.12]}$$

Instead of the wave- parameter angle description, a frequency-angle description can be used. Defining a function $F_2(f, \varphi)$ via the normalizing equation

$$\sigma_h^2 = \int_{0}^{\infty}\int_{-\pi}^{+\pi} F_2(f, \varphi)\, df d\varphi \qquad \text{[Eq. A.13]}$$

the relationship to $X_2(k_x, k_y)$ is

$$F_2(f, \varphi) = \frac{8\pi^2 f^3}{g^2} X_2\left(\frac{2\pi f^2}{g}\cos\varphi, \frac{2\pi f^2}{g}\sin\varphi\right) \qquad \text{[Eq. A.14]}$$

or

$$X_2(k_x, k_y) = \frac{g^2}{8\pi^2 f^{*4}} F_2\left(f^*, \arctan\frac{k_x}{k_y}\right) , \qquad \text{[Eq. A.15]}$$

where again the dispersion relation of Eq. A.6 is used.

$F_2(f, \varphi)$ has the symmetry property

$$F_2(f, \varphi) = F_2(f, \varphi \pm \pi) \quad . \qquad \text{[Eq. A.16]}$$

Inserting Eq. A.15 into Eq. A.5 gives

$$X_3(k_x, k_y, f) = \frac{g^2}{8\pi^2 f^{*5}} F_2\left(f^*, \arctan\frac{k_y}{k_x}\right) W[k_x \mathrm{sgn}(f), k_y \mathrm{sgn}(f)]$$
$$[\delta(f - f^*) + \delta(f + f^*)]. \qquad \text{[Eq. A.17]}$$

The mixing function $W(k_x, k_y)$ can be replaced by another function $W(f, \varphi)$ with the arguments f and φ. This function has the property

$$\left.\begin{aligned} &0 \leq W(f, \varphi) \leq 1 \\ \text{and} \\ &W(f, \varphi) = 1 - W(f, \varphi \pm \pi) . \end{aligned}\right\} \qquad \text{[Eq. A.18]}$$

Although the argument of W has changed, the letter "W" is used for both functions, as there is no danger of confusion. Introducing Eq. A.18 into Eq. A.17 yields

$$X_3(k_x, k_y, f) = \frac{g^2}{8\pi^2 f^{*8}} F_2\left(f^*, \arctan\frac{k_y}{k_x}\right) W\left(f^*, \arctan\frac{k_y}{k_x} + \pi u(-f)\right)$$

$$[\delta(f - f^*) + \delta(f + f^*)] , \qquad \text{[Eq. A.19]}$$

where $u(x)$ is the unit step function

$$u(x) = \begin{cases} 0 & x < 0 \\ \frac{1}{2} & x = 0 \\ 1 & x > 0 . \end{cases} \qquad \text{[Eq. A.20]}$$

In many practical cases the dependance of $F_2(f, \varphi)$ on φ is not known and therefore neglected. Then a wave-parameter spectrum $X_1(k)$ normalized via

$$\sigma_h^2 = \int_0^\infty X_1(k)\, dk \qquad \text{[Eq. A.21]}$$

describes the sea surface. The relation to $X_2(k_x, k_y)$ is

$$X_1\left(\sqrt{k_x^2 + k_y^2}\right) = 2\pi\sqrt{k_x^2 + k_y^2}\; X_2(k_x, k_y) . \qquad \text{[Eq. A.22]}$$

Using again the dispersion relation of Eq. A.6, a frequency spectrum $F_1(f)$ is introduced that is related to $X_1(k)$ via

$$\left.\begin{aligned} F_1(f) &= \frac{4\pi f}{g} X_1\left(\frac{2\pi f^2}{g}\right) \\ \text{or} \\ X_1(k) &= \sqrt{\frac{g}{8\pi k}}\, F_1\left(\sqrt{\frac{kg}{2\pi}}\right) , \end{aligned}\right\} \qquad \text{[Eq. A.23]}$$

where $F_1(f)_\infty$ is normalized with

$$\sigma_h^2 = \int_0^\infty F_1(f)\, df . \qquad \text{[Eq. A.24]}$$

As

$$\int_{-\pi}^{+\pi} F_2(f,\varphi)\, d\varphi = F_1(f) \,, \qquad \text{[Eq. A.25]}$$

the relation to F_2 is

$$F_1(f) = 2\pi F_2(f,\varphi) \,, \qquad \text{[Eq. A.26]}$$

if F_2 is not dependent on φ.

In the case of omnidirectionality the mixing function W is normally set to 0.5. Inserting now Eq. A.26 into Eq. A.19, one obtains, for this special case of practical importance

$$X_3(k_x,k_y,f) = \frac{g^2}{4(2\pi f^*)^3} F_1(f^*)[\delta(f-f^*) + \delta(f+f^*)]. \qquad \text{[Eq. A.27]}$$

In this special case the relation

$$X_3(k_x,k_y,f) = X_3(|k_x|,|k_y|,|f|) \qquad \text{[Eq. A.28]}$$

holds, which is not valid in general.

A.3 The covariance function

A.3.1 General

All relations derived in Chap. A.1 for the wave-parameter frequency domain have consequences for the covariance function $C(x,y,\tau)$ according to the Wiener theorem of Eq. A.3. In this chapter the relations are listed with a few comments.
Introducing Eq. A.5 into Eq. A.3, one obtains

$$C(x,y,\tau) = \int_{-\infty}^{+\infty}\int X_2(k_x,k_y)[W(k_x,k_y)\, \exp\{j2\pi(\tau f^* - k_x x - k_y y)\} + \left(1 - W(k_x,k_y)\right) \exp\{j2\pi(-\tau f^* - k_x x - k_y y)\}]\, dk_x\, dk_y \,. \qquad \text{[Eq. A.29]}$$

If $\tau = 0$, the covariance function $C(x,y,o)$ of the "frozen" sea surface is obtained, which, of course, is independent of the mixing function W.

Equation A.29 can be written in real form using the symmetry relations of X_2 and W. To show this, the following theorem is applied. If $f(x,y) = f_r(x,y) + j\, f_j(x,y) = f^*(-x, -y)$, (* : conjugate complex) then its Fourier transform is

$$F(X,Y) = \int_{-\infty}^{\infty}\int f(x,y)\, \exp\{2\pi j(xX + yY)\}\, dxdy$$

$$= 2 \int_{0}^{\infty}\int_{-\infty}^{\infty} f_r(x,y)\, \cos[2\pi(xX + yY)] - f_j(x,y)\, \sin[2\pi(xX + yY)]\, dxdy.$$

[Eq. A.30]

In this case it is

$$f(k_x,k_y) = X_2(k_x,k_y)[W(k_x,k_y)\exp\{2\pi j\tau f^*\} + (1 - W(k_x,k_y)\exp\{-2\pi j\tau f^*\}],$$

[Eq. A.31]

which equals $f^*(-k_x, -k_y)$ as can be shown simply. Therefore one obtains from Eq. A.29

$$C(x,y,\tau) = \int_{-\infty}^{\infty}\int X_2(k_x,k_y)\{\cos 2\pi f^*\tau \cos 2\pi(k_x x + k_y y)$$

$$+ [2W(k_x,k_y) - 1] \sin 2\pi f^*\tau \sin 2\pi(k_x x + k_y y)\}\, dk_x dk_y .$$

[Eq. A.32]

The introduction of polar coordinates according to Eq. A.12 gives, in the complex form

$$C(x,y,\tau) = \int_{0}^{\infty}\int_{-\pi}^{+\pi} X_2(k\cos\varphi, k\sin\varphi)\{W(k,\varphi)\exp[2\pi j(\tau f^* - k_x x - k_y y)]$$

$$+ [1 - W(k,\varphi)]\exp[2\pi j(-\tau f^* - k_x x - k_y y)]\}\, k\, dk\, d\varphi , \quad \text{[Eq. A.33]}$$

where

$$W(k,\varphi) \le 1$$

and

$$W(k,\varphi) = 1 - W(k, \varphi \pm \pi) .$$

[Eq. A.34]

The real form is

$$C(x,y,\tau) = \int_0^{\infty}\int_{-\pi}^{+\pi} X_2(k\cos\varphi,\ k\sin\varphi)\{\cos 2\pi\tau f^* \cos 2\pi k(x\cos\varphi + y\sin\varphi)$$

$$+ [2W(k,\varphi) - 1]\sin 2\pi\tau f^* \sin 2\pi k(x\cos\varphi + y\sin\varphi)\}\ k\,dk\,d\varphi.$$

[Eq. A.35]

Using again the dispersion relation, one obtains for the complex form in Eq. A.33

$$C(x,y,\tau) = \int_0^{\infty}\int_{-\pi}^{+\pi} X_2\left(\frac{2\pi f^2}{g}\cos\varphi,\ \frac{2\pi f^2}{g}\sin\varphi\right)$$

$$\left(W(f,\varphi)\exp\{2\pi j[\tau f - \frac{2\pi f^2}{g}(x\cos\varphi + y\sin\varphi)]\}\right.$$

$$\left. + (1 - W(f,\varphi))\exp\{2\pi j[-\tau f - \frac{2\pi f^2}{g}(x\cos\varphi + y\sin\varphi)]\}\right)\frac{8\pi^2 f^3}{g^2}\,df\,d\varphi\ ,$$

[Eq. A.36]

where $W(f,\varphi)$ has the property of Eq. A.34.

For the real form one obtains

$$C(x,y,\tau) = \int_0^{\infty}\int_{-\pi}^{\pi} X_2\left(\frac{2\pi f^2}{g}\cos\varphi, \frac{2\pi f^2}{g}\sin\varphi\right)\left\{\cos 2\pi\tau f\cos\frac{(2\pi f)^2}{g}(x\cos\varphi + y\sin\varphi)\right.$$

$$\left. + [2W(f,\varphi) - 1]\sin 2\pi f\tau \sin\frac{(2\pi f)^2}{g}(x\cos\varphi + y\sin\varphi)\right\}\frac{8\pi^2 f^3}{g}\,df\,d\varphi\ .$$

[Eq. A.37]

Using Eq. A.14, Eqs. A.36 and A.37 are formulated in terms of $F_2(f,\varphi)$, yielding

$$C(x,y,\tau) = \int_0^{\infty}\int_{-\pi}^{+\pi} F_2(f,\varphi)\left(W(f,\varphi)\exp\{2\pi j[\tau f - \frac{2\pi f^2}{g}(x\cos\varphi + y\sin\varphi)]\}\right.$$

$$\left. + [1 - W(f,\varphi)]\exp\{2\pi j[-\tau f - \frac{2\pi f^2}{g}(x\cos\varphi + y\sin\varphi)]\}\right)\,df\,d\varphi\ ,$$

[Eq. A.38]

and

$$C(x,y,\tau) = \int_0^{\infty} \int_{-\pi}^{\pi} F_2(f,\varphi) \{ \cos 2\pi f\tau \cos [\frac{(2\pi f)^2}{g} (x\cos\varphi + y\sin\varphi)] + [2W(f,\varphi) - 1] \sin 2\pi f\tau \sin [\frac{(2\pi f)^2}{g} (x\cos\varphi + y\sin\varphi)] \} \, d\varphi \, df \, .$$

[Eq. A.39]

Because of the symmetry properties in Eqs. A.16 and A.34 the integration over φ can be performed from $-\pi/2$ to $+\pi/2$, taking the result twice.

A.3.2 Special case

Now a special case is considered, which simplifies the general formulae. The simplification is applied to Eq. A.39; for the other relations quite similar formulations apply. For the mixing function $W(f,\varphi)$ the following equation is assumed

$$W(f,\varphi) = \begin{cases} W_o, & \text{for } |\varphi - \varphi_w| \leq \frac{\pi}{2}, \; |\varphi_w| \leq \frac{\pi}{2} \\ 1 - W_o, & \text{elsewhere} \end{cases}$$

[Eq. A.40]

Inserting in Eq. A.39 yields

$$C(x,y,\tau) = 2 \int_0^{\infty} \Bigg[\int_{-\pi/2}^{+\pi/2} F_2(f,\varphi) \cos 2\pi f\tau \cos [\frac{(2\pi f)^2}{g} (x\cos\varphi + y\sin\varphi)] \, d\varphi + (2W_o - 1) \int_{\varphi_w - \pi/2}^{\varphi_w + \pi/2} F_2(f,\varphi) \sin 2\pi f\tau \sin [\frac{(2\pi f)^2}{g} (x\cos\varphi + y\sin\varphi)] \, d\varphi \Bigg] \, df.$$

[Eq. A.41]

The second term in Eq. A.41 can be written in this form because the integrand I has the property $I(\varphi) = -I(\varphi \pm \pi)$.
In the extreme case $W_o=1$ and $\varphi_w=0$, Eq. A.41 takes the form

$$C(x,y,\tau) = 2 \int_0^{\infty} \int_{-\pi/2}^{\pi/2} F_2(f,\varphi) \cos [2\pi f\tau - \frac{(2\pi f)^2}{g} (x\cos\varphi + y\sin\varphi)] \, d\varphi \, df.$$

[Eq. A.42]

This case is often assumed in the literature, e.g. [Ref. 10].

For an extremely simplified sea surface, namely a pure sine wave with frequency f_o, travelling in the direction φ_o, Eq. A.42 is solved in closed form. In this case, $F_2(f,\varphi)$ has the form

$$F_2(f,\varphi) = \frac{\sigma_h^3}{2} \left[\delta(f - f_o,\ \varphi - \varphi_o) + \delta(f - f_o,\ \varphi - \varphi_o - \pi)\right] \qquad \text{[Eq. A.43]}$$

and $C(x,y,\tau)$ is

$$C(x,y,\tau) = \begin{cases} \sigma_h^2 \cos\left[2\pi f_o \tau - \dfrac{(2\pi f_o)^2}{g}\,(x\cos\varphi_o + y\sin\varphi_o)\right], & \text{if } |\varphi_o| < \dfrac{\pi}{2} \\ \sigma_h^2 \cos\left[2\pi f_o \tau + \dfrac{(2\pi f_o)^2}{g}\,(x\cos\varphi_o + y\sin\varphi_o)\right], & \text{if } |\varphi_o| > \dfrac{\pi}{2}\ . \end{cases}$$

[Eq. A.44]

The other extreme is $W_o = 0.5$. Then the result is

$$C(x,y,\tau) = \int_0^{\infty} \int_{-\pi}^{+\pi} F_2(f,\varphi) \cos 2\pi f\tau \cos\left[\frac{(2\pi f)^2}{g}(x\cos\varphi + y\sin\varphi)\right] d\varphi\, df.$$

[Eq. A.45]

If, in addition, F_2 is independent of φ, Eq. A.45 becomes

$$C(x,y,\tau) = \int_0^{\infty} F_1(f) \cos 2\pi f\tau\ J_o\left[\frac{(2\pi f)^2}{g}\sqrt{x^2 + y^2}\right] df\ , \qquad \text{[Eq. A.46]}$$

where $J_o(x)$ is the Bessel function of order zero.

The complex form of Eq. A.46 is

$$C(x,y,\tau) = \int_0^{\infty} F_1(f)\ \frac{\exp\{2\pi j\tau f\} + \exp\{-2\pi j\tau f\}}{2}\ J_o\left[\frac{(2\pi f)^2}{g}\sqrt{x^2 + y^2}\right] df.$$

[Eq. A.47]

If the two-sided version of $F_1(f)$,

$$F(f) = \tfrac{1}{2} F_1(|f|)\ , \qquad \text{[Eq. A.48]}$$

is used, Eq. A.47 becomes

$$C(x,y,\tau) = \int_{-\infty}^{+\infty} F(f)\ \exp\{2\pi j\tau f\}\ J_o\left[\frac{(2\pi f)^2}{g}\sqrt{x^2 + y^2}\right] df\ . \qquad \text{[Eq. A.49]}$$

A.3.3 Examples

For use in the application of the general theory, two versions of sea-surface spectra that are of practical importance are described. The first is the well-known Pierson-Moskowitz spectrum that has the form

$$F_2(f,\varphi) = \frac{F_1(f)}{x_n} \cos^n(\varphi - \varphi_o) \quad , \qquad \text{[Eq. A.50]}$$

where

$$F_1(f) = \frac{\alpha g^2}{(2\pi)^4 f^5} \exp\{-\beta(\frac{g}{2\pi f v})^4\} \qquad \text{[Eq. A.51]}$$

and

$$x_n = \int_{-\pi}^{\pi} \cos^n(\varphi - \varphi_o) = 2^{n+1} \frac{\Gamma^2\left(\frac{n+1}{2}\right)}{\Gamma(n+1)} \qquad \text{[Eq. A.52]}$$

$$= 2\pi \frac{(n-1)!!}{n!!} \quad . \qquad \text{[Eq. A.53]}$$

Equation A.53 holds, if n is an even number. The constants α and β in Eq. A.51 are

$$\alpha = 0.0081$$
and $$\beta = 0.74 \quad . \qquad \text{[Eq. A.54]}$$

In the same equation, v is the wind speed.

For calculation purposes, Eq. A.51 is too complicated, therefore it is slightly modified to give a spectrum very similar to the Phillips spectrum. The modification is

$$F_1(f) = \begin{cases} \frac{\alpha g^2}{(2\pi)^4 f^5} \quad , & f \geq f_s \\ 0 \quad , \text{ else} \end{cases} \qquad \text{[Eq. A.55]}$$

where f_s is the frequency, for which the equation

$$\int_0^{\infty} \frac{\alpha g^2}{(2\pi)^4 f^5} \exp\{-\beta(\frac{g}{2\pi f v})^4\}\, df = \int_{f_s}^{\infty} \frac{\alpha g^2}{(2\pi)^4 f^5}\, df \qquad \text{[Eq. A.56]}$$

holds. The solution of Eq. A.56 is

$$f_s = \frac{g}{2\pi v} \sqrt[4]{\beta} \qquad \text{[Eq. A.57]}$$

The second spectrum, due to Scott [Ref. 15], takes into consideration a frequency-dependent directivity of the surface waves. The spectrum has the form

$$\hat{E}_2(f,\varphi) = \hat{A}_S F_1(f) \left|\cos\left(\frac{\varphi - \varphi_o}{2}\right)\right|^{2s} , \qquad \text{[Eq. A.58]}$$

where

$$s = \frac{5.5 \text{ Hz}}{2\pi f} \qquad \text{[Eq. A.59]}$$

and $\hat{A}_S$ is a normalizing factor.

Unfortunately, Eq. A.58 violates Eq. A.16 and hence gives no real covariance function when transformed into the time domain. Therefore Eq. A.58 is interpreted as a product of a two-dimensional spectrum and a mixing function $W(f,\varphi)$:

$$E_2(f,\varphi) = A_S F_1(f) \left[\left|\cos\left(\frac{\varphi - \varphi_o}{2}\right)\right|^{2s} + \left|\sin\left(\frac{\varphi - \varphi_o}{2}\right)\right|^{2s} \right] , \qquad \text{[Eq. A.60]}$$

$$W(f,\varphi) = \frac{\left|\cos\left(\frac{\varphi - \varphi_o}{2}\right)\right|^{2s}}{\left|\cos\left(\frac{\varphi - \varphi_o}{2}\right)\right|^{2s} + \left|\sin\left(\frac{\varphi - \varphi_o}{2}\right)\right|^{2s}} \qquad \text{[Eq. A.61]}$$

and

$$A_S = \frac{1}{\int_{-\pi}^{+\pi} \left[\left|\cos\left(\frac{\varphi - \varphi_o}{2}\right)\right|^{2s} + \left|\sin\left(\frac{\varphi - \varphi_o}{2}\right)\right|^{2s} \right] d\varphi} \qquad \text{[Eq. A.62]}$$

$$= \frac{\Gamma(2s+1)}{2^{2s+2}\,\Gamma^2\left(s+\frac{1}{2}\right)} . \qquad \text{[Eq. A.63]}$$

Equation A.61 is still unsatisfactory as it does not give the omnidirectivity of the high-frequency surface waves.

Therefore the Scott spectrum is modified by introducing

$$W(f,\varphi) = \frac{B + \left|\cos\left(\frac{\varphi - \varphi_o}{2}\right)\right|^{as}}{2B + \left|\cos\left(\frac{\varphi - \varphi_o}{2}\right)\right|^{as} + \left|\sin\left(\frac{\varphi - \varphi_o}{2}\right)\right|^{as}} \quad , \qquad \text{[Eq. A.64]}$$

where

$$B = \left(\frac{f}{f_g}\right)^2 \qquad \text{[Eq. A.65]}$$

and f_g is a limiting frequency.

For $f_g \to 0$, the spectrum is omnidirectional for all surface waves,
for $f_g \to \infty$, it gives the unmodified Scott spectrum.

APPENDIX B

SMALL SCALE ROUGHNESS BACKSCATTERING AND EXTENSION OF THE THEORY

The theory of backscattering of acoustic waves from the moving sea surface is well established for the case of small-sea surface roughness. For sake of completeness, the theory is derived in this appendix, together with a possible extension of the accuracy of the results. However, this extension is not further investigated in the main text.

B.1 Existing theory

The geometry of Fig. 1 of the main text is used.

Combining the results of Ref. 8, pp. 13 and 34 the pressure of a scattered plane wave incident to an aperture ab is approximately in the far field $(r \to \infty)$

$$p(r,\gamma,\varphi,t) = j \frac{\sin\gamma\, p_o}{r} k_o \exp\{2\pi j(-k_o r + f_o t)\}$$

$$\int_{-a/2}^{+a/2}\int_{-b/2}^{+b/2} \exp\{2\pi j\, k_o[x(\alpha - \cos\gamma_o) + y\beta + 2\sin\gamma_o\, h(x,y,t)]\}\, dx\, dy \quad ,$$

[Eq. B.1]

where

α = $\cos\gamma \cdot \cos\varphi$

β = $\cos\gamma \cdot \sin\varphi$

f_o = frequency of incident plane wave

k_o = wave parameter of incident plane wave $= \frac{1}{\lambda_o}$

p_o = pressure of incident plane wave

and

$h(x,y,t)$ = sea-surface function as used in Eq. A.1.

The incident wave is assumed to be in the x-z plane $(\varphi_o = \pi)$, which can be done without loss of generality.

Inserting Eq. B.1 into Eq. 1 of the main text yields

$$\Phi(f,\alpha,\beta) = \frac{\sin^2\gamma \cdot p_0^2 k_0^2}{r^2}$$

$$\int_{-\infty}^{+\infty}\int_{-a/2}^{a/2}\int_{-b/2}^{b/2} \exp\{-2\pi j\, k_0[x_1(\alpha-\cos\gamma_0)+y_1\beta]\}\exp\{-2\pi j f_0 t\}$$

$$\exp\{2\pi j\, k_0[x_2(\alpha-\cos\gamma_0)+y_2\beta]\}\exp\{2\pi j f_0(t+\tau)\}$$

$$E\Big(\exp\{-4\pi j\, k_0 \sin\gamma_0 \cdot [h(x_1,y_1,t)-h(x_2,y_2,t+\tau)]\}\Big)$$

$$\exp\{-2\pi f\tau\}\,dx_1\,dx_2\,dy_1\,dy_2\,d\tau\ . \qquad \text{[Eq. B.2]}$$

With the substitution $x_2 - x_1 = x$, $y_2 - y_1 = y$ and following the derivation in Ref. 8, p. 59 one obtains

$$\Phi(f,\alpha,\beta) = \frac{\sin^2\gamma \cdot p_0^2\, ab\, k_0^2}{r^2}\exp\{-(4\pi k_0 \cdot \sin\gamma_0)^2\, C(0,0,0)\}$$

$$\int_{-\infty}^{+\infty}\int_{-a}^{a}\int_{-b}^{b}\left(1-\frac{|x|}{a}\right)\left(1-\frac{|y|}{b}\right)\exp\{(4\pi k_0 \sin\gamma_0)^2\, C(x,y,\tau)\}$$

$$\exp\{-2\pi j[(f-f_0)\tau - x\,k_0(\alpha-\cos\gamma_0) - y\,k_0\beta]\}\,dx\,dy\,d\tau. \qquad \text{[Eq. B.3]}$$

It is assumed that $a \gg |x|$ and $b \gg |y|$ for all values of x and y where $C(x,y,\tau)$ is different from zero. Then the integration in Eq. B.3 can be performed to infinity and $\frac{|x|}{a}$ and $\frac{|y|}{b}$ are neglected against 1. It follows that

$$\Phi(f,\alpha,\beta) = \frac{\sin^2\gamma \cdot p_0^2\, ab\, k_0^2}{r^2}\exp\{-(4\pi k_0 \sin\gamma_0)^2\, C(0,0,0)\}$$

$$\int_{-\infty}^{+\infty}\int\int \exp\{(4\pi k_0 \sin\gamma_0)^2\ C(x,y,\tau)\}$$

$$\exp\{-2\pi j[(f-f_0)\tau - k_0 x(\alpha-\cos\gamma_0) - k_0 y\beta]\}\,dx\,dy\,d\tau\ . \qquad \text{[Eq. B.4]}$$

For the slightly rough sea surface, it can be assumed that

$$(4\pi k_0 \sin\gamma_0)^2\ C(0,0,0) \ll 1 \qquad \text{[Eq. B.5]}$$

and the exponential in Eq. B.4 is expanded in a power series and only

the first two terms are considered. It is

$$\exp\{(4\pi k_0 \sin\gamma_0)^3\, C(x,y,\tau)\} \approx 1 + (4\pi k_0 \sin\gamma_0)^2\, C(x,y,\tau)\ , \qquad \text{[Eq. B.6]}$$

giving, for Eq. B.4

$$\Phi(f,\alpha,\beta) = \frac{\sin^2\gamma\ p_0^2\ ab\ k_0^2}{r^2}\ [\delta(f-f_0, k_0(\alpha-\cos\gamma_0), k_0\beta) + (4\pi k_0 \sin\gamma_0)^2\ X_3(k_0(\alpha-\cos\gamma_0, k_0\beta, f-f_0)]. \qquad \text{[Eq. B.7]}$$

Equation B.7 makes use of Eq. A.3 and the integral representation of the δ-function. The first term in Eq. B.7 denotes the specular reflection, the second the scattering term. In this case of backscattering, Eq. B.7 takes a special form by putting $\varphi = \pi$ and $\gamma = \gamma_0$. Using the definition for the backscattering doppler density

$$\varphi(f) = \frac{\Phi(f,\alpha,\beta)r^2}{p_0^2 ab}\ , \qquad \text{[Eq. B.8]}$$

the result is

$$\varphi(f) = (4\pi)^2 \sin^4\gamma_0 k_0^4\ X_3(-2k_0\cos\gamma_0, 0, f-f_0). \qquad \text{[Eq. B.9]}$$

This is Eq. 3 of the main text. When integrated over f, Eq. B.9 becomes the backscattering strength q in Eq. 10 of Ref. 5.

If the dispersion relation [Eq. 4] is considered valid, the spectrum $X_3(k_x, k_y, f)$ is replaced by the two-dimensional frequency angle spectrum $F_2(f,\varphi)$. Applying Eq. A.19 one obtains for Eq. B.9

$$\varphi(f) = \frac{2g^2 k_0^4 \sin^4\gamma_0}{f_0^{*3}} F_2(f_0^*, 0)\ [W(f_0^*,\pi)\,\delta(f-f_0-f_0^*) + W(f_0^*,0)\,\delta(f-f_0+f_0^*)] \qquad \text{[Eq. B.10]}$$

which is Eq. 5 of the main text.

Equation B.10 can be simplified by the assumption of omnidirectionality of the wave parameter frequency spectrum for the slightly rough sea surface. In this case, $W = 0.5$ (see App. A) and the sea surface is

described by the frequency spectrum $F_1(f)$. Using Eq. A.2 one obtains

$$\varphi(f) = \frac{\sin^4\gamma_0 \sqrt{g\pi k_0^5}}{2\sqrt{\cos^3\gamma_0}} F_1(|f-f_0|)\,[\delta(f-f_0-f_0^*) + \delta(f-f_0+f_0^*)]. \quad \text{[Eq. B.11]}$$

This equation, when integrated over f gives the result known from Eq. 18 of Ref. 5.

B.2 Extension of the theory for the doppler spectrum of the small-scale roughness sea surface

The present theory, as is seen from Eq. B.10 gives two δ-functions for the backscattered doppler spectrum of an incident monochromatic plane wave.
A possible extension would be to consider one more term in the series expansion of Eq. B.6. This third term has the form

$$T_3 = \tfrac{1}{2}(4\pi k_0 \sin\gamma_0)^4 \; C^2(x,y,\tau). \quad \text{[Eq. B.12]}$$

Here only this term is considered.

Inserting Eq. B.12 into Eq. B.4 gives

$$\Phi^{(3)}(f,\alpha,\beta) = \frac{\sin^2\gamma\; p_0^2\; ab\; k_0^2}{r^2} \exp\{-(4\pi k_0 \sin\gamma_0)^2\, C(0,0,0)\}$$

$$\int_{-\infty}^{+\infty}\!\!\int\!\!\int \tfrac{1}{2}(4\pi k_0 \sin\gamma_0)^4 \; C^2(x,y,\tau)$$

$$\exp\{-2\pi j[(f-f_0)\tau - k_0 x(\alpha - \cos\gamma_0) - k_0 y\,\beta]\}\; dx\, dy\, d\tau. \quad \text{[Eq. B.13]}$$

Equation B.13 has to be added to the first order result Eq. B.7 to obtain a second-order formula.

For the covariance function, omni-directionality and $W = 0.5$ is assumed. Then $C(x,y,\tau)$ is represented by Eq. A.49, which

is inserted into Eq. B.13, yielding

$$\Phi^{(3)}(f,\alpha,\beta) = G \int_{-\infty}^{+\infty}\int_{-\infty}^{+\infty}\int_{0}^{\infty}\int_{0}^{\infty} F(f_1)\,F(f_2)\,\exp\{2\pi j f_1 \tau\}\,\exp\{2\pi j f_2 \tau\}$$

$$J_0\left[\frac{(2\pi f_1)^2}{g}\sqrt{x^2+y^2}\right] J_0\left[\frac{(2\pi f_2)^2}{g}\sqrt{x^2+y^2}\right]$$

$$\exp\{-2\pi j[(f-f_0)\,\tau - k_0 x(\alpha-\cos\gamma_0) - k_0 y\,\beta]\}\,df_1\,df_2\,dx\,dy\,d\tau,$$

[Eq. B.14]

where

$$G \equiv \frac{\sin^2\gamma_0\, p_0^2\, ab\, k_0^2}{2r^2}\,(4\pi k_c \sin\gamma_0)^4\,\exp\{-(4\pi k_0 \sin\gamma_0)^2\, C(0,0,0)\}.$$

[Eq. B.15]

Equation B.14 can be integrated over τ in closed form. The result is

$$\Phi^{(3)}(f,\alpha,\beta) = G \int_{-\infty}^{+\infty}\int\int\int\int F(f_1)F(f_2)\,J_0\left[\frac{(2\pi f_1)^2}{g}\sqrt{x^2+y^2}\right]J_0\left[\frac{(2\pi f_2)^2}{g}\sqrt{x^2+y^2}\right]$$

$$\exp\{2\pi j\, k_0[x(\alpha-\cos\gamma_0)+y\,\beta]\}\,\delta(f_1+f_2-f+f_0)\,df_1\,df_2\,dx\,dy.$$

[Eq. B.16]

Next the integration over f_1 or f_2 is performed. The result, after integration over f_2, is

$$\Phi^{(3)}(f,\alpha,\beta) = G \int_{-\infty}^{+\infty}\int\int F(f_1)F(f-f_0-f_1)J_0\left[\frac{(2\pi f_1)^2}{g}\sqrt{x^2+y^2}\right]$$

$$J_0\left[\frac{[2\pi(f-f_0-f_1)]^2}{g}\sqrt{x^2+y^2}\right]$$

$$\exp\{2\pi j\, k_0[x(\alpha-\cos\gamma_0)+y\,\beta]\}\,df_1\,dx\,dy. \qquad \text{[Eq. B.17]}$$

Changing to polar coordinates, where

$$x = R\cos\varphi\,,$$
$$y = R\sin\varphi$$

gives

$$\Phi^{(3)}(f,\alpha,\beta) = G\int_{-\infty}^{+\infty}\int_{0}^{\infty}\int_{-\pi}^{+\pi} F(f_1)\,F(f-f_0-f_1)\,J_0\left[\frac{(2\pi f_1)^2}{g}R\right]J_0\left[\frac{[2\pi(f-f_0-f_1)]^2}{g}R\right]$$

$$\exp\{2\pi j\,R\,k_0\sqrt{(\alpha-\cos\gamma_0)^2+\beta^2}\,\cos(\varphi-\psi)\}R\,dR\,d\varphi\,df_1\ , \qquad \text{[Eq. B.18]}$$

where

$$\cos\psi = \frac{\alpha-\cos\gamma_0}{\sqrt{(\alpha-\cos\gamma_0)^2+\beta^2}} \quad \text{and} \quad \sin\psi = \frac{\beta}{\sqrt{(\alpha-\cos\gamma_0)^2+\beta^2}}\ .$$

Integration over φ gives a Bessel function again

$$\Phi^{(3)}(f,\alpha,\beta) = G\int_{-\infty}^{+\infty}\int_{0}^{\infty} F(f_1)F(f-f_0-f_1)J_0\left[\frac{(2\pi f_1)^2}{g}R\right]J_0\left[\frac{[2\pi(f-f_0-f_1)]^2}{g}R\right]$$

$$2\pi\,J_0[2\pi R\,k_0\sqrt{(\alpha-\cos\gamma_0)^2+\beta^2}\,]\,R\,dR\,df_1\ . \qquad \text{[Eq. B.19]}$$

Using a result from Ref. 12, p. 412 and Ref. 13, p. 334

$$I = \int_0^{\infty} J_0(at)\,J_0(bt)\,J_0(ct)\,t\,dt$$

$$= \begin{cases} \dfrac{1}{\pi bc\sin A}\ , & \text{if } |\cos A| = \left|\dfrac{b^2+c^2-a^2}{2bc}\right| \le 1 \\ 0\ , & \text{otherwise} \end{cases} \qquad \text{[Eq. B.20]}$$

and inserting into Eq. B.20 gives the final result, which is written down for the backscattering case using the normalized backscattering doppler density as defined in Eq. 2

$$\varphi^{(3)}(f) = 4k_0^6 g^2 \sin^6\gamma_0\,\exp\{-(4\pi k_0\sin\gamma_0)^2\,C(0,0,0)\}$$

$$\int_{-\infty}^{+\infty} F(f_1)\,F(f-f_0-f_1)\,\frac{df_1}{f_1^2(f-f_0-f_1)^2\,\sin A(f_1)}\ . \qquad \text{[Eq. B.21]}$$

The integration over f_1 is performed only for those values of f_1, where $|\sin A(f_1)| < 1$.

For $\cos A$, one obtains

$$\cos A = \frac{f_1^2}{2(f-f_o-f_1)^2} + \frac{(f-f_o-f_1)^2}{2f_1^2} - \frac{g^2 f_o^2 \cos^2 \gamma_o}{2(\pi c f_1)^2 (f-f_o-f_1)^2} \; . \qquad \text{[Eq. B.22]}$$

The evaluation of Eq. B.21 seems possible only by numerical methods. This is not investigated here.

APPENDIX C

STATISTICAL DESCRIPTION OF THE FACETS

C.1 Introductory

The starting equations for the derivations of the statistical properties of the facets are Eqs. 12 to 18 of the main text. These equations lead to the facet inclination σ_c, the vertical and horizontal velocities u_x and u_z, and the crossmoments. Further on in this appendix the sea-surface roughness on the facet $\sigma_h(L)$ is calculated. For $\sigma_h(L)$, Eqs. 39 and 40 are the starting point.

This appendix has two sections. Firstly, a general result in terms of the sea-surface covariance function $C(x,y,\tau)$ is derived which is evaluated in the second section for a Pierson Moskowitz sea-surface spectrum.

C.2 General results

C.2.1 Formulation in terms of the covariance function $C(x,y,\tau)$

The facet is represented by a straight line

$$f(x,t) = \epsilon(t) + b(t) , \qquad \text{[Eq. C.1]}$$

such that the mean-square error $e(t)$ between the surface function $h(x,y,t)_{|y=0}$ and the facet equation $f(x,t)$

$$e(t) = \int_{-L/2}^{L/2} [h(x,y,t) - \epsilon(t)\,x - b(t)]^2 \, dx \qquad \text{[Eq. C.2]}$$

is a minimum. Taking the derivative of $e(t)$ with respect to $\epsilon(t)$ and $b(t)$ leads to the equations

$$\epsilon(t) = \frac{12}{L^3} \int_{-L/2}^{L/2} x\, h(x,y,t)\, dx \qquad \text{[Eq. C.3]}$$

and

$$b(t) = \frac{1}{L} \int_{-L/2}^{L/2} h(x,y,t)\, dx \, . \qquad \text{[Eq. C.4]}$$

The velocities in vertical and horizontal directions are repeated here for completeness. It follows from Eqs. 15 and 18 of the main text that

$$u_z(t) = \frac{1}{L} \int_{-L/2}^{L/2} \frac{\partial h(x,y,t)}{\partial t} \, dx \qquad \text{[Eq. C.5]}$$

and

$$u_x(t) = -\frac{g}{L} \int_{t_0}^{t} [h(\tfrac{L}{2}, y, t_1) - h(-\tfrac{L}{2}, y, t_1)] \, dt_1 + u_x(t_0) \, . \qquad \text{[Eq. C.6]}$$

The roughness on the facet $\rho^2(t)$ is expressed by the mean-square error $e(t)$, normalized by the facet length L. It is

$$\rho^2(t) = \frac{1}{L} e(t) \quad ,$$

which is identical to Eq. 40 of the main text.

All these quantities are stochastic variables with the mean values zero and variances that depend on the sea-surface properties and the facet length L.

The calculation of the variances and crossvariances is demonstrated in detail for one example. The facet slope $\epsilon(t)$ has the variance

$$E_t\{\epsilon^2\} = E\left\{\left(\frac{12}{L^3}\right)^2 \int_{-L/2}^{L/2} \int_{-L/2}^{L/2} x_1 \, h(x_1, y_1, t_1) \; x_2 \, h(x_2, y_2, t_2) \, dx_1 \, dx_2 \right\} , \qquad \text{[Eq. C.7]}$$

where $t_1 = t_2$ and $y_1 = y_2$.

Taking the expectation E inside the integral and using the rect-function

$$\text{rect } x = \begin{cases} 1, & |x| \le \frac{1}{2} \\ 0, & \text{else} \end{cases} \qquad \text{[Eq. C.8]}$$

one obtains

$$E_t\{\epsilon^2\} = \frac{144}{L^6} \int_{-\infty}^{\infty} \int x_1 x_2 \; \text{rect} \, \frac{x_1}{L} \; \text{rect} \, \frac{x_2}{L} \; E\{h(x_1, y_1, t_1) \, h(x_2, y_2, t_2)\} \, dx_1 \, dx_2 \, . \qquad \text{[Eq. C.9]}$$

From Eq. A.1 it is seen that the expectation in Eq. C.9 is the covariance function $C(x_1, x_2, y_1, y_2, t_1, t_2)$ of the sea surface. As stationarity in space and time is assumed, C depends only on the space and time differences. Therefore the substitutions $x = x_1 - x_2$, $y = y_1 - y_2$ and $\tau = t_1 - t_2$ are made, which transform Eq. C.9 to

$$E_t\{\epsilon^2\} = \frac{144}{L^6} \int_{-\infty}^{\infty}\int (x_2+x)\, x_2\, \mathrm{rect}\frac{x+x_2}{L}\, \mathrm{rect}\frac{x_2}{L}\, C(x,y,\tau)\, dx\, dx_2 . \qquad [\text{Eq. C.10}]$$

The integration over x_2 is performed by considering two cases $x > 0$ and $x < 0$. For $x > 0$ one obtains

$$E_t\{\epsilon^2\} = \frac{144}{L^6} \int_0^L C(x,y,\tau) \left[\frac{x_2^3}{3} + \frac{x\, x_2^2}{2}\right]_{-L/2}^{L/2-x} dx \qquad [\text{Eq. C.11}]$$

$$= \frac{12}{L^3} \int_0^L C(x,y,\tau) \left(1 - 3\frac{x}{L} + \frac{2x^3}{L^3}\right) dx . \qquad [\text{Eq. C.12}]$$

For $x < 0$ the result is

$$E_t\{\epsilon^2\} = \frac{12}{L^3} \int_{-L}^{0} C(x,y,\tau) \left(1 + 3\frac{x}{L} + 2\frac{x^2}{L^3}\right) dx . \qquad [\text{Eq. C.13}]$$

Combining Eqs. C.12 and C.13 gives

$$E_t\{\epsilon^2\} = \frac{12}{L^3} \int_{-L}^{L} C(x,y,\tau) \left(1 - 3\frac{|x|}{L} + 2\frac{|x|^3}{L^3}\right) dx . \qquad [\text{Eq. C.14}]$$

It was mentioned before that this expectation has to be taken for $t_1 = t_2$, and $y_1 = y_2$, viz. for $\tau = y = 0$. Then $C(x,y,\tau)\big|_{\tau=y=0}$ is an even function in x. Therefore Eq. C.14 is rewritten as

$$E_t\{\epsilon^2\} = \frac{24}{L^3} \int_0^L C(x,y,\tau)\Big|_{\substack{y=0\\ \tau=0}} \left(1 - 3\frac{x}{L} + 2\frac{x^3}{L^3}\right) dx . \qquad [\text{Eq. C.15}]$$

which is Eq. 19 of the main text.

The calculation of $E_t\{u_x^2\}$ and $E_t\{u_z^2\}$ is performed analogously. For $E_t\{u_z^2\}$ the fact is used that

$$\frac{\partial^2 C(x,y,\tau)}{\partial \tau^2}\Big|_{y=\tau=0}$$

is an even function in x, while $E_t\{u_x^2\}$ is calculated using the relation that $E_t\{u_x\} = 0$ and therefore $C(x,y,\tau) = 0$ for $\tau \to \infty$. The results are Eqs. 20 and 21.

For the crossmoments a similar derivation applies. For $E_t\{\epsilon\, u_x\}$ one has

$$E_t\{\epsilon\, u_x\} = \frac{12}{L^4} \int_{-L/2}^{L/2} \int_{-L/2}^{L/2} x_1\; h(x_1, y_1, t_1)\; u(x_2, y_2, t_2)\, dx_1\, dx_2 \,. \qquad [\text{Eq. C.16}]$$

Again, the substitutions $y_1 - y_2 = y$, $t_1 - t_2 = \tau$ and for the first summand $x_1 - \frac{L}{2} = x$, for the second $x_1 + \frac{L}{2} = x$, are made. It follows

$$E\{\epsilon\, u_x\} = \frac{12\, g}{L^4} \left\{ \int_{-L}^{0} \left(x + \frac{L}{2}\right) \int_{-\infty}^{\tau} C(x,y,\tau')\, d\tau' \Big|_{\substack{\tau=0 \\ y=0}} dx \right.$$

$$\left. + \int_{0}^{L} \left(x - \frac{L}{2}\right) \int_{-\infty}^{\tau} - C(x,y,\tau')\, d\tau' \Big|_{\substack{\tau=0 \\ y=0}} dx \right\} \,. \qquad [\text{Eq. C.17}]$$

As $C(x,y,\tau)_{|y=\tau=0}$ is even in x, the integral over C is uneven in x. Therefore both summands cancel out and the result is

$$E_t\{\epsilon\, u_x\} = 0 \,. \qquad [\text{Eq. C.18}]$$

The same argument leads to

$$E_t\{u_z\, u_x\} = 0 \,. \qquad [\text{Eq. C.19}]$$

This is Eq. 23 of the main text.

For $E_t\{\epsilon\, u_z\}$ the result is different from zero.

It is

$$E_t\{\varepsilon\, u_z\} = \frac{12}{L^4} \int_{-L/2}^{L/2} \int_{-L/2}^{L/2} x_1\, E\left\{ h(x_1, y_1, t_1)\, \frac{\partial h(x_2, y_2, t_2)}{\partial t_2} \right\} dx_1\, dx_2$$

[Eq. C.20]

$$= \frac{12}{L^4} \int_{-\infty}^{\infty}\int_{-\infty}^{\infty} (x + x_2)\, \mathrm{rect}\, \frac{x + x_2}{L}\, \mathrm{rect}\, \frac{x_2}{L}\, \frac{-\partial C(x,y,\tau)}{\partial \tau}\Big|_{\substack{\tau=0\\ y=0}} dx\, dx_2 \,.$$

[Eq. C.21]

The integration over x_2 is performed for $x > 0$ and $x \leq 0$. It follows for $x > 0$ that

$$E_t\{\varepsilon\, u_z\} = -\frac{12}{L^4} \int_0^L \frac{\partial C(x,y,\tau)}{\partial \tau}\Big|_{\substack{\tau=0\\ y=0}} \left[x\, x_2 - \frac{x_2^2}{2} \right]_{-L/2}^{-L/2-x} dx \qquad \text{[Eq. C.22]}$$

$$= -\frac{12}{L^4} \int_0^L \frac{\partial C(x,y,\tau)}{\partial \tau}\Big|_{y=\tau=0} \left(\frac{L}{2}\, x - \frac{x^2}{2} \right) dx \,. \qquad \text{[Eq. C.23]}$$

For $x \leq 0$ the result is

$$E_t\{\varepsilon\, u_z\} = -\frac{12}{L^4} \int_{-L}^{0} \frac{\partial C(x,y,\tau)}{\partial \tau}\Big|_{y=\tau=0} \left(\frac{L}{2}\, x + \frac{x^2}{2} \right) dx \,. \qquad \text{[Eq. C.24]}$$

The function

$$f(x) = \begin{cases} \dfrac{L}{2}\, x - \dfrac{x^2}{2}\,, & \text{if } x > 0 \\[2ex] \dfrac{L}{2}\, x + \dfrac{x^2}{2}\,, & \text{if } x \leq 0 \end{cases} \qquad \text{[Eq. C.25]}$$

is uneven in x. As $\dfrac{\partial C}{\partial \tau}$ is also uneven in x, the result

is

$$E_t\{\varepsilon\, u_z\} = -\frac{12}{L^3}\int_0^L \left.\frac{\partial C(x,y,\tau)}{\partial \tau}\right|_{\substack{\tau=0\\ y=0}} \left(x - \frac{x^2}{L}\right) dx \qquad \text{[Eq. C.26]}$$

which is Eq. 22 of the main text.

Next the roughness $\sigma_h^2 = E_t\{\rho^2\}$ is calculated. Inserting Eq. C.2 into Eq. C.6 and taking the expectation gives

$$E_t\{\rho^2\} = \frac{1}{L}\int_{-L/2}^{L/2} E\{[h(x,y,t) - \varepsilon(t)\, x - b(t)]^2\}\, dx \qquad \text{[Eq. C.27]}$$

Inserting Eqs. C.3 and C.4 for $\varepsilon(t)$ and $b(t)$ gives, after a straightforward calculation,

$$E_t\{\rho^2\} = \frac{1}{L}\int_{-L/2}^{L/2} E\{h^2(x,y,t)\}dx - \frac{12}{L^4}\int_{-L/2}^{L/2}\int_{-L/2}^{L/2} E\{x_1\, h(x_1,y_1,t_1) x_2\, h(x_2,y_2,t_2)\}\, dx_1\, dx_2$$

$$- \frac{1}{L^2}\int_{-L/2}^{L/2}\int_{-L/2}^{L/2} E\{h(x_1,y_1,t_1)\, h(x_2,y_2,t_2)\}\, dx_1\, dx_2 \,. \qquad \text{[Eq. C.28]}$$

Now the integration technique used for the facet statistics is applied again, giving

$$E_t\{\rho^2\} = C(0,0,0) - \frac{12}{L^4}\int_{-\infty}^{\infty}\int (x + x_2)\, x_2\, \text{rect}\frac{x + x_2}{L}\, \text{rect}\frac{x_2}{L}\, C(x,y,\tau)\, dx\, dx_2$$

$$- \frac{1}{L^2}\int_{-\infty}^{\infty}\int \text{rect}\frac{x + x_2}{L}\, \text{rect}\frac{x_2}{L}\, C(x,y,\tau)\, dx\, dx_2 \,. \qquad \text{[Eq. C.29]}$$

The integration over x_2 yields the final result

$$E_t\{\rho^2\} = C(0,0,0) - \frac{4}{L}\int_0^L \left.C(x,y,\tau)\right|_{\substack{\tau=0\\ y=0}} \left(1 - \frac{2x}{L} + \frac{x^3}{L}\right) dx \,, \qquad \text{[Eq. C.30]}$$

which is Eq. 42 of the main text.

C.2.2 Formulation in terms of the frequency angle spectrum $F_2(f,\varphi)$

The derivations make use of the relationship between the covariance function $C(x,y,\tau)$ and the frequency angle sea-surface spectrum $F_2(f,\varphi)$. This relationship is calculated in Eq. A.39 and is repeated here for convenience

$$C(x,y,\tau) = \int_{-\pi}^{\pi}\int_{0}^{\infty} F_2(f,\varphi)\{\cos 2\pi f\tau \cos[\frac{(2\pi f)^2}{g}(x\cos\varphi + y\sin\varphi)]$$

$$+ [2W(f,\varphi) - 1]\sin 2\pi f\tau \sin[\frac{(2\pi f)^2}{g}(x\cos\varphi + y\sin\varphi)]\}\, d\varphi\, df\,. \qquad [\text{Eq. C.31}]$$

This equation is inserted into the expressions for the facet statistics and the roughness on the facet σ_{1l}. Then the integration over x is performed. The calculation is given for one example, all other formulae follow in a similar manner.

From Eq. C.15

$$E_t\{\varepsilon^2\} = \frac{24}{L^3}\int_0^L\int_{-\pi}^{\pi}\int_0^{\infty} F_2(f,\varphi)\cos\left[\frac{(2\pi f)^2}{g}\,x\,\cos\varphi\right]\left(1 - \frac{3x}{L} + \frac{2x^3}{L^3}\right) dx\, d\varphi\, df\,. \qquad [\text{Eq. C.32}]$$

As $\tau = 0$, the mixing function $W(f,\varphi)$ has no influence.

The integration over x is performed giving

$$E_t\{\varepsilon^2\} = \frac{24}{L^3}\int_{-\pi}^{\pi}\int_0^{\infty} F_2(f,\varphi)\{(1+\cos a L)\frac{3}{La^2} + (1-\cos a L)\frac{12}{L^3 a^4}$$

$$- \frac{12}{L^3 a^3}\sin a L\}\, df d\varphi\,, \qquad [\text{Eq. C.33}]$$

where the abbreviation

$$a = \frac{(2\pi f)^2}{g}\cos\varphi \qquad [\text{Eq. C.34}]$$

is used. Equation C.33 can be shown to be

$$E_t\{\varepsilon^2\} = \frac{144}{L^6}\int_{-\pi}^{\pi}\int_0^{\infty} \frac{F_2(f,\varphi)}{a^4}\left(La\cos\frac{aL}{2} - 2\sin\frac{aL}{2}\right)^2 df d\varphi \qquad [\text{Eq. C.35}]$$

which is Eq. 24 of the main text.

The calculation for the other moments and the crossmoment is not made here as it is straight forward and follows the above derivation strictly. The resulting formulae are found in the main text.

C.2.3 Limiting cases

To gain a better understanding of the physical meaning of the expressions derived in the preceding section it is instructive to consider two limiting cases. They are connected with the correlation distance x_R of the surface covariance function $C(x,y,\tau)$. The distance x_R is defined as the 3 dB-width of $C(x,y,\tau)$ in the x-direction. The two cases $L >> x_R$ and $L << x_R$ are considered.

a) $L >> x_R$

If the facet length $L >> x_R$, then $C(x,y,\tau) \approx 0$ for all values of x in the order of L, that means, $\frac{x}{L}$ can be neglected against 1 in the formulae for the facet statistics. This gives immediately the limiting cases

$$E_t\{\varepsilon^2\} \approx \frac{24}{L^3} \int_0^L C(x,y,\tau)\,|_{y=\tau=0}\ dx\,, \qquad \text{[Eq. C.36]}$$

$$E_t\{u_z^2\} \approx -\frac{2}{L}\int_0^L \frac{\partial^2 C(x,y,\tau)}{\partial \tau^2}\,|_{y=\tau=0}\ dx\,, \qquad \text{[Eq. C.37]}$$

$$E\{u_x^2\} \approx -\frac{2g^2}{L^2} \int_{-\infty}^{\tau}\int^{t_1} C(0,y,\tau)\,dt\,dt_1\,|_{y=\tau=0}\,, \qquad \text{[Eq. C.38]}$$

and

$$E_t\{\varepsilon\, u_z\} \approx -\frac{12}{L^3} \int_0^L \frac{\partial C(x,y,\tau)}{\partial \tau}\,|_{y=\tau=0}\ x\,dx\,. \qquad \text{[Eq. C.39]}$$

For the roughness on the facet $E_t\{p^2\}$ follows

$$E_t\{p^2\} \approx C(0,0,0) - \frac{4}{L}\int_0^L C(x,y,\tau)\,|_{y=\tau=0}\ dx\,. \qquad \text{[Eq. C.40]}$$

From the equations it is seen that all facet statistics [Eqs. C.36 to C.39] tend to zero for $L \to \infty$ while $E_t\{p^2\}$ equals the sea-surface roughness $C(0,0,0)$ in the limiting case $L \to \infty$.

Again, the above expressions are formulated in terms of the frequency angle spectrum $F_a(f,\varphi)$.

For completeness the results are listed below

$$E_t\{\varepsilon^2\} \approx \frac{24}{L^3} \int_{-\pi}^{\pi} \int_{o}^{\infty} \frac{F_2(f,\varphi)}{a} \sin aL \, df \, d\varphi \ , \qquad \text{[Eq. C.41]}$$

$$E_t\{u_z^2\} \approx \frac{2g}{L} \int_{-\pi}^{\pi} \int_{o}^{\infty} F_2(f,\varphi) \frac{\sin aL}{\cos \varphi} \, df \, d\varphi \ , \qquad \text{[Eq. C.42]}$$

$$E_t\{u_x^2\} \approx \frac{2g^2}{L^2} \int_{-\pi}^{\pi} \int_{o}^{\infty} \frac{F_2(f,\varphi)}{(2\pi f)^2} \, df \, d\varphi \ , \qquad \text{[Eq. C.43]}$$

$$E_t\{\varepsilon u_z\} \approx \frac{12}{L^3} \int_{-\pi}^{\pi} \int_{o}^{\infty} F_2(f,\varphi) \, [2W(f,\varphi) - 1] \, 2\pi f \left(\frac{\sin aL}{a^2} - \frac{L}{a} \cos aL \right) df \, d\varphi \ , \qquad \text{[Eq. C.44]}$$

and

$$E_t\{\rho^2\} \approx \int_{-\pi}^{\pi} \int_{o}^{\infty} F_2(f,\varphi) \, df \, d\varphi - \frac{4}{L} \int_{-\pi}^{\pi} \int_{o}^{\infty} F_2(f,\varphi) \frac{\sin aL}{a} \, df \, d\varphi \ . \qquad \text{[Eq. C.45]}$$

b) $L \ll x_R$

In this case it can be assumed that $C(x,y,\tau)$ changes very little in the integration range 0 to L. Therefore $C(x,y,\tau)$ is expanded in a power series and the first two terms are considered. This gives the limiting cases

$$E_t\{\varepsilon^2\} \approx - \frac{\partial^2 C(x,0,0)}{\partial x^2} \Big|_{x=0} \ , \qquad \text{[Eq. C.46]}$$

$$E_t\{u_z^2\} \approx - \frac{\partial^2 C(0,0,\tau)}{\partial \tau^2} \Big|_{\tau=0} \ , \qquad \text{[Eq. C.47]}$$

$$E_t\{u_x^2\} \approx g^2 \int_{-\infty}^{\tau} \int^{t_1} \frac{\partial^2 C(x,y,\tau)}{\partial x^2} \, dt \, dt_1 \Big|_{x=y=\tau=0} \ , \qquad \text{[Eq. C.48]}$$

$$E_t\{\varepsilon u_z\} \approx - \frac{\partial^2 C(x,y,\tau)}{\partial \tau \, \partial x} \Big|_{x=y=\tau=0} \ , \qquad \text{[Eq. C.49]}$$

and

$$E_t\{\rho^2\} \approx 0 \ . \qquad \text{[Eq. C.50]}$$

In terms of the frequency angle spectrum $F_2(f,\varphi)$ the above equations are

$$E_t\{\varepsilon^2\} \approx \int_{-\pi}^{\pi}\int_{0}^{\infty} F_2(f,\varphi)\ a^2\,df\,d\varphi\ , \qquad \text{[Eq. C.51]}$$

$$E_t\{u_z^2\} \approx \int_{-\pi}^{\pi}\int_{0}^{\infty} F_2(f,\varphi)\ (2\pi f)^2\,df\,d\varphi\ , \qquad \text{[Eq. C.52]}$$

$$E_t\{u_x^2\} \approx \int_{-\pi}^{\pi}\int_{0}^{\infty} F_2(f,\varphi)\ (2\pi f\cos\varphi)^2\,df\,d\varphi\ , \qquad \text{[Eq. C.53]}$$

and

$$E_t\{\varepsilon\, u_z\} \approx \int_{-\pi}^{\pi}\int_{0}^{\infty} F_2(f,\varphi)\,[2W(f,\varphi)-1]\ 2\pi f\,a\,df\,d\varphi\ . \qquad \text{[Eq. C.54]}$$

C.3 Application to a Pierson-Moskowitz spectrum

C.3.1 Solution for general directivity

For practical purposes the general formulae in Eqs. 24 to 28 of the main text have to be evaluated for a special frequency angle spectrum $F_2(f,\varphi)$ and a mixing function $W(f,\varphi)$. The functions chosen are a Pierson-Moskowitz spectrum and a simple mixing function, which is found in App. A in Eqs. A.50, A.51 and A.40.

First, the expression for $E_t\{\varepsilon^2\}$ is derived. Inserting Eq. A.50 with Eq. A.55 into Eq. C.33 gives

$$E_t\{\varepsilon^2\} = \frac{24\,A_n}{L^3}\int_{-\pi}^{\pi}\int_{0}^{\infty}\frac{\cos^n(\varphi-\varphi_0)}{f^5}\Big\{(1+\cos aL)\,\frac{3}{La^2}+(1-\cos aL)\,\frac{12}{L^2a^4}$$

$$-\frac{12}{L^2a^3}\sin aL\Big\}\,df\,d\varphi\ . \qquad \text{[Eq. C.55]}$$

In Eq. C.55, the factor a is an abbreviation seen from Eq. C.34 and

$$A_n = \frac{\alpha\, g^2}{(2\pi)^4\, x_n}\ , \qquad \text{[Eq. C.56]}$$

where x_n is defined in Eq. A.52.

Equation C.55 is integrated over f in closed form. The derivation is lengthy but straightforward. It is denoted that

$$I_f = \int_{f_s}^{\infty} \frac{1}{f^5} \left[(1 + \cos bf^2) \frac{3L}{b^2 f^4} + (1 - \cos bf^2) \frac{12L}{b^4 f^8} - \frac{12L}{b^3 f^6} \sin bf^2 \right] df \qquad \text{[Eq. C.57]}$$

where

$$b = \frac{(2\pi)^2 L \cos \varphi}{g} = \frac{aL^2}{f^2} \quad . \qquad \text{[Eq. C.58]}$$

With the substitution $u = bf^2$ and continuous application of partial integration, Eq. C.57 becomes

$$I_f = \frac{3L}{2f_s} \left[\frac{1}{4u_o^3} + \frac{2}{3u_o^4} + \cos u_o \left(\frac{-1}{72} + \frac{1}{12u_o^2} - \frac{2}{3u_o^4} \right) + \sin u_o \left(\frac{u_o}{72} - \frac{1}{36u_o} - \frac{2}{3u_o^3} \right) + \frac{u_o^2}{72} \int_{|u_o|}^{\infty} \frac{\cos u}{u} \, du \right] , \qquad \text{[Eq. C.59]}$$

where

$$u_o = a_o \cos \varphi = bf_s^2$$

and

$$a_o = \frac{(2\pi f_s)^2 L}{g} = \frac{\sqrt{\beta}\ Lg}{v^2} \qquad \text{[Eq. C.60]}$$

As the integration over φ is performed numerically in the digital computer, the problem of numerical stability occurs for small u_o. Therefore an approximation for $|u_o| < 0.2$ is calculated by expanding the sine and cosine terms in Eq. C.59 in a power series and taking the first few terms.

This leads to

$$I_f = \frac{3L}{2f_s^4} \left[\frac{7u_o^3}{288} - \frac{u_o^4}{320} + \frac{u_o^2}{72} \int_{|u_o|}^{\infty} \frac{\cos u}{u} \, du \right] , \quad \text{if} \quad |u_o| < 0.2 \qquad \text{[Eq. C.61]}$$

Inserting the result for I_f in Eq. C.55 gives finally

$$E_t\{\varepsilon^2\} = \frac{\alpha v^4}{\beta x_n L^2 g^2} \int_0^{\pi} \cos^n(\varphi - \varphi_0) \left\{ \frac{18}{u_0^2} + \frac{48}{u_0^4} \right.$$

$$+ \cos u_0 \left(-1 + \frac{6}{u_0^2} - \frac{48}{u_0^4} \right) + \sin u_0 \left(u_0 - \frac{2}{u_0} - \frac{48}{u_0^3} \right)$$

[Eq. C.62]

$$\left. - u_0^2 \, \mathrm{Ci}(|u_0|) \right\} d\varphi \quad , \quad \text{if} \quad u_0 > 0.2 \quad ,$$

and

$$E_t\{\varepsilon^2\} = \frac{\alpha v^4}{\beta x_n L^2 g^2} \int \cos^n(\varphi - \varphi_0) \left\{ \frac{7u_0^2}{4} - \frac{9u_0^4}{40} - u_0^2 \mathrm{Ci}(|u_0|) \right\} d\varphi \quad ,$$

$$\text{if} \quad u_0 \leq 0.2$$

This is Eq. 57 of the main text.

For the other facet statistics the calculations are made in a similar way. The main steps are listed below.

Inspection of Eqs. 25 and 26 of the main text shows that $E_t\{u_z^2\}$ and $E_t\{u_x^2\}$ are identical in respect to the integration over the frequency f. Inserting the Pierson-Moskowitz spectrum into Eq. 25 gives

$$E_t\{u_z^2\} = \frac{2 g^2 A_n}{L^3} \int_{-\pi}^{\pi} \int_{f_s}^{\infty} \frac{\cos^n(\varphi - \varphi_0)(1 - \cos aL)}{f^5 (2\pi f \cos\varphi)^2} \, df \, d\varphi \, . \qquad \text{[Eq. C.63]}$$

The integral I_f is in this case

$$I_f = \int_{f_s}^{\infty} \frac{1 - \cos bf^2}{f^5 (2\pi f \cos\varphi)^2} \, df \quad , \qquad \text{[Eq. C.64]}$$

with the solution

$$I_f = \frac{(2\pi L)^2}{6 g^2 f_s^2 u_0^2} \left[1 + \left(-1 + \frac{u_0^2}{2} \right) \cos u_0 + \frac{u_0^2}{2} \sin u_0 + \frac{|u_0|^3}{2} \int_{|u_0|}^{\infty} \frac{\sin u}{u} \, du \right] .$$

[Eq. C.65]

The approximation of Eq. C.65 for small u_o is

$$I_f = \frac{(2\pi L)^2}{6g^2 f_s^2}\left\{\frac{3}{2} - \frac{3u_o^2}{8} + \frac{19u_o^4}{720} + \frac{|u_o|}{2}\int_{|u_o|}^{\infty}\frac{\sin u}{u}\,du\right\}, \quad \text{if } |u_o| < 0.2 \ .$$

[Eq. C.66]

Inserting this into Eq. C.63 gives the result

$$E_t\{u_z^2\} = \frac{2\alpha v^2}{3\sqrt{\beta}\, x_n}\int_o^{\pi}\cos^n(\varphi-\varphi_o)\left\{\frac{1}{u_o^2} + \cos u_o\ \frac{1}{2} - \frac{1}{u_o^2}\right\}$$

$$+ \frac{\sin u_o}{2u_o} + \frac{|u_o|}{2}\,\mathrm{Si}\,(|u_o|)\ \ d\varphi\ , \quad \text{if } |u_o| > 0.2\ , \qquad \text{[Eq. C.67]}$$

and

$$E_t\{u_z^2\} = \frac{2\alpha v^2}{3\sqrt{\beta}\, x_n}\int_o^{\pi}\cos^n(\varphi-\varphi_o)\left\{\frac{3}{2} - \frac{3}{8}u_o^2 + \frac{19u_o^4}{720} + \frac{|u_o|}{2}\,\mathrm{Si}(|u_o|)\right\}d\varphi\ ,$$

$$\text{if } |u_o| \le 0.2$$

For $E_t\{u_x^2\}$ the result is

$$E_t\{u_x^2\} = \frac{2\ \alpha v^6}{3\beta^{1.5} x_n L^2 g^2}\int_o^{\pi}\cos^n(\varphi-\varphi_o)\left\{1 + \cos u_o\left(-1 + \frac{u_o^2}{2}\right)\right.$$

$$\left. + \frac{u_o \sin u_o}{2} + \frac{|u_o|^3}{2}\,\mathrm{Si}(|u_o|)\right\}d\varphi\ , \quad \text{if } |u_o| > 0.2\ ,$$

and [Eq. C.68]

$$E_t\{u_x^2\} = \frac{2\alpha v^6}{3\beta^{1.5} x_n L^2 g^2}\int_o^{\pi}\cos^n(\varphi-\varphi_o)\left\{\frac{3}{2}u_o^2 - \frac{3}{8}u_o^4 + \frac{19u_o^6}{720}\right.$$

$$\left. + \frac{|u_o|^3}{2}\,\mathrm{Si}(|u_o|)\right\}d\varphi\ , \quad \text{if } |u_o| \le 0.2$$

Equations C.67 and C.68 are Eqs. 58 and 59 of the main text, respectively.

The crossmoment $E_t\{\varepsilon u_z\}$ is derived in the following way. With the Pierson-Moskowitz spectrum and the mixing function $W(f,\varphi)$

$$W(f,\varphi) = \begin{cases} W_o, & \text{if } |\varphi - \varphi_w| < \frac{\pi}{2} \ , \quad |\varphi_w| < \frac{\pi}{2} \\ 1 - W_o \ , & \text{else} \end{cases} \qquad \text{[Eq. C.69]}$$

Equation 27 of the main text has the form

$$E_t\{\varepsilon u_z\} = \frac{-12\ An\ 2\pi}{L^3} \int_{-\pi}^{\pi} \int_{f_s}^{\infty} \frac{\cos^n(\varphi - \varphi_o)}{f^4} \left[2W(f,\varphi) - 1\right]$$

$$\left\{ \frac{-\sin aL}{a^2} + \frac{2}{La^3} (1 - \cos aL) \right\} df\, d\varphi \ . \qquad \text{[Eq. C.70]}$$

As $W(f,\varphi)$ is independent of f in this special example, the integral over f has the form

$$I_f = \int_{f_s}^{\infty} \frac{1}{f^4} \left\{ \frac{-\sin aL}{a^2} + \frac{2}{La^3} (1 - \cos aL) \right\} df \ . \qquad \text{[Eq. C.71]}$$

The result of the integration is

$$I_f = \frac{L^2}{2f_s^3} \left\{ \sin u_o \left(\frac{k_1}{u_o^2} + k_2 \right) + \cos u_o \left(\frac{k_3}{u_o^3} + \frac{k_4}{u_o} + k_5 u_o \right) - \frac{k_3}{u_o^3} \right.$$

$$\left. - 2\, k_5 u_o \sqrt{|u_o|} \frac{\pi}{2} \left(\frac{1}{2} - S\left(\sqrt{\frac{2|u_o|}{\pi}} \right) \right) \right\} \ , \qquad \text{[Fq. C.72]}$$

where $S(x)$ is the Fresnel integral and the constants k_1 to k_5 have the values $k_1 = -10/63$, $k_2 = 8/189$, $k_3 = -4/9$, $k_4 = -4/63$, and $k_5 = 16/189$.

Now Eqs. C.72 and C.69 are inserted into Eq. C.70, giving the desired result

$$E_t\{\varepsilon u_z\} = \frac{24(1-2W_o)\,\pi A_n}{L f_s^3} \int_{\varphi_w-\pi/2}^{\varphi_w+\pi/2} \cos^n(\varphi-\varphi_o)$$

$$\left\{ \sin u_o \left(\frac{k_1}{u_o^2} + k_2 \right) + \cos u_o \left(\frac{k_3}{u_o^3} + \frac{k_4}{u_o} + k_5 u_o \right) - \frac{k_3}{u_o^3} \right.$$

$$\left. - 2\, k_5 u_o \sqrt{\frac{\pi}{2}\,|u_o|} \left(\frac{1}{2} - S\left(\sqrt{\frac{2|u_o|}{\pi}} \right) \right) \right\} d\varphi, \quad \text{if} \quad |u_o| > 0.2$$

[Eq. C.73]

The factor before the integral is

$$\frac{24(1-2\,W_o)\,\pi A_n}{L f_s^3} = \frac{12(1-2\,W_o)\,\alpha\, v^3}{g\,\beta^{0.75} L\, x_n} \quad ; \qquad \text{[Eq. C.74]}$$

then Eq. C.73 equals Eq. 60 of the main text. For small $|u_o| < 0.2$, Eq. C.73 is approximated by

$$E_t\{\varepsilon u_z\} = \frac{12(1-2W_o)\,\alpha\, v^3}{g\,\beta^{0.75} L\, x_n} \int_{\varphi_w-\pi/2}^{\varphi_w+\pi/2} \cos^n(\varphi-\varphi_o)$$

$$\left\{ \frac{u_o}{6} \frac{299}{5670} u_o^3 - 2k_5 u_o \sqrt{\frac{\pi}{2}\,|u_o|} \left(\frac{1}{2} - S\left(\sqrt{\frac{2|u_o|}{\pi}} \right) \right) \right\} d\varphi, \quad \text{if} \quad |u_o| < 0.2$$

[Eq. C.75]

The roughness on the facet $E_t\{\rho^2\}$ is derived in a similar form. The starting equation is Eq. 43 of the main text, in which the Pierson-Moskowitz spectrum is inserted. It is, in this case,

$$I_f = \int_{f_s}^{\infty} \frac{1}{f^5} \left\{ 1 - \frac{4}{a^2 L^2} \left[\left(1 - \frac{6}{a^2 L^2} \right) \cos aL - \frac{6}{aL} \sin aL + 2 + \frac{6}{L^2 a^2} \right] \right\} df.$$

[Eq. C.76]

The result of the integration is

$$I_f = \frac{1}{f^4}\left(\frac{1}{4} - \frac{1}{u_o^2} - \frac{2}{u_o^4} + \frac{2\cos u_o}{u_o^4} + \frac{2\sin u_o}{u_o^3}\right). \qquad \text{[Eq. C.77]}$$

For small $|u_o| < 0.2$, this is expanded in a power series and the first terms are taken. Inserting Eq. C.77 into Eq. 43 gives the result for $|u_o| > 0.2$ and $|u_o| \le 0.2$

$$E_t\{\rho^2\} = \frac{2\alpha v^4}{\beta g^2 x_n}\int_o^{\pi} \cos^n(\varphi - \varphi_o)\left\{\frac{1}{4} - \frac{1}{u_o^2} - \frac{2}{u_o^4} + \frac{2\cos u_o}{u_o^4} + \frac{2\sin u_o}{u_o^3}\right\} d\varphi ,$$

$$\text{if} \quad |u_o| > 0.2 \qquad \text{[Eq. C.78]}$$

and

$$E_t\{\rho^2\} = \frac{2\alpha v^4}{\beta g^2 x_n}\int_o^{\pi} \cos^n(\varphi - \varphi_o)\,\frac{u_o^2}{72}\, d\varphi , \quad \text{if} \quad |u_o| \le 0.2 .$$

This is Eq. 67 of the main text.

The factor before the integral is the explicit expression of

$$\frac{2A_n}{f_s^4} = \frac{2\alpha v^4}{\beta g^2 x_n} . \qquad \text{[Eq. C.79]}$$

C.3.2 Approximale Analytic solution for cosine square directivity

The expressions of Eqs. 57 to 62 of the main text derived in the preceding section are evaluated here for the case $n = 2$, the cosine square directivity law, to obtain an approximate analytic solution that does not need a digital computer for numerical evaluation. For most practical cases these approximations are considered of sufficient accuracy.

In this section, the expressions of Eq. 64 are derived.

C.3.2.1 $\sigma_\epsilon = \sqrt{E_t\{\epsilon^2\}}$

a) $a_o \ll 1$

$$a_o = \frac{(2\pi f)^2 L}{g} = \frac{\sqrt{\beta}\, Lg}{v^2}$$

The starting point is Eq. C.62 for $u_o = a_o \cos\varphi < 0.2$. The sine integral $Ci(|u_o|)$ is expanded in a series, giving

$$\sigma_\varepsilon^2 = \frac{\alpha v^4}{\beta x_2 L^2 g^2} \int_o^\pi \cos^2(\varphi - \varphi_o) \left\{ \frac{7u_o^2}{4} - \underline{\frac{9u_o^4}{40}} - u_o^2 \left(\gamma + \ln|u_o| - \underline{\frac{u_o^2}{4}} + \ldots\right)\right\} d\varphi \qquad \text{[Eq. C.80]}$$

The underlined terms in Eq. C.80 are neglected, with the result

$$\sigma_\varepsilon^2 = \frac{\alpha}{\pi} \int_o^\pi \cos^2(\varphi - \varphi_o) \cos^2\varphi \left(\ln|u_o| - \gamma - \frac{7}{4}\right) d\varphi \ . \qquad \text{[Eq. C.81]}$$

This integral can be solved in closed form with the substitution $\cos\varphi = x$, the result being

$$\sigma_\varepsilon^2 = \frac{\alpha}{8}\left[3\cos^2\varphi_o \left(-\ln a_o - \gamma + \frac{7}{4} - 1 + \frac{1}{2} - \frac{1}{3} + \frac{1}{4} + \ln 2\right)\right.$$

$$\left. + \sin^2\varphi_o \left(-\ln a_o - \gamma + \frac{7}{4} - \frac{1}{2}\left(1 - \frac{1}{2} + \frac{1}{3} - \frac{1}{4} - \frac{1}{6} - \ln 2\right)\right)\right] . \qquad \text{[Eq. C.82]}$$

Equation C.82 equals σ_ε^2 in Eq. 64 of the main text.

b) $a_o >> 1$

If $a_o >> 1$, this also has the consequence that $u_o = a_o \cos\varphi_o$ is much greater than one in most of the range from 0 to π. However, if $\varphi = \frac{\pi}{2}$, then $u_o = 0$, and it is necessary to split the integral in Eq. C.62 into two parts, one for $u_o << 1$ and one for $u_o >> 1$. If $u_o >> 1$, the cosine integral $Ci(|u_o|)$ in Eq. C.62 is replaced by its asymptotic expansion for large arguments. Then it can be shown that, neglecting all terms containing powers more than $1/u_o^2$, Eq. C.62 takes the simple form

$$\sigma_\varepsilon^2 = \frac{\alpha v^4}{\beta \pi L^2 g^2}\left[\int_o^{\pi/2-\varepsilon'} + \int_{\pi/2+\varepsilon'}^{\pi} \cos^n(\varphi - \varphi_o) \ \frac{18}{u_o^2}\, d\varphi\right] . \qquad \text{[Eq. C.83]}$$

For the integration range $\varphi = \frac{\pi}{2} - \varepsilon'$ to $\varphi = \frac{\pi}{2} + \varepsilon'$, the approximation for small u_o in Eq. C.81 has to be taken. The

sum of both gives the desired result. The choice of ε' contains a certain amount of arbitrariness; for lack of a better possibility $\varepsilon' = \frac{1}{a_o}$ was taken.

Then it can be shown that the part of the integral where $a_o \ll 1$ can be neglected, therefore Eq. C.83 gives the complete result. The integration of Eq. C.83 is straightforward, leading to the form

$$\sigma_\varepsilon^2 = \frac{18\,\alpha\,v^4}{\beta\,\pi\,L^2\,g^2\,a_o^2}\left[\varphi\cos^2\varphi_o + \sin^2\varphi_o(\tan^3\varphi - \varphi)\right]_o^{\frac{\pi}{2}-\frac{1}{a_o}} + \Bigg|_{\frac{\pi}{2}+\frac{1}{a_o}}^{\pi} \qquad \text{[Eq. C.84]}$$

The $\tan^2\varphi$ terms is expanded for arguments near $\frac{\pi}{2}$, giving the result

$$\sigma_\varepsilon^2 = \frac{18\,\alpha}{\beta^2 g^4\left(\frac{L}{v^2}\right)^4}\left(\cos\varphi_o^2 + \frac{(2\,a_o - \pi)}{\pi}\sin^2\varphi_o\right) \qquad \text{[Eq. C.85]}$$

which is part of Eq. 64

C.3.2.2 $\dfrac{\sigma_z}{v} - \dfrac{\sqrt{E_t\{u_z^2\}}}{v}$

a) $a_o \ll 1$

From Eq. C.67 it is seen that for $a_o \ll 1$ the vertical velocity has the variance

$$\left(\frac{\sigma_z}{v}\right)^2 = \frac{2\alpha}{3\sqrt{\beta}\,\pi}\int_o^{\pi}\frac{3}{2}\cos^2(\varphi - \varphi_o)\,d\varphi, \qquad \text{[Eq. C.86]}$$

which leads easily to

$$\frac{\sigma_z}{v} = \sqrt{\frac{\alpha}{2\sqrt{\beta}}}\,. \qquad \text{[Eq. C.87]}$$

This is the result given in Eq. 64 of the main text.

b) $a_o \gg 1$

Again, Eq. C.67 shows the approximation for $a_o \gg 1$

$$\left(\frac{\sigma_z}{v}\right)^2 = \frac{2\alpha}{3\sqrt{\beta}\,\pi}\int_o^{\pi} \frac{\cos^2(\varphi - \varphi_o)}{u_o^2}\, d\varphi \quad , \qquad \text{[Eq. C.88]}$$

as all sine and cosine terms cancel out if the sine integral is expanded into an asymptotic expansion. This is a form of the integrand identical to that of Eq. C.83. Therefore the same argument applies and the result is

$$\left(\frac{\sigma_z}{v}\right)^2 = \frac{2\alpha}{3\beta^{1.5}\, g\, \frac{L}{v^2}} \left(\cos^2\varphi_o + \frac{2a_c - \pi}{\pi}\sin^2\varphi_o\right) , \qquad \text{[Eq. C.89]}$$

which is listed in Eq. 64

C.3.2.3 $\dfrac{\sigma_x}{v} = \dfrac{\sqrt{E_t\{u_x^2\}}}{v}$

a) $a_o \ll 1$

The asymptotic expansion of the sine integral $si(x)$ in Eq. C.69 shows that also here the sine and cosine terms cancel out leaving an integral of the form

$$\left(\frac{\sigma_x}{v}\right)^2 = \frac{\alpha\, v^4\, a_o^2}{\beta^{1.5}\,\pi\, L^2 g^2}\int_o^{\pi} \cos^2(\varphi - \varphi_o)\cos^2\varphi\, d\varphi \quad . \qquad \text{[Eq. C.90]}$$

The evaluation of Eq. C.90 gives

$$\left(\frac{\sigma_x}{v}\right)^2 = \frac{\alpha}{8\sqrt{\beta}}\,(3\cos^2\varphi_o + \sin^2\varphi_o) \quad . \qquad \text{[Eq. C.91]}$$

b) $a_o \gg 1$

The sine and cosine terms cancel out in this case, too. Then it follows from Eq. C.68 that

$$\left(\frac{\sigma_x}{v}\right)^2 = \frac{2\alpha v^4}{3\beta^{1.5}\pi L^3 g^2} \int_o^{\pi} \cos^2(\varphi - \varphi_o)\, d\varphi \quad , \qquad \text{[Eq. C.92]}$$

which leads to the result

$$\left(\frac{\sigma_x}{v}\right)^2 = \frac{\alpha}{3\beta^{1.5} g^2 \left(\frac{L}{v^2}\right)^2} \quad . \qquad \text{[Eq. C.93]}$$

C.3.2.4 $\dfrac{\sigma_{\varepsilon z}}{v} = \dfrac{E_t\{\varepsilon u_z\}}{v}$

a) $a_o \ll 1$

For small arguments the sine integral in Eq. C.75 tends to zero. The term with u_o^3 is neglected against u_o, leaving an integral of the form

$$\frac{\sigma_{\varepsilon z}}{v} = \frac{12(1-2W_o)\alpha v^2 a_o}{g\,\beta^{0.75} L\,\pi} \int_{\omega_w-\pi/2}^{\varphi_w+\pi/2} \cos^2(\varphi - \varphi_o)\cos\varphi \left[\frac{1}{6} - \frac{16}{3\cdot 7\cdot 9}\sqrt{\frac{\pi a_o}{2}}\sqrt{|\cos\varphi|}\right] d\varphi \quad , \qquad \text{[Eq. C.94]}$$

For most practical cases is seems reasonable to assume that $\varphi_o = \varphi_w$. For this special case the above integral is evaluated. Application of known integration formulae gives

$$\frac{\sigma_{\varepsilon z}}{v} = \frac{24\alpha(1-2W_o)\cos\varphi_o}{\pi\sqrt[4]{\beta}}\left(\frac{y_3}{6} - \frac{16\sqrt{\pi a_o}}{21\cdot 9\sqrt{2}}\, y_{3.5}\right) \quad , \qquad \text{[Eq. C. 95]}$$

where

$$y_n = \int_0^{\pi/2} \cos^n \varphi \, d\varphi = \frac{\Gamma^2\left(\frac{n+1}{2}\right) 2^{n-1}}{\Gamma(n+1)} \quad . \qquad \text{[Eq. C.96]}$$

Numerical evaluation of Eq. C.95 and Eq. C.96 gives Eq. 65 of the main text.

b) $a_0 \gg 1$

This case leads to a similar form to that for the standard deviation σ_ξ of the facet slope. Starting from Eq. C.73, all terms containing sine and cosine functions cancel out, the fresnel integral can also be neglected in this case. The remaining equation is simply for $\varphi_0 = \varphi_w$

$$\frac{\sigma_{\varepsilon z}}{v} = \frac{16(1 - 2W_0)\,\alpha\, v^2}{3\, g\, \beta^{0.75}\, L\pi\, a_0^3} \int_{\varphi_0-\pi/2}^{\varphi_0+\pi/2} \frac{\cos^2(\varphi - \varphi_0)}{\cos^3 \varphi}\, d\varphi \quad . \qquad \text{[Eq. C.97]}$$

The integrand is diverging at $\varphi = \frac{\pi}{2}$. But, as it is known that the integrand of the original integral is vanishing for $\cos \varphi = 0$, as is seen from Eq. C.94, again the technique of splitting the integral is performed. The contribution for small $\cos \varphi$ can be neglected. Two cases have to be considered: $\varphi_0 = 0$ and $\varphi_0 \neq 0$.

The first case leads to

$$\frac{\sigma_{\varepsilon z}}{v} = \frac{16(1 - 2W_0)\,\alpha}{3\, \varphi_0^4\, \pi\, \sqrt[4]{\beta}} \int_{-\pi/2+1/a_0}^{\pi/2-1/a_0} \frac{d\varphi}{\cos \varphi} \quad , \quad \text{if} \quad \varphi_0 = 0 \quad . \qquad \text{[Eq. C.98]}$$

The evaluation gives approximately

$$\frac{\sigma_{\varepsilon z}}{v} = \frac{16(1 - 2W_0)\,\alpha}{3\, a_0^4\, \pi\, \sqrt[4]{\beta}}\, 2\, \ell n\, 2a_0 \quad , \quad \text{if} \quad \varphi_0 = 0 \quad . \qquad \text{[Eq. C.99]}$$

The general case $\varphi_0 \neq 0$ leads to the form

$$\frac{\sigma_{\varepsilon z}}{v} = \frac{16(1-2W_0)\alpha}{3a_0^4\, \pi\, \sqrt[4]{\beta}} \left[\int_{\varphi_0-\pi/2}^{\pi/2-\varepsilon'} + \int_{\pi/2+\varepsilon'}^{\varphi_0+\pi/2} \left[\frac{\cos^2 \varphi_0}{\cos \varphi} + \frac{2 \sin \varphi_0 \cos \varphi_0 \sin \varphi}{\cos^2 \varphi} \right.\right.$$

$$\left.\left. + \frac{\sin^2 \varphi_0 \sin^3 \varphi}{\cos^3 \varphi} \right] d\varphi \right] \quad . \qquad \text{[Eq. C.100]}$$

The result of the integration is

$$\frac{\sigma_{ez}}{v} \approx \frac{16(1-2W_o)\,\alpha}{3\,a_o^4\,\pi\,\sqrt[4]{\beta}} \left[\left(\cos^2\varphi_o - \frac{1}{2}\sin^2\varphi_o\right) \ln \frac{1+\cos\varphi_o}{1-\cos\varphi_o} + 4\cos\varphi_o(1+a_o|\sin\varphi_o|)\right] , \qquad \text{[Eq. C.101]}$$

where the approximation

$$\ln \sqrt{\frac{1+\sin\left(-\frac{\pi}{2}+\frac{1}{a_o}\right)}{1-\sin\left(-\frac{\pi}{2}+\frac{1}{a_o}\right)}} \approx -\ln 2a_o \qquad \text{[Eq. C.102]}$$

is used. Eq. C.101 is a part of Eq. 64 of the main text.

C.3.2.5 $\dfrac{\sigma_h}{v^2}$ $\dfrac{\sqrt{E_t\{\rho^2\}}}{v^2}$

a) $a_o \ll 1$

Starting from the second part of Eq. C.78 one obtains

$$\left(\frac{\sigma_h}{v^2}\right)^2 = \frac{2\,\alpha\,a_o^2}{36\,\beta\,g^2} \int_0^{\pi} \cos^2(\varphi-\varphi_o)\,\cos^2\varphi\,d\varphi \qquad \text{[Eq. C.103]}$$

which leads directly to the desired result

$$\frac{\sigma_h}{v^2} = \sqrt{\frac{\alpha}{18\cdot 16}\,(3\cos^2\varphi_o + \sin^2\varphi_o)} \qquad \text{[Eq. C.104]}$$

This is part 1 of Eq. 69 of the main text.

b) $a_o \gg 1$

For a large a_o, the bracket in Eq. C.78 (first part) reduces to $\frac{1}{4}$, as all other terms can be neglected against it. Then the integral is solved quite easily. Starting from

$$\left(\frac{\sigma_h}{v^3}\right)^2 = \frac{\alpha}{2\beta g^2 \pi} \int_o^{\pi} \cos^3(\varphi - \varphi_o)\, d\varphi \qquad \text{[Eq. C.105]}$$

gives

$$\frac{\sigma_h}{v^3} = \sqrt{\frac{\alpha}{\beta}}\ \frac{1}{2g} \qquad \text{[Eq. C.106]}$$

which is part 2 of Eq. 69 of the main text.

APPENDIX D

CALCULATION OF THE DOPPLER SPECTRUM FOR AN ARBITRARY SEA-SURFACE ROUGHNESS

The starting point for the calculation is Eq. 46 which is repeated here for convenience

$$\varphi(f) = 2g^2 \int_{-\infty}^{\infty}\int\int\int \frac{k_{of}^4 \sin^4 \gamma_f}{f_f^{*3}} F_2(f_f^*, 0)$$

$$\left[W(f_f^*, \pi)\, \delta(f - f_f - f_f^*) + W(f_f^*, 0)\, \delta(f - f_f + f_f^*) \right] w_3(\varepsilon, u_z, u_x)\, d\varepsilon\, du_z\, du_x .$$

[Eq. D.1]

Making use of Eq. 6 and replacing k_{of} by $\frac{f_f}{c}$ gives a form of Eq. D.1 better suited for the following calculations

$$\varphi(f) = 2\pi \int_{-\infty}^{\infty}\int\int\int \frac{\sin^4 \gamma_f \sqrt{g\pi f_f^5}}{\sqrt{c^5 \cos^3 \gamma_f}} F_2(f_f^*, 0)$$

$$\left[W(f_f^*, \pi)\delta(f - f_f - f_f^*) + W(f_f^*, 0)\, \delta(f - f_f + f_f^*) \right] w_3(\varepsilon, u_z, u_x)\, d\varepsilon\, du_z\, du_x .$$

[Eq. D.2]

To solve this threefold integral, Eqs. 44, 45 and 29 are inserted and the integrations are performed step by step. As it is assumed that σ_ε is a small angle, the following approximation is valid

$$\sin \gamma_f = \sin(\gamma_0 + \varepsilon) \approx \sin \gamma_0 + \varepsilon \cos \gamma_0$$

and

$$\cos \gamma_f = \cos(\gamma_0 + \varepsilon) \approx \cos \gamma_0 \; . \qquad \text{[Eq. D.3]}$$

The first integration is performed over the variable u_z. Because of the δ-function, this is possible by setting

$$f - f_f \pm f_f^* = 0 \qquad \text{[Eq. D.4]}$$

and inserting into Eq. D.1 the value $u_{z-,+}$ that fulfils Eq. D.4. It is

$$f - f_f \pm f_f^* = f - f_0 - \frac{2f_0}{c}(u_z \sin\gamma_f - u_x \cos\gamma_f) \pm \sqrt{\frac{g f_f \cos\gamma_f}{\pi c}} \qquad \text{[Eq. D.5]}$$

Inserting Eq. 45 into Eq. D.5, the square root can be drawn approximately, as σ_z and σ_x are very much smaller than c. Applying Eq. D.2 and using the abbreviation Eq. 6

$$f_0^* = \sqrt{\frac{g f_0 \cos\gamma_0}{\pi c}} \quad , \qquad \text{[Eq. D.6]}$$

the result is

$$f - f_f \pm f_f^* = f - f_0 \pm f_0^* + \frac{u_x \cos\gamma_f}{c}(2f_0 \mp f_0^*) + \frac{u_z \sin\gamma_f}{c}(-2f_0 \pm f_0^*) = 0 \; . \qquad \text{[Eq. D.7]}$$

As f_0^* is very much smaller than f_0, it is neglected in the terms with u_x and u_z. Furthermore, $\sin\gamma_f$ is replaced in Eq. D.7 by $\sin\gamma_0$, which simplifies the mathematical effort considerably and causes a negligible error in all practical cases, where γ_0 is a small angle. Then Eq. D.7 becomes

$$u_{z-,+} = \frac{(f - f_0 \mp f_0^*)\, c}{2f_0 \sin\gamma_0} + u_x \operatorname{cotan}\gamma_0 \qquad \text{[Eq. D.8]}$$

Inserting it into Eq. 45 gives, for the doppler frequency f_f,

$$f_f(u_{z-,+}) = f \mp f_0^* \qquad \text{[Eq. D.9]}$$

and for f_f^*

$$f_{-,+}^* = \sqrt{\frac{g \cos\gamma_0 \,(f \mp f_0^*)}{\pi c}} \; . \qquad \text{[Eq. D.10]}$$

Inserting Eqs. D.8 and D.9 into Eq. D.2 and using Eq. gives

$$\varphi(f) = \frac{\sqrt{\pi^3 g}}{f_o \sin\gamma_o \sqrt{c^3 \cos^3\gamma_o}} \int\int_{-\infty}^{\infty} \sin^4(\gamma_o + \varepsilon)$$

$$\left[\sqrt{(f - f_o^*)^5}\, F_2(f_-^*, 0)\, W(f_-^*, \pi)\ \ w_2(\varepsilon, u_{z-}) \right.$$

$$\left. + \sqrt{(f + f_o^*)^5}\ F_2(f_+^*, 0)\, W(f_+^*, 0)\ \ w_2(\varepsilon, u_{z+}) \right] w_1(u_x)\, d\varepsilon\, du_x$$

[Eq. D.11]

$$= \frac{\sqrt{\pi^3 g}}{f_o \sin\gamma_o \sqrt{c^3 \cos^3\gamma_o}} \left[\sqrt{(f - f_o^*)^5}\, F_2(f_-^*, 0)\, W(f_-^*, \pi)\ \ I_- \right.$$

$$\left. + \sqrt{(f + f_o^*)^5}\, F_2(f_+^*, 0)\, W(f_+^*, 0)\ \ I_+ \right] ,$$

[Eq. D.12]

where

$$I_{-,+} = \int\int_{-\infty}^{\infty} (\sin\gamma_o + \varepsilon \cos\gamma_o)^4\ \ w_1(u_x)\ w_2(\varepsilon, u_{z-,+})\, d\varepsilon\, du_x . \qquad \text{[Eq. D.13]}$$

The function $w_2(\varepsilon, u_{z-,+})$ is rewritten in the form

$$w_2(\varepsilon, u_{z-,+}) = N(u_{z-,+}, 0, \sigma_z)\ \ N(\varepsilon, m_{\varepsilon-,+}, \sigma_\varepsilon^*) , \qquad \text{[Eq. D.14]}$$

where

$$m_{\varepsilon-,+} = \frac{\rho_{\varepsilon z}\, \sigma_\varepsilon\, u_{z-,+}}{\sigma_z}$$

and

$$\sigma_\varepsilon^* = \sigma_\varepsilon \sqrt{1 - \rho_{\varepsilon z}^2} \quad . \qquad \text{[Eq. D.15]}$$

Using the well known relations for the higher moments of the normal distribution density, Eq. D.13 is integrated over ϵ, yielding

$$I_{-,+} = \int_{-\infty}^{\infty} N(u_{z-,+},\ 0,\ \sigma_z)\ [(\sin\gamma_0 + \cos\gamma_0\ \ m_{\epsilon-,+})^4$$

$$+ 6\cos^2\gamma_0\ (\sin\gamma_0 + \cos\gamma_0\ \ m_{\epsilon-,+})^2\ \sigma_\epsilon^{*2} + 3\cos^4\gamma_0\ \sigma_\epsilon^{*4}]\ w_1(u_x)\ dx.$$

[Eq. D.16]

The product

$$P = N(u_{t-,+},\ 0,\ \sigma_t)\ \ w_1(u_x) \qquad \text{[Eq. D.17]}$$

is split up into a term containing the variable u_x and one without u_x. It is

$$P = N(u_{-,+},\ 0,\ \sigma_1)\ \ N(u_x,\ m_{x-,+},\ \sigma) \qquad \text{[Eq. D.18]}$$

where

$$u_{-,+} = \frac{(f - f_0 \mp f_0^*)\ c}{2\ f_0 \sin\gamma_0}\ , \qquad \text{[Eq. D.19]}$$

$$\sigma_1 = \frac{\sqrt{\sigma_x^2 + \sigma_z^2\ \tan^2\gamma_0}}{\tan\gamma_0}\ , \qquad \text{[Eq. D.20]}$$

$$m_{x-,+} = \frac{u_{-,+}\ \ \sigma_x^2\ \ \tan\gamma_0}{\sigma_z^2\ (\sigma_x^2 + \sigma_z^2\ \tan^2\gamma_0)}\ , \qquad \text{[Eq. D.21]}$$

and

$$\sigma = \frac{\sigma_x\ \sigma_z\ \tan\gamma_0}{\sqrt{\sigma_x^2 + \sigma_z^2\ \tan^2\gamma_0}} \qquad \text{[Eq. D.22]}$$

To obtain the final result, the integration over u_x is now performed, applying again the relation for the moment calculation

of normal processes. It is

$$I_{-,+} = N(u_{-,+}, 0, \sigma_1) \cos^4 \gamma_o$$

$$[3\,\sigma_\epsilon^{*4} + 6\,\sigma_\epsilon^{*2}(\sigma_2^2 + m_{-,+}^2) + 3\,\sigma_2^4 + 6\,\sigma_2^2\,m_{-,+}^2 + m_{-,+}^4]\,, \qquad \text{[Eq. D.23]}$$

where

$$\sigma_2 = \frac{\sigma_\epsilon\ \sigma_x\ \rho_{\epsilon z}}{\sqrt{\sigma_x^2 + \sigma_z^2 \tan^2 \gamma_o}} \qquad \text{[Eq. D.24]}$$

and

$$m_{-,+} = \frac{\sigma_\epsilon\ \sigma_z\ \rho_{\epsilon z}\ u_{-,+}\ \tan^2 \gamma_o}{\sigma_x^2 + \sigma_z^2 \tan^2 \gamma_o} + \tan \gamma_o\,. \qquad \text{[Eq. D.25]}$$

The combination of Eqs. D.12 and D.23 gives the general result of Eqs. 47 and 49 of the main text.

REFERENCES

1. MARSH, H.W. Sound reflection and scattering from the sea surface. Jnl Acoustical Society America 35 (2) 1963: 240-244.

2. PARKINS, B.E. Scattering from the time-varying surface of the ocean. Jnl Acoustical Society America 42 (6) 1967: 1262-1267.

3. KURYANOV, B.F. The scattering from the time-varying surface of the ocean. Soviet Physics - Acoustics 8 (3) 1963: 252-257.

4. BACHMANN, W. Verallgemeinerung und Anwedung der Rayleighschen Theorie der Schallstreuung [Generalization and application of Rayleigh theory of scattering of sound]. Acustica 28 (4) 1973: 223-228.

5. BACHMANN, W. A theoretical model for the backscattering strength of a composite-roughness sea surface. Jnl Acoustical Society America 54 (3) 1973: 712-716.

6. ESSEN, H.H. Wave-facet interpretation model applied to acoustic scattering from a rough sea surface. Acustica 31 (2) 1974: 107-113.

7. BACHMANN, W. and RAIGNAC, B. de. The calculation of reverberation and average intensity of broadband acoustical signals in the ocean by means of the RAIBAC computer model. Jnl Acoustical Society America 59 (1) 1976: 31-39.

8. CLARKE, R.H. Theory of acoustic propagation in a variable ocean, SACLANTCEN Memorandum SM-28. La Spezia, Italy, SACLANT ASW Research Centre, 1973. [AD 770 247]

9. URICK, R.J. Principles of Underwater Sound for Engineers. New York, N.Y., McGraw-Hill, 1967: p. 188.

10. NEUMAN, G. and PIERSON, W.J. Principles of Physical Oceanography. Englewood Cliffs, N.J. Prentice-Hall, [1966].

11. STRUTT, J.W. [Lord Rayleigh]. The Theory of Sound, Vol. II. New York, N.Y., Dover, 1945: p. 89.

12. WATSON, G.N. Theory of Bessel Functions. New York, N.Y., McMillan, 1948.

13. ABRAMOWITZ, M. and STEGUN, I.A., eds. Handbook of Mathematical Functions. Washington, D.C., National Bureau of Standards, 1968.

14. BACHMANN, W. Calculation of rms slope of carrier waves in a composite-roughness sea-surface model, SACLANTCEN Memorandum SM-38. La Spezia, Italy, SACLANT ASW Research Centre, 1974. [AD 776 583]

15. SCOTT, J.R. Some average wave lengths on short crested seas. Quart Jnl Royal Meteorological Society 95, 1969: 621-634.

[Documents with AD numbers may be obtained from the US National Technical Information Service or national outlets in other nations]

INITIAL DISTRIBUTION

	Copies
MINISTRIES OF DEFENCE	
MOD Belgium	2
DND Canada	10
CHOD Denmark	8
MOD France	8
MOD Germany	15
MOD Greece	11
MOD Italy	10
MOD Netherlands	12
CHOD Norway	10
MOD Portugal	5
MOD Turkey	5
MOD U.K.	16
SECDEF U.S.	60
NATO AUTHORITIES	
Defence Planning Committee	3
NAMILCOM	2
SACLANT	10
SACLANTREPEUR	1
CINCWESTLANT/COMOCEANLANT	1
COMIBERLANT	1
CINCEASTLANT	1
COMSUBACLANT	1
COMCANLANT	1
COMMAIREASTLANT	1
SACEUR	2
CINCNORTH	1
CINCSOUTH	1
COMNAVSOUTH	1
COMSTRIKFORSOUTH	1
COMEDCENT	1
COMSUBMED	1
COMMARAIRMED	1
CINCHAN	1
SCNR FOR SACLANTCEN	
SCNR Belgium	1
SCNR Canada	1
SCNR Denmark	1
SCNR Germany	1
SCNR Greece	1
SCNR Italy	1
SCNR Netherlands	1
SCNR Norway	1
SCNR Portugal	1
SCNR Turkey	1
SCNR U.K.	1
SCNR U.S.	2
NATIONAL LIAISON OFFICERS	
NLO Denmark	1
NLR Italy	1
NLO U.K.	1
NLO U.S.	1
NLR TO SACLANT	
NLR Belgium	1
NLR Canada	1
NLR Germany	1
NLR Greece	1
NLR Italy	1
NLR Norway	1
NLR Portugal	1
NLR Turkey	1
ESRO/ELDO Doc. Service	1
Total initial distribution	230
SACLANTCEN library	10
Stock	40
Total number of copies	280